

QATAR UNIVERSITY

COLLEGE OF ENGINEERING

SHEAR BEHAVIOR OF FIBER REINFORCED CONCRETE BEAMS REINFORCED
WITH BASALT FRP BARS AND GFRP STIRRUPS

BY

ABATHAR ABDULKARIM HASSON ALHRANI

A Thesis Submitted to
the Faculty of The College of
Engineering
In Partial Fulfillment
of the Requirements
for the Degree of
Master of Science in Civil Engineering

June 2018

© 2018 Abathar Abdulkarim Hasson Alhrani. All Rights Reserved

COMMITTEE PAGE

The members of the Committee approve the thesis of Abathar Abdulkarim Hasson
AlHrani defended on 06/05/2018.

Dr. Wael Alnahhal
Thesis/Dissertation Supervisor

Dr. Usama Ebead
Committee Member

Dr. Wasim Barham
Committee Member

Dr. Okan Sirin
Committee Member

Approved:

Khalifa Al-Khalifa, Dean, College of Engineering

ABSTRACT

ALHRANI, ABATHAR, A, Masters

June: 2018, Master of Science in Civil Engineering

Title: Shear Behavior of Fiber Reinforced Concrete Beams Reinforced with Basalt FRP Bars and Glass FRP Stirrups

Supervisor of Thesis: Dr. Wael Alnahhal.

Qatar suffers from a harsh environment in the form of high temperature that prevails almost all year round in addition to severe humidity and coastal conditions. This exposure leads to the rapid deterioration and the reduction of the life span of reinforced concrete (RC) infrastructure. With the developments in materials science, the advanced composites, especially fiber reinforced polymer (FRP) materials are becoming viable alternatives to the traditional construction materials. Having superior durability against corrosion, versatility for easy in-situ applications and enhanced weight-to-strength ratios compared to their counterpart conventional materials, FRPs are promising to be the future of construction materials.

This study is focusing mainly on studying the shear behavior of basalt fiber reinforced concrete (BFRC) beams reinforced with basalt FRP bars and glass FRP (GFRP) stirrups. The experimental work comprises 14 beams of size $165 \times 260 \times 2000$ mm. The beams were tested under four-point loading test by universal testing machine (UTM) until failure. The beams were reinforced with sand coated basalt FRP bars (BFRP) as a flexural reinforcement, in addition to the discrete, chopped basalt fibers, which were added to the

concrete mix at two different volume fractions namely, 0.75%, and 1.5%. Two mixes with the aforementioned volume fractions were prepared and cured for 28 days before testing. The main parameters investigated in this study were the reinforcement ratio, the span to depth ratio and the volume fraction of basalt macro-fibers (BMF). Test Results showed a significant increase in the shear strength as the reinforcement ratio increases. In addition, using lower span to depth ratio resulted in an increase in the shear capacity. It has also revealed that using higher percentages of BMF enhanced the shear capacity, reduced the beam deflection, reduced the cracks width and propagation, and improve the beam ductility before failure.

DEDICATION

“To my grandparents, parents, and lovely brothers”

ACKNOWLEDGMENTS

I would like sincerely to thank almighty Allah for all his grants that he bestowed on me.

I would also like to thank the following people for their support, without whose help this work would never have been possible: I am indebted particular grateful to Dr. Wael Alnahhal for his continuous support along 6 years in the university during my bachelor and master studies in which he has enrich my knowledge level and provide me with an excellent tools for an engineering thinking. I would like to thank him for being a great brother before being my supervisor.

The deepest gratitude at the end to my parents and brothers for their great effort in meeting all my needs and their continuous encouragement to finish this work.

TABLE OF CONTENTS

DEDICATION	v
ACKNOWLEDGMENTS	vi
LIST OF TABLES	xi
LIST OF FIGURES.....	xii
CHAPTER 1: INTRODUCTION	1
1.1. Corrosion of Steel in Concrete.....	1
1.2. Qatar’s Environment.....	3
1.3. FRP Composites.....	3
1.3.1. FRP Constituents	4
1.3.2. FRPs as a Structural Element	5
1.3.3. Mechanical Behavior of FRP Bars Compared to Steel Reinforcement.	7
1.3.4. Advantages of FRP Composites	9
1.3.5. Limitations of FRP Composites	11
1.4. FRP Bars	12
1.5. Chopped (discontinuous) FRP Fibers	13
1.5.1. Fibers Classification and Geometry	15
1.5.2. Failure Mechanism of Fibers.....	17
1.6. Basalt FRP Composites.....	20
1.6.1. Basalt Macro Fibers	22
1.6.2. Basalt Fibers Characteristics	23
1.7. Shear in Beams.....	24
1.7.1. Types of Shear Cracks	27
1.7.1.1. Flexure Shear Cracks.....	27
1.7.1.2. Web Shear Crack	27
1.7.2. Types of Shear Failures	28
1.7.3. The Internal Shear Transfer Actions.....	31
1.7.4. Factors Affecting the Shear Strength of RC Beams	33
1.8. Research Significance	34
1.9. Aim of the Study	35
1.10. Thesis Organization	36
CHAPTER 2: LITERATURE REVIEW	37
2.1. Cracks Pattern	37

2.2.	Load Deflection Behavior.....	38
2.3.	Load Strain Behavior	39
2.4.	Effect of Reinforcement Ratio (ρ) and (E) on the Shear Strength of Concrete	39
2.5.	The effect of span to depth (a/d) ratio on the shear strength.....	40
2.6.	The Effect of Compressive Strength on the shear strength.....	41
2.7.	The use of FRP as a Shear Reinforcement.....	41
2.8.	The use of Macro Fibers in Concrete Mix and its Effect on the Shear Behavior	42
2.9.1.	<i>Fibers Advantages over Stirrups</i>	45
CHAPTER 3: EXPERIMENTAL PROGRAM.....		47
3.1.	The Concrete Ingredients Used in the Concrete Mix.....	47
3.1.1.	<i>Cement</i>	47
3.1.2.	<i>Water</i>	48
3.1.3.	<i>Sand</i>	48
3.1.4.	<i>Coarse Aggregate</i>	48
3.1.5.	<i>Basalt Macro Fibers</i>	48
3.2.	Concrete Mixture Proportions.....	49
3.3.	Flexural and Shear Reinforcement Used in this Study	49
3.4.	Material Characterization Tests	50
3.4.1.	<i>The Fresh Concrete Test</i>	51
3.4.1.1.	<i>Slump Test</i>	51
3.4.2.	<i>The Hardened Concrete Tests</i>	51
3.4.2.1.	<i>Compressive Strength Test</i>	51
3.4.2.2.	<i>Flexural Strength Test</i>	52
3.4.2.3.	<i>The Direct Tensile Test</i>	53
3.5.	Beam Tests.....	55
3.5.1.	<i>Test Setup and Instrumentation</i>	55
3.5.2.	<i>The Test Variables</i>	59
3.5.3.	<i>Beams Designations</i>	60
CHAPTER 4: RESULTS AND DISCUSSION.....		64
4.1.	The Mechanical Properties of Fresh Concrete.....	64
4.1.1.	<i>Slump Test Results</i>	64
4.2.	The Mechanical Properties of Hardened Concrete	66
4.2.1.	<i>Compressive Test Results</i>	66

4.2.2.	<i>Flexural Test Results</i>	67
4.2.3.	<i>Direct Tensile Test Results</i>	69
4.3.	<i>Large – Scale BFRP-RC Beams</i>	71
4.3.1.	<i>Beam A1(2.5-ρf1-0.75%-G250)</i>	71
4.3.2.	<i>Beam A2 (2.5-ρf1-1.5%-G250)</i>	73
4.3.3.	<i>Beam A3 (2.5-ρf2-0.75%-G250)</i>	74
4.3.4.	<i>Beam A4 (2.5-ρf2-0.75%-G170)</i>	76
4.3.5.	<i>Beam A5 (3.3-ρf2-1.5%-G250)</i>	78
4.3.6.	<i>Beam A6 (3.3-ρf2-0%-G170)</i>	80
4.3.7.	<i>Beam A7 (3.3-ρf2-0.75% -G170)</i>	82
4.3.8.	<i>Beam A8 (3.3-ρ2-1.5% -G170)</i>	84
4.3.9.	<i>Beam A9 (3.3-ρ3-0.75%-G170)</i>	86
4.3.10.	<i>Beam A10 (2.5-ρ3-1.5% -G170)</i>	87
4.3.11.	<i>Beam A11 (2.5-ρ3-0.75%-G250)</i>	89
4.3.12.	<i>Beam A12 (2.5-ρ3-0.75%-G170)</i>	91
4.3.13.	<i>Beam A13 (2.5-ρ3-0.75%-S170)</i>	92
4.3.14.	<i>Beam A14 (2.5-ρ3-1.5%-S170)</i>	94
4.4.	<i>Discussion of Test Results</i>	96
4.4.1.	<i>The Effect of Fiber Percentage</i>	98
4.4.2.	<i>The Effect of Reinforcement Ratio</i>	107
4.4.3.	<i>The Effect of Span to Depth Ratio</i>	113
4.4.4.	<i>The Effect of Stirrups Spacing</i>	116
4.4.5.	<i>The GFRP Stirrups Vs Steel Stirrups</i>	120
CHAPTER 5: ANALYTICAL PROGRAM.....		123
5.1.	<i>Design Equations for Shear Strength</i>	123
ACI 440.1R-15 [9]......		123
CSA-S806-12 [31]......		124
JSCE-97 [10]......		125
ISIS 2007 [30]......		126
5.1.1.	<i>Design Equations for Concrete Beams Reinforced with Longitudinal FRP Bars.</i>	126
5.1.2.	<i>Design Equations for Beams with FRP Stirrups</i>	130
5.1.3.	<i>Design Equations for FRC Beams Reinforced with Basalt Chopped Fibers</i>	135
Narayanan and Darwish [85]......		135

Ta'an and Feel [86].	135
Swamy et al [87].	135
Khuntia [88].	136
CHAPTER 6: SUMMARY, CONCLUSIONS AND RECOMMENDATIONS	144
Summary	144
Conclusions	144
Recommendations	147
References	148

LIST OF TABLES

Table 1: Properties of various types of FRP materials	19
Table 2: Basalt fibers characteristics	23
Table 3: Ingredients proportions	49
Table 4: Steps of beam specimen's preparation.....	57
Table 5: Testing parameters.....	60
Table 6: Tentative testing matrix of tested beams	63
Table 7: Compressive test results.....	67
Table 8: Flexural test results.....	69
Table 9: Direct tensile test results	70
Table 10: Summary of test results	97
Table 11: Statistics summary for the experimental concrete shear capacity compared to the predicted ones	128
Table 12: Statistics summary for the experimental shear capacity of beams reinforced FRP bars and stirrups compared to the predicted ones	134
Table 13: Results for evaluating the shear behavior of beams reinforced with longitudinal basalt bars and basalt chopped fibers.....	138
Table 14: Results for evaluating the shear behavior of beams reinforced with longitudinal basalt bars, GFRP stirrups, and basalt chopped fibers.....	140

LIST OF FIGURES

Figure 1. Corrosion stages.	3
Figure 2. Stress strain diagram for: Fibers, FRP & matrix [6].	5
Figure 3. FRP sheets.	6
Figure 4. Different types of FRP rebars.....	6
Figure 5. FRP Macro-fibers.	7
Figure 6. Stress strain diagram of FRP bars Vs Steel bars.	9
Figure 7. a) RC deterioration; b) Basalt FRP rebar mesh.	11
Figure 8. Different surface texture of FRP bars [11].	13
Figure 9. Stress strain behavior of plain concrete Vs Fiber reinforced concrete [16].	14
Figure 10. Monofilament & Multifilament.	16
Figure 11. Various geometries of the commercial discrete fibers [17].....	17
Figure 12. failure mechanisms of fibers.	18
Figure 13. Basalt discrete fibers.....	22
Figure 14. Beam under loading.....	24
Figure 15. Internal moment and shear at section A-A.....	25
Figure 16.(a) Shear and flexural stresses; (b) Normal Principal stresses; (c) Compressive stress trajectories; (d) Crack pattern.	26
Figure 17. Types of shear cracks; (a) flexure- shear cracks, (b) Web shear cracks.....	28
Figure 18. Diagonal tension. failure	29
Figure 19. Shear compression failure.	30

Figure 20. Shear tension failure.....	30
Figure 21. (a)The internal shear actions in cracked section, (b) the interlocking mechanism	32
Figure 22. a) BFRP bars; b) GFRP stirrup.....	50
Figure 23. Compressive test setup	52
Figure 24. Flexural test setup.....	53
Figure 25. Formwork and dimensions for direct tensile test specimen	54
Figure 26. a) Direct tensile test setup; b) 200 mm LVDT	54
Figure 27. Strain gauges used: (a) FRP- strain gauge, (b) Steel- strain gauge, (c) Concrete- strain gauge	58
Figure 28. The data acquisition system.....	58
Figure 29. Stirrups spacings: 170 mm; and 250 mm	60
Figure 30. Beams and their sections details.....	62
Figure 31. Fibers distribution.....	65
Figure 32. a) Slump for plain concrete; b) Slump for concrete with 1.5% basalt volume fraction.....	65
Figure 33. Failure modes of a) Plain concrete; b) 0.75% and 1.5% concrete cylinders under compressive test.....	66
Figure 34. Failure types of prisms under flexural strength test	68
Figure 35. (a) Stress strain diagram; (b) Failure occurs at the mid height; (c) Failure occurs near the upper neck.....	70
Figure 36. Beam A1 (Diagonal tension failure).....	72

Figure 37. Beam A2 (Diagonal tension failure).....	74
Figure 38. Beam A3 (Diagonal tension failure).....	76
Figure 40. Beam A4 (Compression flexural failure)	78
Figure 41. Beam A5 (Compression flexural failure)	80
Figure 42. Beam A6 (Compression shear failure)	82
Figure 43. Beam A7 (Compression flexural failure).	83
Figure 44. Beam A8 (Compression flexural failure)	85
Figure 45. Beam A9 (Compression flexural failure).	87
Figure 46. Beam A10 (Compression flexural failure)	89
Figure 47. Beam A11 (Diagonal tension failure).....	90
Figure 48. Beam A12 (Diagonal tension failure).....	92
Figure 49. Beam A13 (Diagonal tension failure).....	94
Figure 50. Beam A14 (Compression flexural failure)	96
Figure 51. a) fibers bridging the flexural crack; b) fibers across inclined crack.	101
Figure 52. a) Concrete spallation in beam A6 (without fibers); b) The effect of fibers in partially substituting the glass stirrups.....	102
Figure 53. Load displacement diagrams for identical beams with different fiber percentages.....	103
Figure 54. Load vs Crack width diagrams for identical beams with different fiber percentages.....	104
Figure 55. Load vs longitudinal FRP strain diagrams for identical beams with different fiber percentages	105

Figure 56. Load vs concrete strain diagrams for identical beams with different fiber percentages.....	106
Figure 57. Load displacement diagrams for identical beams with different reinforcement ratios.....	109
Figure 58. Load vs crack width diagrams for identical beams with different reinforcement ratios.....	110
Figure 59. Load vs Longitudinal FRP strain diagrams for identical beams with different reinforcement ratios	111
Figure 60. Load vs concrete strain diagrams for identical beams with different reinforcement ratios	112
Figure 61. Load displacement diagrams for identical beams with different span to depth (a/d) ratios	114
Figure 62. Load vs crack width diagrams for identical beams with different span to depth (a/d) ratios	115
Figure 63. Load vs longitudinal FRP strain diagrams for identical beams with different span to depth (a/d) ratios.....	115
Figure 64. Load vs concrete strain diagrams for identical beams with different span to depth (a/d) ratios	116
Figure 65. Load displacement diagrams for identical beams with different spacings of stirrups.....	118
Figure 66. Load vs crack width diagrams for identical beams with different spacings of stirrups.....	119

Figure 67. Load vs stirrups strain diagrams for identical beams with different type of stirrups (GFRP vs Steel)	120
Figure 68. Load displacement diagrams for identical beams with different type of stirrups (GFRP vs Steel)	121
Figure 69. Load vs crack width diagrams for identical beams with different type of stirrups (GFRP vs Steel).	121
Figure 70. Load vs longitudinal FRP strain diagrams for identical beams with different type of stirrups (GFRP vs Steel).	122
Figure 71. Load vs concrete strain diagrams for identical beams with different type of stirrups (GFRP vs Steel)	122
Figure 72. Comparison of experimental and predicted shear strength for beams reinforced with longitudinal FRP bars only.	129
Figure 73. Comparison of experimental and predicted shear strength for beams reinforced with longitudinal FRP bars and stirrups.....	134
Figure 74. The effect of $\rho^{1/3}$ on the shear contribution of chopped fibers	137
Figure 75. Comparison between the experimental and predicted values by equation (20)	142
Figure 76. Comparison between the experimental and predicted values by equation (21)	143

CHAPTER 1: INTRODUCTION

In the field of construction, it is a common knowledge that the steel reinforcement represents the most commonly reinforcing component used for concrete structures. This can be attributed to their distinct mechanical characteristics, as they have proved since the start of their use to be feasible and well-performing material in terms of reinforcing and strengthening concrete structures with a high tensile strength, high stiffness, and high ductility. However, one of the major problems that steel reinforcement faces is the problem of corrosion, which is considered as the key factor for the evident widespread deterioration of infrastructure buildings around the world. Engineers, in turn, have developed new techniques to overcome this issue such as using epoxy coatings, galvanized coatings, polymer impregnated concrete, and cathodic protection. Nevertheless, and with all intensive efforts of engineers, the corrosion problem has not been completely eliminated.

In this chapter, the corrosion mechanism in concrete along with its consequences is discussed, then an alternative solution will be introduced and explained in detail.

1.1. Corrosion of Steel in Concrete

Corrosion is defined as "the degradation of materials by chemical reaction with the environment in which the material resides" [1]. In order for the corrosion action to take place in the steel reinforcement, the availability of two sources: the oxygen and the moisture are highly responsible for the initiation of the corrosion activity, both of them can diffuse inside the concrete cover through the cracks, reducing, as a result, the concrete alkalinity from 13 to below 10, at which the corrosion activity can start in the steel bars.

Therefore, corrosion has a harmful effect on metals due to its tendency to attack and destroy their strength, thus, the situation becomes more critical and destructive failure of structure can occur. Although that the concrete cover provides an excellent protection for the reinforcement from being corroded, it is known that after the curing process of concrete the concrete will dry, and the extra water used for mixing begins to find its way to the outer surface of concrete, where it evaporates. As a result, concrete starts shrinking, and cracks will appear on the surface. Also, some cracks such as the flexural cracks which are usually formulated at the maximum moment zone are penetrating the concrete cover. Hence, both crack types will pave the way for the chloride, moisture, and oxygen agents to reach bars surface, and thereby, the probability of corrosion attack increases. After the corrosion occurrence, the formulated oxides will be accumulated around the metal, and will occupy larger space than that of the original steel, therefore, the steel will be expanding, leading to an internal pressure that tends to move outward, creating with it an excessive cracks, and concrete spallation in the later stages, and hence a bond loss between steel and concrete will exist [2] as shown in Figure 1. These factors are capable of threatens the structure, shortens its lifespan, and make it less liable in the future. Figure 1 describes the corrosion occurrence steps in a reinforced concrete.

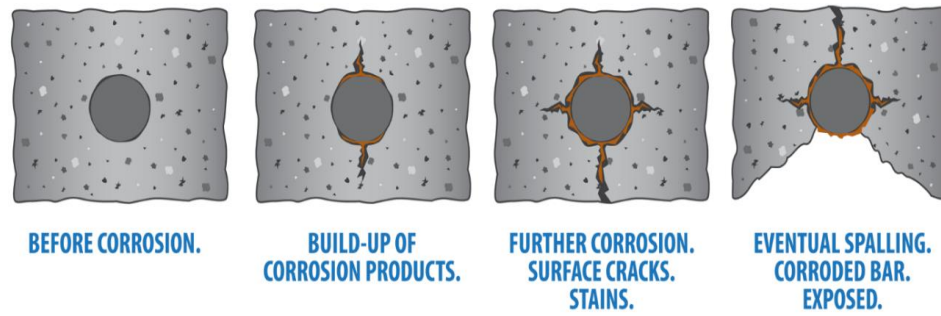


Figure 1. Corrosion stages.

1.2. Qatar’s Environment

Qatar is known by its harsh environment that is represented by high periodical humidity, in addition to the dust accompanied by the temperature fluctuation. Also, geographically Qatar is considered a peninsula, this in turn makes it highly susceptible to the spray from the seawater which contains high chloride contents. All of the aforementioned factors consequently made from Qatar a corrosive environment. Hence, this dilemma drew the attention toward what is known as the “Fiber reinforced polymers or FRPs”.

1.3. FRP Composites

As the time is passing, an obvious development and prosperity in various fields of science can be witnessed worldwide. However, introducing a new idea in the field of science whose researchers are intended to implement it in the real life needed to be highly justified, especially if the idea is related to the structural engineering domain, where people

safety constitute the top priority requirement to be met. The construction industry is always aiming to develop a new, safe, and economical materials that would improve the structural behavior of concrete buildings and would create an alternative to the conventional reinforcement that would tackle the problems of the harsh environments around the world. In the last century [3], manufacturing composite materials (Fiber reinforced polymers, FRPs) has become a hot subject among researchers due to their striking remarkable features such as high strength and high corrosion resistance. According to Balagury et al. and Bakis et al. [4,5] FRPs have been used as a strengthening material for Civil Engineering structures since 1980s. However, these materials have been originally made to be used in aircrafts and high-speed trains as the FRP materials are characterized by their low weight and high strength.

1.3.1. FRP Constituents

FRPs are composite materials that are comprised of fibers and matrix. The fibers are the parts that are responsible for providing both stiffness and strength to the composite material. Fibers are embedded in a relatively ductile polymer matrix such as: epoxy and vinyl ester which are constituting 30% to 60% by volume of the composite. These matrixes are taking charge of binding the fibers together and as a result the load will be transferred among the individual fibers. Also, the matrix can help in protecting the fibers from the outer environment and from being appraised. As a result, the matrix can be considered as a protection and a structural component [3]. Figure 2 shows the typical stress - strain diagrams for the following: the fiber, the matrix and the composite material FRP.

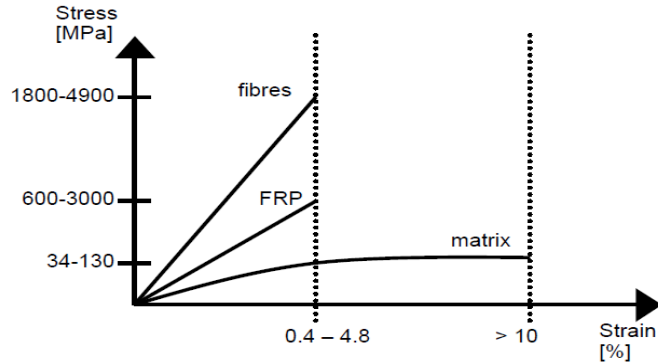


Figure 2. Stress strain diagram for: Fibres, FRP & matrix [6].

1.3.2. FRPs as a Structural Element

As a structural reinforcement, FRPs was recognized to be utilized in different shapes and forms in structures such as:

a) FRP sheets: They are thin, flexible and light in weight. They are mainly used for strengthening and retrofitting of an existing structural element by increasing its bearing capacity without the need for drilling concrete to add additional reinforcement. This provide a very beneficial solution for the structural element that requires a change in function. FRP sheet along with its application can be shown in Figure 3.

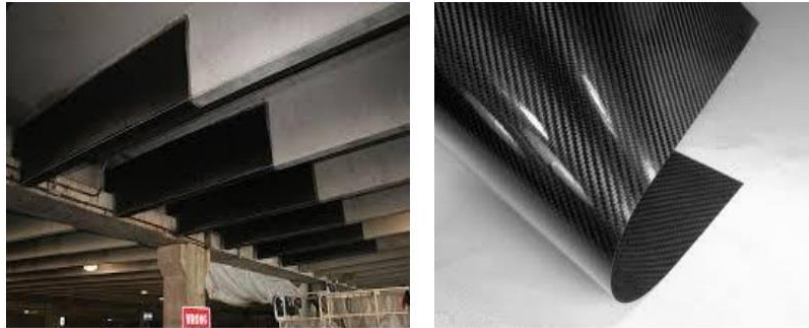


Figure 3. FRP sheets.

b) FRP Bars: Many kinds of rebars with different treated surfaces are available nowadays with a lighter weight and much greater tensile strength than the conventional steel reinforcement. Different FRP rebars are shown in Figure 4.



Figure 4. Different types of FRP rebars.

c) FRP Macro-fibers: The FRP can also be fabricated as a randomly oriented and discrete fibers known as chopped fiber added to the concrete in order to provide the concrete with higher durability and more ability to resist the damaging effects of loads, especially under tensile loadings. These fibers can be depicted from Figure 5.



Figure 5. FRP Macro-fibers.

1.3.3. Mechanical Behavior of FRP Bars Compared to Steel Reinforcement.

The main goal of expanding the FRP material and its behavioral knowledge as structural element (mainly the reinforcing bars) stems from the fact that it is required to be developed through different practical application studies, so that eventually the calibration of design codes can be enabled and the practicing engineers can use it in the practical life. It is important here to understand the main behavior of the FRP reinforcement and how

does it differ from the conventional steel reinforcement in concrete structures, in order to take the required considerations for an efficient and safe design.

The stress strain behavior of an FRP material is elastic up to the failure point, which means that it does not experience any yielding behavior up to the point where it ruptures. Thus, the failure of reinforced concrete members reinforced with an FRP material is brittle either by the rupture of FRP reinforcement or crushing of concrete [3]. This is one of the main differences between FRP materials and steel which starts yielding after slightly exceeding the elastic limit (this is termed as elastic plastic behavior). As a result the steel RC member will show large deflection and excessive cracks prior to failure with a little loss in load carrying capacity, giving by that enough warning before total collapse. However, this lack of warning in FRP-RC members has been compensated by designing them for a higher reserve of strength through the use of smaller strength reduction factors than steel. At failure FRP bars exhibit lower strains than that in steel bars. However, the ultimate tensile strength of FRP bars are ranging from 3 to 5 times that of steel reinforcement [3]. In most FRP materials the elastic modulus is lower than steel except for carbon which can have an elastic modulus exceeding that for steel bars [3]. To understand the stress strain behavior graphically, the reader can be referred to Figure 6 that illustrates the stress - strain behavior of the GFRP and carbon FRP (CFRP) bars versus steel bars.

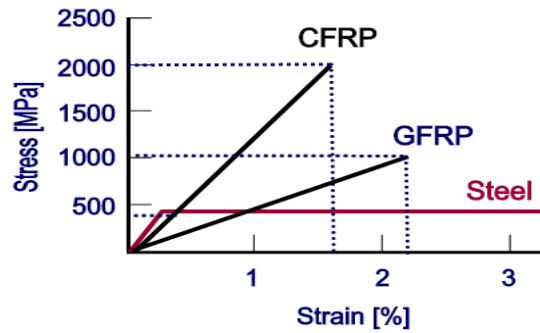


Figure 6. Stress strain diagram of FRP bars Vs Steel bars.

In addition, FRPs are orthotropic material, which means that their mechanical properties are affected by the fibers orientation. The fibers are considered to be more effective in resisting the tensile stresses as long as their alignment is in same direction of the applied stresses [3]. The steel bars show similar stiffness in tension and compression, while FRP bars are not recommended to be used in compression zones, because their stiffness in compression is way less than that in tension [3].

Furthermore, because FRP material is a non-corrosive material, the ACI 318 limitations on the crack width for RC members reinforced with steel can be relaxed in FRP-RC members. However, in certain cases, this relaxation might be inappropriate due to aesthetic reasons or to guarantee the required shear capacity.

1.3.4. Advantages of FRP Composites

The conventional materials such as steel had a successful usage history in concrete structures. However, in some cases RC buildings might be exposed to a rapid deterioration that takes place due to the corrosion problem as can be depicted from Figure 7a. Therefore,

FRP composites are attracting a widespread interest due to some remarkable features that can't be found in a conventional steel material. The FRP composites are characterized by [4,6,7]:

- Higher ultimate tensile strength than steel
- High strength to weight ratio
- Excellent resistance to corrosion
- Electromagnetic neutrality, which means that it can be used in magnetic imaging facilities
- Low thermal conductivity
- High durability in a wide range of environments including the aggressive ones
- Requires little or no maintenance
- High flexibility, ease of handling, and fast in installation because of their light weight. According to Neuvokas Corporation [8] two workers are able to lift and move 20 x 20 ft mat of basalt FRP bras and place it in its suitable location as shown by Figure 7b.



(a) RC deterioration



(b) Basalt FRP rebar mesh

Figure 7. a) RC deterioration; b) Basalt FRP rebar mesh.

1.3.5. Limitations of FRP Composites

On the other hand, the use of FRP as a structural reinforcement has some disadvantages such as:

- Low modulus of elasticity
- Low strain at failure
- FRP is not an isotropic material, which indicates that FRP can take the load in one direction, and hence low transverse strength in comparison with axial strength the FRP will undergoes
- Higher cost than steel [3].

1.4. FRP Bars

In infrastructure applications, there are four types of FRP bars that are available in the market which are:

Aramid,
Carbon,
Glass and
Basalt.

In the research field there is a lack of data related to the long-term behavior of FRP bars in different environmental conditions. Consequently, the ACI 440.1R-15 [9] and JSCE [10] code standards have introduced an environmental reduction factors, that would ensure being in the safe side as the FRP bars might show some reduction in strength when exposed to various exposure conditions. Furthermore, if the bars are exposed to sustained loadings, the available codes specify a very conservative upper limit for the developed stresses for each FRP type, to prevent the use of full FRP capacity.

To enhance the bond efficiency between the FRP bars and the surrounding concrete, the commercially available FRP rebars have been manufactured with different surface texture such as sand coated texture, helical wrapping texture, helical wrapping and sand coated texture, and indented texture. Examples of different surface textures are illustrated in Figure 8.

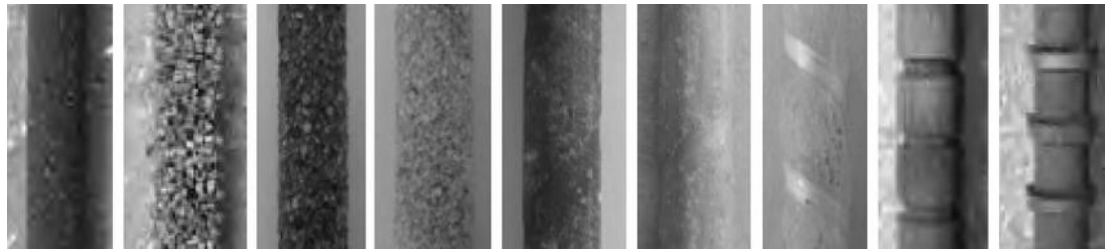


Figure 8. Different surface texture of FRP bars [11].

1.5. Chopped (discontinuous) FRP Fibers

The chopped fibers in a concrete mix can be considered as a discrete reinforcement dispersed randomly all over the entire concrete section of a structural element [12].

Some natural materials such as asbestos and basalt can be used to make fibers. Fibers can also be manufactured as steel, carbon, glass and synthetic such as polypropylene [13]. However, steel, glass, synthetic fibers and the ones made from natural material are most commonly used fibers in the practical life [14]. Basalt fibers is used in this study.

In Civil Engineering, concrete is considered as the most important material that is commonly used in structural applications with low cost, high compressive strength, and an abundant raw material. However, the common concrete is known by its brittle behavior at failure, low ductility, poor toughness and weakness in the zone under tension stresses, which restrict its applications. Therefore, to overcome these shortcomings, the chopped fibers have been introduced to improve the concrete tensile strength, delay crack

formulation, provide an excellent permeability, and boost the concrete toughness by increasing the cracked concrete ability to resist more stress beyond the peak stress without fracturing, and the structural integrity preserved as a result past the failure load of normal RC beams [15]. In other words, the general response of plain concrete against the fiber reinforced concrete (FRC) can be shown in Figure 9, where it can be seen that FRC undergoes a large plastic deformation after reaching the peak load, thus a relatively ductile failure was assured. However, in the plain concrete a sudden brittle failure was occurred immediately after reaching the peak load.

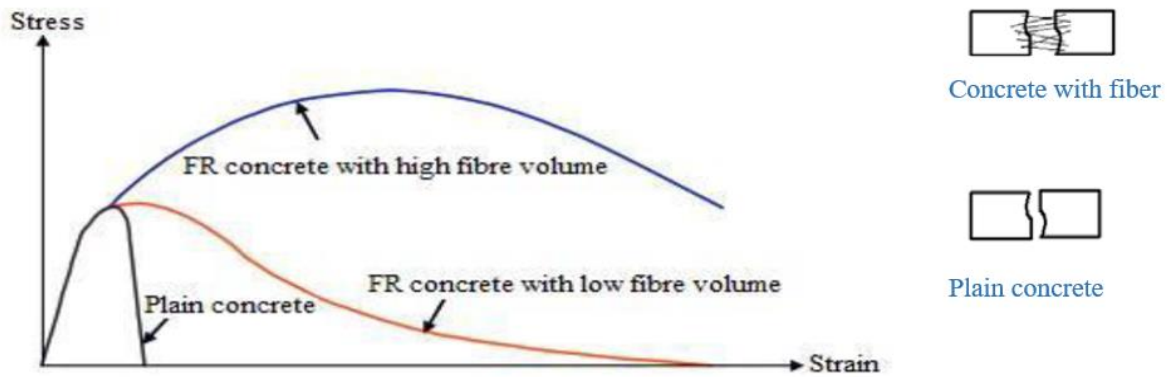


Figure 9. Stress strain behavior of plain concrete Vs Fiber reinforced concrete [16].

1.5.1. Fibers Classification and Geometry

The chopped fibers can be made in two configurations: sometimes fibers come in the form of monofilament where each fiber is separated from the other fiber. Whereas occasionally fibers come in the form of multifilament where many fibers are bundled together as shown in Figure 10. In general, the discrete fibers are available with a length varying from few millimeters up to 80 millimeters, and a very small diameter ranging from only tenth of millimeters to 2 millimeters [17].

Based on their length and diameters the fibers can be classified as either macrofibres or microfibers. In case their length and diameter are greater than the maximum aggregate size and the cement grain diameter respectively, then they are considered as macrofibres, but if their length and diameter are less than the maximum aggregate size and equal diameter to that of cement grains respectively, then they are considered as microfibers [18].

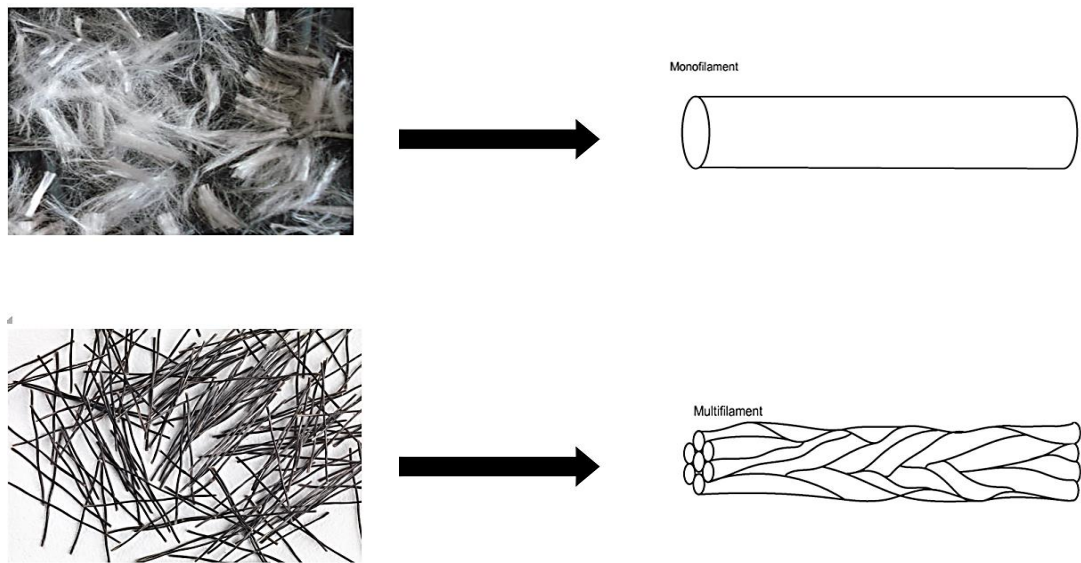


Figure 10. Monofilament & Multifilament.

The improvement in the mechanical performance of concrete by the addition of the discrete fibers is substantially dependent on two types of interactions between the fibers and the cementitious matrix that surrounds the fibers which are: the chemical adhesion and the frictional bonding [19]. However, these types of interactions might not be enough, and uneffiecient reinforcing might be induced when using the conventional fibers (straight fibers). Consequently, fibers have been deformed on their surface, and many complex geometries have been developed to create a mechanical anchorage between the fiber and the surrounding matrix [19]. Many forms of fibers can be depicted from Figure 11.

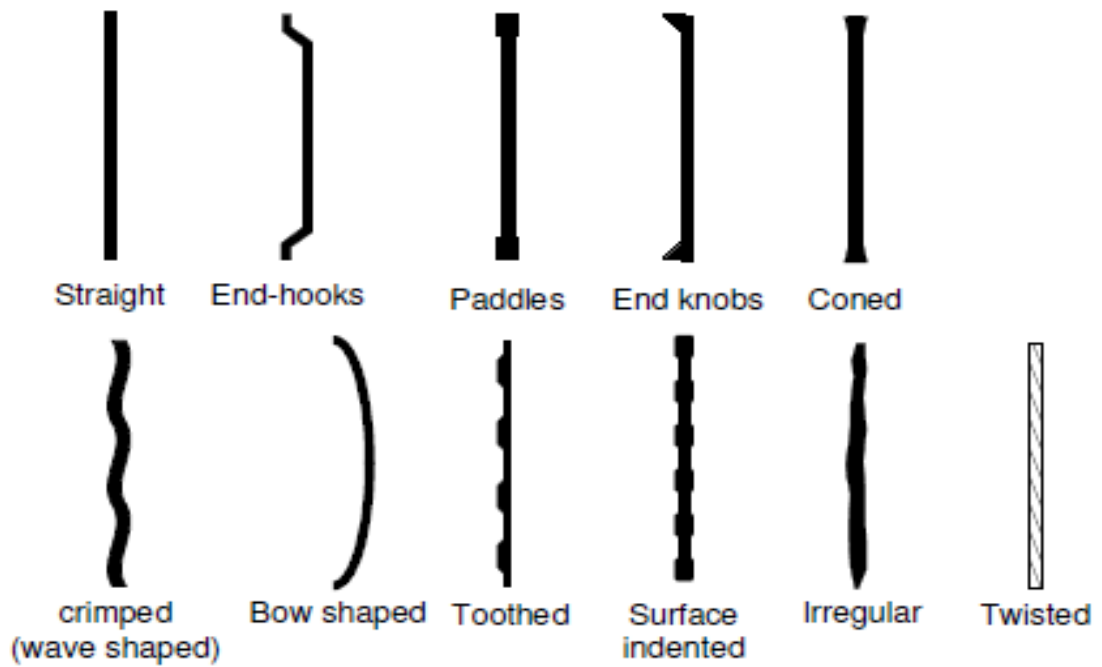


Figure 11. Various geometries of the commercial discrete fibers [17].

1.5.2. Failure Mechanism of Fibers

The failure mechanisms of fibers with the surrounding matrix are:

Fiber rupture: when the maximum tensile strength is developed in the minibar after cracking of concrete and exceeded, the macro fibers will be ruptured.

Fiber pullout: this type of failures usually depends on the location of the crack with respect to the macro fibers. Sometimes the crack develops on the last portion of minibar,

therefore the embedded length will not be capable to develop the full tensile strength capacity, this in turn will cause the pullout failure. This failure also depends on the bond characteristics between the concrete matrix and the macro fibers, where it can be found that there is a space at the interfacial zone (which is known as debonding) making a quite loose bonding between the two surfaces [15]. The two failure types are illustrated in Figure 12.

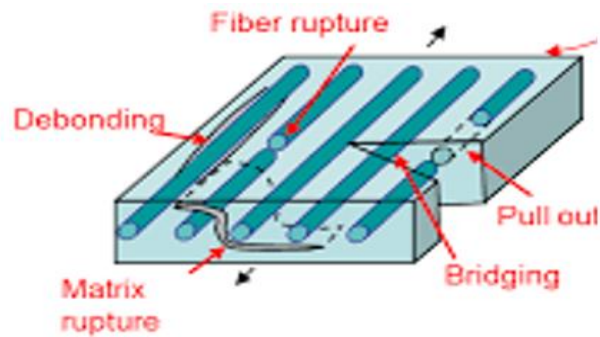


Figure 12. failure mechanisms of fibers.

1.5.3. Properties of Various Types of FRP Materials

The following table illustrates the different types of FRP material available in the market along with their mechanical properties and geometry [3]:

Table 1

Properties of various types of FRP materials

Fiber type	Tensile strength (MPa)	Modulus of Elasticity (GPa)	Ultimate strain (%)	Density (kg/m ³)	Fiber Diameter (μm)
E-glass	1800-3500	70-75	2.0-3.5	2500-2600	5-25
S-glass	3400-4800	85-100	3.5-5.0	2500-2600	5-25
Carbon-pitch HM (High Modulus)	3000-3500	400-800	0.4-1.5	1900-2100	9-18
Carbon-PAN HM (High Modulus)	2500-4000	350-700	0.4-0.8	1800-2000	5-8
Carbon-PAN HT (High Tensile Strength)	3500-5000	200-260	1.2-1.8	1700-1800	5-8
Aramid-IM (Intermediate Modulus)	2700-4500	60-80	4.0-4.8	1400-1450	12-15
Aramid-HM (High Modulus)	2700-4500	115-130	2.5-3.5	1400-1450	12-15
Basalt	1850-4800	70-110	2.5-3.5	2500-2900	6-13

1.6. Basalt FRP Composites

The main source of basalt fiber reinforced polymers (BFRP) is basalt rocks. The basalt rocks categorized as an extrusive igneous rocks which exist in the planet after the action of volcanic eruptions which expel them into the earth crust in the form of lava, then and after the lava being exposed to rapid cooling, lava changes into basalt rocks. These rocks are considered as the most type of rocks that are occupying the earth crust space [20]. Therefore, and proceeding from this point engineers start thinking about how to exploit this widespread source in proportion to the engineering applications.

The basalt fiber reinforced polymer is relatively new material that is fabricated by melting the basalt rocks through the exposure to very high values of melting temperatures above 1400 C° [3]. Then continuous basaltic fiber filaments are extruded through small nozzles [20].

The BFRP material starts gaining a noticeable popularity [21-24] in the FRP field of applications. This is because BFRP is characterized by some outstanding features that attract the engineers' attention such as high corrosion resistance [25], high thermal resistance, where Sim et al [26] in his research have shown that BFRP keeps maintaining its shape and its mechanical integrity after 2 hours of 1200 C° heat exposure. However Sim et al [26] on the other hand have also investigated the alkali resistance for several fibers, then he observed that basalt and glass fibers experience a significant reduction in tensile strength after placing them into 1 molar solution of sodium hydroxide for 7, 14, 21, and 28 days, whereas carbon fibers encounters a minor reduction in strength. Additionally, BFRP materials are characterized by their light weight material (one third of the steel fibers

weight) [27], 3 times higher strength than that of steel [28], and greater strain at failure than carbon fibers as shown in Table 1.

A number of guidelines provide guidance on design and construction of structural concrete reinforced with glass, aramid and carbon FRP bars available in USA [9], Japan [10], and Canada [29,30]. These documents, however, do not provide specific provisions for structural concrete reinforced with BFRP bars.

Although the initial cost of FRP reinforcement is more expensive than the conventional reinforcement, there are several factors creating from basalt fibers a suitable product that can be used in building constructions. Firstly, basalt rocks are forming most of the earth crust, this, as a result, gives an additional advantage in terms of cost due to the fact that the BFRP will be available plentifully and there will be no lack of source like other rocks material such as carbon. This fact made from basalt fibers much cheaper product than carbon fibers [28]. Secondly, the production process of basalt fibers contains no additives [29]. Thirdly, because basalt fibers are lighter material than steel, then it can be easily installed, and less number of trucks is required to deliver FRP reinforcement to the site, this will reduce total duration and the number of workers required for installation, as a result the labor cost will be reduced. Finally, the FRP material becomes cost effective when considering the entire life cycle cost for a structure, this is because of the excellent durability of FRP reinforcement in RC structure which will reduce both the maintenance and inspection costs.

1.6.1. Basalt Macro Fibers

The basalt fibers used in this study were an innovative product made by the Norwegian company known as (ReforceTech AS) with trademark brand name of (MiniBar™ ReforceTech). These fibers can be mixed with concrete in a large quantity without impairing the concrete workability. According to [21] no difficulties were faced when dosage of 4% of fibers by volume (corresponds to 72 kg/m^3) were mixed with concrete. The basalt fibers are characterized by their density of 2 gm/cc , which is closer to concrete than synthetic fibers (0.9 gm/cc) or steel (7 gm/cc), this in terms of mixing gives the used BMF an advantage over the rest of the available fibers [21]. The BMF have an average diameter of 0.66 mm and a length of $43 \pm 1 \text{ mm}$ as shown in Figure 13. They have a tensile strength of 1100 MPa and an elastic modulus of 90 GPa . Adhikari [32] stated that higher tensile strength can be possessed by basalt fibers than other synthetic fibers. For more details about the tested basalt fibers the reader can be referred to Table 2.



Figure 13. Basalt discrete fibers.

1.6.2. Basalt Fibers Characteristics

Table 2

Basalt fibers characteristics

Diameter (mm)	0.66
Length (mm)	45
Specific Gravity (g/cm ³)	2.68
Water Absorption	None
Tensile Strength (Mpa)	1100
E modulus (Gpa)	90
Alkaline Resistance	Excellent
Thermal Operating Range (c)	-260 to +700
Electrical Conductivity	None
Resistance to Corrosion	Non Corrosive

1.7. Shear in Beams

The applied loads on Reinforced concrete beams are usually resisted through the internal actions of moments and shears that are developed inside the beam as shown in Figure 14 and 15. Therefore, a beam under loading might encounter two main types of failures resulted from shear or bending stresses such as: the flexural failure and the shear failure. Design codes used for designing RC beams are specifying some limits on the quantity of flexural reinforcement that must be used in a concrete section, in order to ensure the gradual flexural failure of a beam that would inform the occupants to escape the building before its total collapsing. However, this is not the case for the failure under shear, because this failure usually behaves in a brittle and sudden manner with little or without prior warning. Consequently, one of the most important conditions that engineers must satisfy when they are carrying the design procedures for RC beams, is making sure that the shear strength exceeds that of the flexural strength, so that beams under a certain loading would fails under flexure before it fails under shear. Following this method will ensure the ductile behavior of our RC members under failure [33]. This study will only focus on studying the shear behavior of fiber reinforced concrete beams reinforced with FRP bars.

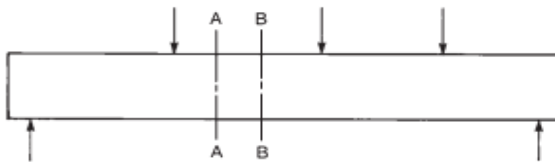


Figure 14. Beam under loading

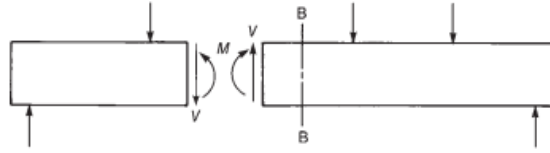


Figure 15. Internal moment and shear at section A-A

Figure 16a shows the developed stresses on two infinitesimal elements 1 & 2. Due to the effect of combined shear and bending stresses shown on the two elements, maximum and minimum normal stresses might be created as a result with the orientation shown which can be determined from the in-plane principal stresses equations or from establishing the Mohr's circle concept. These stresses are known as principal stresses and are acting along the compressive stress trajectories shown in Figure 16c. It can be noticed that the normal tension stresses will be acting perpendicular to the trajectories while the normal compression stresses will be acting parallel to the trajectories. According to the fact that the concrete is strong in compression and weak in tension, then the crack pattern can be expected to move along the compressive stress trajectories in case the maximum tensile strength of concrete is exceeded, which will cause a diagonal cracks resulted from the diagonal tension effect as illustrated in Figure 16d [33].

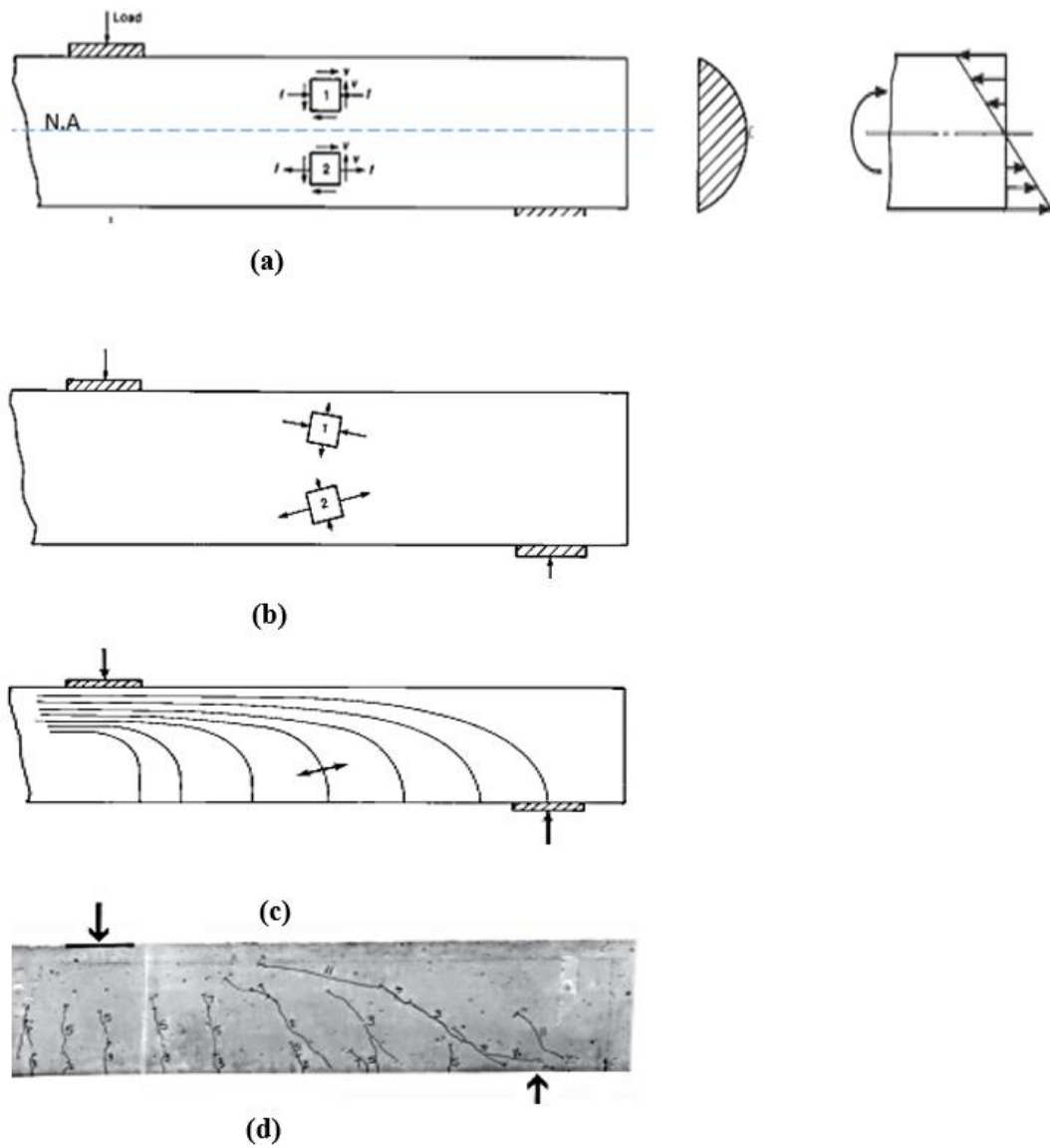


Figure 16.(a) Shear and flexural stresses; (b) Normal Principal stresses; (c) Compressive stress trajectories; (d) Crack pattern.

1.7.1. Types of Shear Cracks

1.7.1.1. Flexure Shear Cracks

Cracking of RC beams due to the shear action takes more than one shape. Occasionally, after the development of flexure cracks which takes the vertical shape, some cracks that are making an angle of 45 degrees with the horizontal axis of beam starts developing on top of the flexural cracks as an extension for them, these cracks are known as flexure-shear cracks. This type of cracks usually appears at the locations with relatively high comparable shear and moment, at which vertical cracks perpendicular to the extreme tension surface starts showing up due to the effect of high moment, then the vertical crack will acquire a progressive increasing in the inclination as it gets closer to the neutral axis where the shear stress is at maximum. The cracks then changes their direction and becomes steeply inclined as shown in Figure 17a due to the high shearing stress effect on the neutral axis of the beam [34].

1.7.1.2. Web Shear Crack

The other type of cracks is known as a web shear cracks, where they are developing diagonally at the mid height of the beam and keeps spreading along the diagonal path as the load increases, a typical web shear crack can be observed in Figure 17b. They are usually formed at high shear and low moment locations such as the locations which are near the simple supports caused by the diagonal tension stress. This will result in a reduction in the shear capacity of a beam section since cracks has reduced the contact area between the opposite sides of concrete located at the crack location and as a result shear

stress will be increasing and concentrating mainly above the crack, the location where the crack still not reached [35].

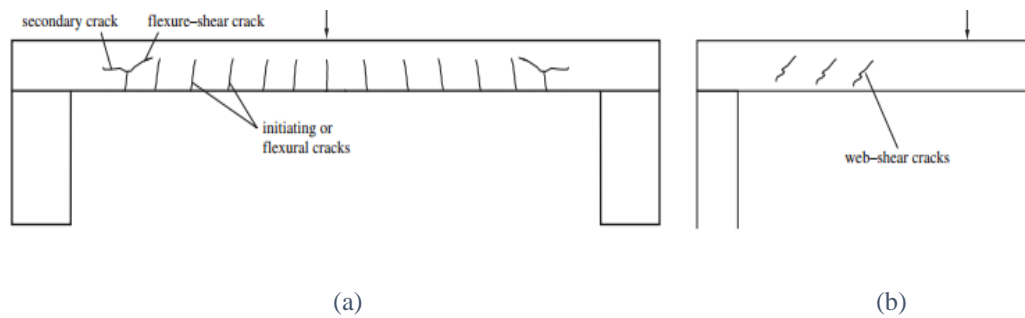


Figure 17. Types of shear cracks; (a) flexure- shear cracks, (b) Web shear cracks

1.7.2. Types of Shear Failures

Concrete begins to crack when the applied loadings create tensile stresses that exceeds the maximum tensile strength of concrete. When the effect of shear force in a concrete beam governs, diagonal tension and compression stresses will be generated simultaneously leading as a result to the formation of inclined cracks [34]. Concrete beams that are failing under shear force, observed according to previous studies to fail in two failure modes of inclined cracks such as:

- 1- Diagonal tension failure: this type of failures usually occurs in beams with span to depth ratio ranging from 2.5 to 6, where the critical crack starts at the mid height of the beam, as the load increases as the crack begins to propagate diagonally in the opposite directions, up toward the upper face of the beam and down until it reaches the flexural reinforcement level [36]. This failure can be depicted in Figure 18.

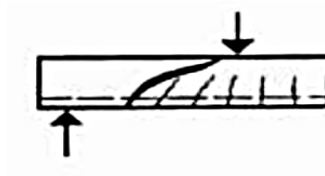


Figure 18. Diagonal tension. failure

- 2- Shear compression failure: this type of failures usually occurs in beams with short span to depth ratio ranging from 1-2.5. Such failures will be caused by crushing of the concrete in the compression zone at the top of the inclined crack as shown in Figure 19 [36].

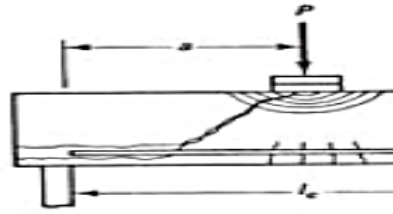


Figure 19. Shear compression failure.

- 3- Shear tension failure: this type of failures is similar to that in the diagonal tension failure, however, once the crack reaches the main reinforcement, it remains increasing along the level of reinforcement up to failure, which will cause loss of bond between the concrete and the reinforcement as illustrated in Figure 20 [36].



Figure 20. Shear tension failure.

1.7.3. The Internal Shear Transfer Actions

Once the inclined crack appears in a beam, the mechanism of shear transfer at the interface starts, where several internal actions that take place inside the diagonally cracked beam section are contributing in resisting the shearing force that is developing along the inclined crack. Around 20% to 40 % of the shear force is resisted by the uncracked compression zone located above the neutral axis. The interlocking mechanism of the aggregates relative to each other and with the surrounding cementitious material that is preventing the two concrete surfaces from slippage due to shear stresses as shown in Figure 21b were estimated to resist shear by 33% to 50% of the total resistance. In addition, once the inclined crack appears and starts to split the concrete, the main flexural reinforcement running crosswise the crack will act as a dowel that is connecting the opposite concrete pieces formed after crack together, preventing them from being split. This counteract to the splitting action is known as the “Dowel Action” and its resistance to shear was estimated to be 15% to 25% [30]. Despite all the internal actions resisting shear force, the resulted inclined crack will decline the shear strength capacity of the beam below its flexural strength capacity, especially when the load increases, the beam will witness wider cracks, and as a consequence, beam would fail in shear, which is from safety point of view undesirable. This problem has been solved by introducing the vertical reinforcement which are known as “stirrups”. Stirrups will decrease the crack width and will also ensure the flexural failure by ensuring that the maximum flexural capacity of a beam can be reached before the ultimate shear capacity [35]. Referring back to the available design codes [9,10,29,30], the methods used to predict the ultimate shearing force for a beam are primarily considering the concept of equilibrium of forces through a diagonal crack, where

the external shear is resisted by the aforementioned internal actions which includes: the concrete compression zone (V_{cy}), the aggregate interlock (V_{ay}), the dowel action (V_d) and the vertical stirrups (V_{sy}). The equilibrium for these forces is acting in the y-direction and denoted as (V), this concept has been clarified in figure (21):

$$V = V_{cy} + V_{ay} + V_d + V_{sy} \quad \text{eq (1)}$$

The first three terms in the above equation are representing the concrete contribution to the external shear force, therefore they were lumped together and expressed as V_c , thus, the equation becomes:

$$V = V_c + V_{sy} \quad \text{eq (2)}$$

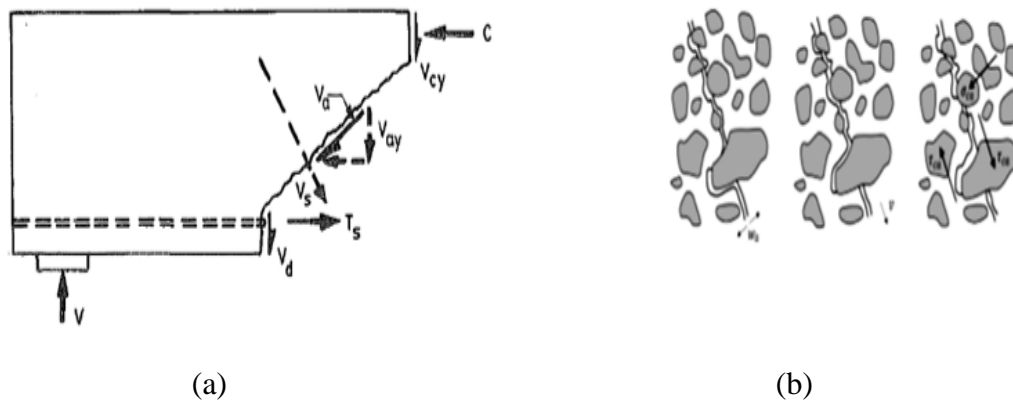


Figure 21. (a)The internal shear actions in cracked section, (b) the interlocking mechanism

1.7.4. Factors Affecting the Shear Strength of RC Beams

In order to study the shear behavior of RC beams reinforced with FRP bars, there are several parameters usually considered by researchers due to their effect on the shear strength of beams such as:

- 1- Span to depth ratio
- 2- Beam dimensions
- 3- Concrete compressive strength
- 4- Ratio of longitudinal reinforcement
- 5- Vertical reinforcement (stirrups)
- 6- Volume of fraction of chopped fibers

1.8. Research Significance

Having in mind the harsh environmental conditions in Qatar especially in view of high temperature and humidity and their effect on the lifespan of the traditional concrete, it is imperative to work on developing a material that would resolve the issue of corrosion. Therefore this study has a significant payoff to the Qatari construction industry and in making Qatar a leader in applying the research results for constructing durable concrete. Conducting such a study will help in providing better understanding and create new knowledge on the shear design of RC structures using unconventional materials in Qatar, the region, and the world. It will also help to promote the use of FRP reinforced concrete in Qatar and establishing a leadership role of the country at the forefront of advanced structural engineering research. Furthermore, this research can open the door for other important research areas in which the same FRP material can be used in other infrastructure facilities. The advanced composites, especially FRP materials are becoming viable alternatives to the traditional construction materials. Nowadays, basalt fibers are even gaining more popularity in the construction field than other FRPs as they are produced with a lower price than Carbon fibers and with a suitable constructional features. The use of basalt fibers intended to provide a less overall life cycle cost of RC structures if taking the maintenance cost into consideration as the basalt material is a sustainable material that does not require much maintenance as the normal steel do.

1.9. Aim of the Study

The design of this study is set to achieve a number of important objectives. The objectives are summarized under three main themes:

1. Study and quantify experimentally the shear capacity of the FRC beams reinforced with BFRP bars. Failure mechanisms, mode of failures, and ductility of the beams are among the scope of the study.
2. Investigate the effect of the main reinforcement ratio, spacing of stirrups, volume fraction of basalt fibers, and span to depth ratio on the shear performance of concrete beams reinforced with BFRP bars.
3. Evaluate the concrete contribution to shear strength of FRC beams reinforced with BFRP reinforcing bars analytically by comparing the experimental findings of this proposed research with the available code-based equations.

1.10. Thesis Organization

This thesis is divided into 6 chapters:

Chapter 1 gives an overview of the topic, in addition to research significance and objectives.

Chapter 2 conducts a detailed literature review describing researches related to the shear behavior of FRP-RC beams to point out the results emerging from previous studies.

Chapter 3 explains in detail the experimental procedure followed throughout the test and the main variables which their effects are to be evaluated.

Chapter 4 covers all the results obtained from the carried tests. It also provides a detailed discussion by studying the test variables effects on the general behavior of the tested beams.

Chapter 5 Evaluates the accuracy of the available design codes equations in predicting the shear strength of the tested beams and proposes a new analytical approach.

Chapter 6 summarizes conclusion of this study and recommendations for future work.

CHAPTER 2: LITERATURE REVIEW

This chapter aims to look deeply at previous studies conducted on the shear behavior of beams reinforced with FRP as flexural and shear reinforcement, then the most prominent achieved results will be summarized and illustrated. The investigation on this chapter will shed the light on four main different variables: 1)- Span to depth ratio; 2)- Flexural reinforcement ratio; 3)- Modulus of elasticity; 4)- Spacing between stirrups; 5)- The macro fibers percentage. Considering the above, the effect of each of the four variables on the cracks pattern, the deflection behavior, and the strain behavior in both concrete and FRP bars will be investigated.

2.1. Cracks Pattern

Several researchers [25,38] have studied the shear behavior of FRP-RC beams without shear reinforcement. In their researches Elrefai et al [25] and Elsayed et al [38] have observed that after the load application, cracks were initiated vertically at the extreme tension zone in the mid span of the beam where the maximum constant moment is located. Increasing the load resulted in more flexural cracks started to show up in the shear span zone with a progressive inclination keeps increasing toward the points load. Shanour et al [39] observed that the inclined cracks begin at 50.1% of the peak load for GFRP beams without shear reinforcement, while it was started at 29.6-43.6 % for GFRP beams with GFRP shear reinforcement. Some beams were observed to experience a horizontal crack (an extension of the diagonal crack) that keeps propagating parallel to the reinforcement level toward the support [25,38,40]. As a result, splitting of the reinforcement from the concrete was reported by Issa et al [40]. This phenomenon was attributed to the sudden

increase in the dowel action that succeed the failure in the aggregate interlock and to the splitting tensile stresses developed around the longitudinal bar [41].

When the shear span increased more number of cracks was realized than that with a smaller span, this is because having a larger moment arm will result in a larger moment value and hence more cracks [25]. In addition, beams with higher reinforcement ratio of basalt FRP bars have also observed the formulation of more cracks prior to failure but with a lesser width [25,40]. The same behavior was reported for beams reinforced with GFRP [37], however, authors realized that as the reinforcement ratio increases as the shear failure becomes more brittle [25].

2.2. Load Deflection Behavior

Researchers have divided the load deflection behavior of FRP beams into two stages: pre-cracking and post cracking [25,40 ,42,43]. In terms of deflection behavior before cracking for BFRP and GFRP beams, previous studies have shown a linear relationship between the load and deflection until the occurrence of the first crack [25,40 ,42,43]. However, this relationship no longer exists after cracks appeared, because with a small increment in the applied load deflection increased more due to the reduction in the stiffness of BFRP beams, which depends mainly on the reinforcement ratio. It was noticed that beams with higher reinforcement ratio experienced less reduction in the stiffness of beams and as a result less deflection [25, 40, 42, 43]. In comparison to RC beams reinforced with steel reinforcement, GFRP beams witnessed a lot of curvature before failure due to the relatively low elastic modulus and as a consequence, this have resulted in an increased deflection and crack openings [25,44].

2.3. Load Strain Behavior

The strain values for both the reinforcement and concrete were mainly dependent on the reinforcement ratio and the (a/d) ratio. Elrefai et al [25] observed that at the same load level, beams with higher BFRP reinforcement ratio ρ experienced less strain in both concrete and reinforcement than that with less ρ , also using higher (a/d) ratio resulted in higher strains, this is due to the increased number of cracks caused by the increased shear span. However, there was a marginal effect on the ultimate strain at failure when fixing the ρ and changing the (a/d) ratio [40].

2.4. Effect of Reinforcement Ratio (ρ) and (E) on the Shear Strength of Concrete

It has been established that shear capacity of concrete is strongly dependent on the dowel action of the main reinforcement where the transverse rigidity of the main reinforcement significantly contributes to the dowel action [37]. Knowing that FRP bars are anisotropic materials with weaker strength in the transverse direction compared with the longitudinal direction and having a relatively low modulus of elasticity compared with steel reinforcement, it is important to investigate the concrete contribution to shear strength for beams reinforced with FRP bars. The dowel action of the longitudinal reinforcements is highly affected by the size of the bar and the amount of the reinforcement area. Issa et al [40], Yost et al [41], Kalpana et al [42], Mahmoud et al [43], and Sergery et al [44] noticed a significant reduction in the contribution of the bars to the dowel action when less bar diameter was used, Issa et al [40] concluded that the increase of the main reinforcement area of beams reinforced with BFRP bars has increased the shear capacity of the tested beams. As well, Tomlinson and Fam [50] stated that increasing the reinforcement ratio of

the longitudinal reinforcement in beams reinforced with BFRP bars from 0.0039 to 0.0084 increased the shear strength by 54 percent. Elrefai et al [25] attributed this enhancement in the shear strength of beams with high reinforcement ratio due to the increased compression zone required to balance the high ratio of reinforcement, the reduced crack width that will maintain the effectiveness of the aggregate interlocking mechanism, and the boosted dowel capacity. However, Ahmed et al [51] have indicated that the FRP bars contribution to the dowel action is way less than that for steel. The lowest contribution was demonstrated by GFRP, whereas Carbon FRP (CFRP) shows a slightly better performance [51]. This can be justified by considering the effect of axial rigidity (ρE) which causes a high improvement in the shear strength as it increases [25, 37, 52, 53]. Since CFRP have a higher modulus of elasticity (E) than other FRPs it is expected to have a better performance in terms of shear strength.

2.5. The effect of span to depth (a/d) ratio on the shear strength

It was revealed that for BFRP-RC beams that the shear strength was decreased as (a/d) increases [25,40]. Similar outcomes were reported for CFRP beams [37]. The shear failure of FRP beams without shear reinforcement is governed by the aggregate interlock, therefore the decrease in the shear strength can be related to the increase in the cracks width caused by increasing (a/d) ratio which consequently reduces the shear transfer mechanism through cracks [45,54].

2.6. The Effect of Compressive Strength on the shear strength

Shanour et al [39] have tested GFRP beams using three different compressive strength values: 20 MPa, 45 MPa, and 70 MPa. His results revealed an increase in the shear capacity by 49% for beams with similar reinforcement ratio when 45 MPa concrete was used instead of 20 MPa concrete. Moreover, increasing the concrete compressive strength to 70 MPa demonstrated a 104% increase in the shear capacity over that with 20 MPa concrete strength.

2.7. The use of FRP as a Shear Reinforcement

Unlike steel, FRP has to be pre-bent by the manufacturer before coming to the site, which is considered as one of the main disadvantages for using FRP as a shear reinforcement. In addition, the FRP bar will encounter a significant reduction in strength after being bent into the shape of stirrups, thus this will create a weakNess at the bent locations [47]. This weakNess in FRP resulted from the kinked shape of fibers at the bent region [51]. Grace et al [52] indicated that GFRP bars have a higher sensitivity toward bending into stirrups than that of CFRP bars. Therefore, in case of using FRP bars as a shear reinforcement, Bentz et al [48] recommended the use of double layer reinforcement as it appears to protect the stirrups from being ruptured at the weak bend regions. The bend region requires special treatment during its design, because Ehsani et al [49] recognized that the ratio of internal radius of the stirrups at the bended locations to the bar diameter (r_b / d_b) has a clear effect on the tensile forces developed at these regions, his results revealed that the GFRP stirrups tends to fail at very low load levels when zero (r_b / d_b) ratio

was used. Subsequently, [49] recommended to avoid such detail and (r_b / d_b) of not less than 3 should be used instead.

The use of BFRP stirrups in BFRP-RC beams shows an evident increase in the shear strength compared to those beams without shear reinforcement, however, this increase was less apparent as the reinforcement ratio was increased [40]. Likewise when Shanour et al [39] introduced GFRP stirrups for 300 mm height beams spaced at 215 mm and 100 mm, the corresponding increase in shear capacity was 41 % and 82 %, respectively. This increase in shear capacity according to Massam et al [55] is referred to the load that has been distributed among the present stirrups and due to the confinement they provide for the concrete section which in turn enhance the contribution of the aggregate interlock in resisting shear force developed along the shear failure plane.

2.8. The use of Macro Fibers in Concrete Mix and its Effect on the Shear Behavior

Using fibers in concrete mix has a clear advantage on the cracking mechanism of concrete, Patnaik et al [56] stated that when the fibers were introduced smaller cracks were appeared with lesser width. This can be attributed to the fibers which are acting as a proactive reinforcement that provides the immediate tensile load carrying capacity when micro cracks develop in concrete which will slow down the process of cracking propagation and as a result the ultimate tensile cracking strain of concrete is increased [57]. The reduction in cracks number and width can result into several quantifiable benefits where the concrete will be less permeable and all from the impact resistance, fatigue strength, and surface abrasion resistance will be increased [57]. Moreover, the lesser width of cracks will provide a concrete with higher durability because of the increased aggregate

interlock [49,55], and an enhanced bonding in the interface between the aggregates and the cementitious composites due to the fiber presence which is bridging the cracks and keeps carrying stresses up to their fracture point [59].

The increase in the fiber content avoids the brittle failure of concrete because it allows the formulation of multiple cracks distributed along the shear span [59-62] and not localized at one location, which consequently will delay the development of major crack that can cause brittle collapsing [12,61,63,64]. However, incorporating fibers in concrete needs special attention as it might result in a poor workability and an improper consolidation of the concrete mix which leads to the existence of voids like honeycombs [15].

Previous investigations have shown that using discrete steel fibers in concrete increases its ductility due to the large compressive strains exhibited at failure [65-67].

To enhance the shear capacity of RC beams, fibers can be used, and they can partially substitute the stirrups [68, 69], previous research studies demonstrated that the shear strength of RC members is significantly improved by adding adequate quantity of steel or synthetic fibers [70–72]. ACI 318-08 recommends the use of a minimum volume fraction of 0.75 % of steel fiber to partially replace the internal steel stirrups in RC beams [73].

Some researchers aimed to find the optimum amount of fibers that should be incorporated in a concrete mix to replace the shear reinforcement. The approach to this issue has been proposed by Sahoo et al [72], where they have studied the effect of using different volume fractions of polypropylene and steel fibers in the concrete mix in order to

investigate their contribution to shear strength in the absence of lateral reinforcement (stirrups). The obtained results indicate that replacing polypropylene fibers by stirrups reduces the shear resistance by 30% compared to that of normal RC beams. However, similar peak shear resistance to that of normal RC beams was achieved using the steel fibers in the FRC beams. Combining both fibers in similar proportions of 0.5% polypropylene and 0.5% steel fibers in FRC beams lead to similar shear strength of RC beams, and it can be even better by 22.5% if 1% of each fiber is added to the FRC beams with better stress redistribution, and post yield ductile behavior due to the fiber bridging effect.

El-deib et al [74] have demonstrated that the shear capacity of concrete beams without stirrups can be increased by the addition of steel fibers to the extent where it exceeds the shear capacity of the normal reinforced concrete beams with internal stirrups. Further, using steel fibers in concrete beams tends to restrict the cracks propagation and widening.

Ding et al [75] have also found that increasing the steel fiber content increases the shear strength, and by the addition of a sufficient steel fiber amount the failure behavior changes from brittle shear collapse into ductile flexure behavior. It was observed that the stirrups can be partially substituted by steel fibers. However, combining both steel fibers and stirrups improves the mechanical behavior.

Amin and Foster [76] show that beams with higher steel fiber ratio exhibited more cracks but with finer openings due to the crack arresting mechanism. Moreover, they have

similarly found as the previous researchers found that adding adequate fiber content could partially replace the shear reinforcement.

It was noticed by Mansur et al [77] that the shear resistance of FRC beams was enhanced more than the corresponding strength of bending when the fiber content was increased. This had affected the mode of failure for beams where it was changed from shear failure into flexural failure.

However, among the disadvantages of using steel fibers is corrosion, especially in the harsh environment that characterizes the Arabian Gulf area. Therefore, basalt fibers is proposed in this study. Basalt fibers are characterized by their flexible structure and therefore they can be easily dispersed in the concrete mix without causing segregation [78-80]. However, increasing the fiber dosage will decrease the measured slump [81].

Bajaj [82] reported that the crack width that develops in plain concrete is larger than the crack width in polypropylene fiber concrete, which is larger than the crack width obtained in reinforced concrete having basalt fibers in the mix.

In terms of shear, Krassowska et al [27] stated that the experimental results showed an increase of 36 % in the shear strength value over the theoretical shear value (with no fibers) when the basalt fibers were added to the RC beam.

2.9.1. Fibers Advantages over Stirrups

Several reasons have been stated by Li et al [83] which makes from fibers a preferable product than stirrups to be used in RC structures to resist the shearing forces.

- 1- Fibers in a concrete mix usually have a random distribution in all directions with a small spacing separate them, thus an approximate even resistance to stresses in all directions will be created. In particular, such reinforcement would be of great advantages in terms of resisting shear forces for buildings that exposed to wind and earthquake loadings.
- 2- In addition, fibers can reduce the cracks sizes and deflection, thereby the ultimate limit state design might be carried without being restricted by serviceability considerations. The reduction in the cracks sizes will also result in preventing the internal reinforcement from being exposed to the aggressive environments, and hence the reinforcement will be protected from corrosion.
- 3- Additionally, fibers can partially substitute the stirrups, therefore using fibers will reduce the labor cost and time to install the stirrups which requires many laborers to bend them and fix them in their suitable locations, especially in the period where the market is witnessing an increase in the labor cost, or a shortage in the laborers.
- 4- Fiber reinforced concrete can be easily placed in irregular structural shapes such as: architectural panels, while it would be difficult to place the stirrups in such shapes.

CHAPTER 3: EXPERIMENTAL PROGRAM

In this chapter, the details of the materials used, the mix design, the preparation of cages and formwork will be presented. Also, this chapter will comprise the laboratory tasks that were conducted to investigate and study the mechanical characteristics of the basalt fiber reinforced concrete according to the ASTM standards for both the fresh and hardened concrete to help in understanding the behavior of large scale beams which will be tested in a later stage. The experimental program will be carried out at two levels:

- (a) Material characterization tests: where the mechanical properties of FRC cylinders and prisms with three different volume fractions of basalt fibers were obtained through lab testing.
- (b) Large scale beams test: where four-point loaded tests were conducted on BFRC beams reinforced with BFRP bars and GFRP stirrups.

3.1. The Concrete Ingredients Used in the Concrete Mix

3.1.1. Cement

Cement is one of the basic material in a concrete mix which is acting as a glue (when water is added) that binds the aggregates to each other to make Portland cement concrete. In this research work, the cement used was an ordinary Portland cement (OPC) produced by Al- Wataniya Concrete company. This type of cement has been chosen because it is the most available type of cement used in the industry field of the state of Qatar.

3.1.2. Water

A potable water was used in the mix. The presence of water is a prominent requirement in any concrete mix, because in order for the hydration process to take place (which will solidify the concrete), water is required to react with cement.

3.1.3. Sand

Washed sand was used as fine aggregates in all concrete mixes that were prepared in the laboratory, and in order to meet the fine aggregates specifications of ASTM, the sand was tested in accordance with ASTM C33.

3.1.4. Coarse Aggregate

The aggregate used in this research was gabbro aggregate. Gabbro aggregate is a natural coarse aggregate, which characterized by its dark color, and categorized as an intrusive igneous rock. Gabbro aggregates are not available in Qatar but imported from Oman to supersede the local limestone aggregates. To meet the coarse aggregate specifications of ASTM, the gabbro aggregate was tested in accordance with ASTM C33.

3.1.5. Basalt Macro Fibers

The discontinuous, discrete basalt fibers (MinibarsTM) were purchased from the Norwegian company known as (ReforceTech AS). Basalt macro fibers properties and geometry were described in the previous chapter.

3.2. Concrete Mixture Proportions

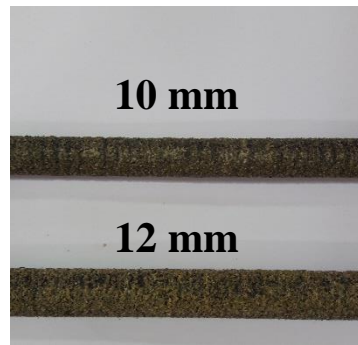
Table 3

Ingredients proportions

	Concrete Mix with % Volume Fraction of BMF		
	0%	0.75%	1.5%
Target Strength (MPa)	35	35	35
Cement (Kg/m ³)	440	440	440
Water (Kg/m ³)	60	60	60
Sand (Kg/m ³)	752	752	752
20 mm gabbro coarse aggregate (Kg/m ³)	1158	1158	1158
BMF (Kg/m ³)	0	14.25	28.5

3.3. Flexural and Shear Reinforcement Used in this Study

For the beam tests, sand coated BFRP bars were used as a longitudinal reinforcement with two nominal diameters of 10 mm, and 12 mm as shown in Figure 23a. A (GFRP) stirrups with a nominal diameter of 9.5 mm were selected to be as a transverse reinforcement. Stirrup geometry is shown in Figure 23b. The ACI requirements regarding the minimum radius of bend (r_b) was considered while designing the stirrups, which specify a minimum r_b to bar diameter (d_b) ratio (r_b/ d_b) of 3.



(a)



(b)

Figure 22. a) BFRP bars; b) GFRP stirrup

3.4. Material Characterization Tests

In the mix design, two volume fractions of basalt fibers were used (0.75%, and 1.5%) which correspond to 14.25 Kg/m^3 and 28.5 Kg/m^3 , respectively. Plain concrete cylinders and prisms with no basalt fibers will be tested to serve as control. The tensile strength and modulus of elasticity of the basalt reinforcing bars will be attained through lab testing. The relevant ASTM material test standards will be followed. Tests on the beam specimens will then be accomplished as described in the following section. In this subsection, fresh and hardened concrete will be studied. To study the properties of the fresh concrete, the laboratory tasks involve one test:

- 1- Slump of Hydraulic Cement Concrete (ASTM C143).

To study the properties of the hardened concrete, the laboratory tasks involve three tests:

- 1- Compressive Strength of Cylindrical Concrete Specimens (ASTM C 39).
- 2- Four- Point Bending Test (ASTM C1609).
- 3- Direct Tensile Test (not a standard test).

3.4.1. The Fresh Concrete Test

3.4.1.1. Slump Test

To check for concrete consistency, and how it can be placed and compacted (workability), the slump test has been conducted in accordance with ASTM (C143), and the slumps values for each mix were recorded.

3.4.2. The Hardened Concrete Tests

3.4.2.1. Compressive Strength Test

The compressive strength test has been conducted in accordance with ASTM (C39). Three cylinders from each mix with a dimension of 100×200 mm were molded for 24 hours, then they were removed and moist-cured for 28 days, then they were tested. The average value of the three tested cylinders was taken as the representative value for the corresponding mix. The test setup can be shown in Figure 24.

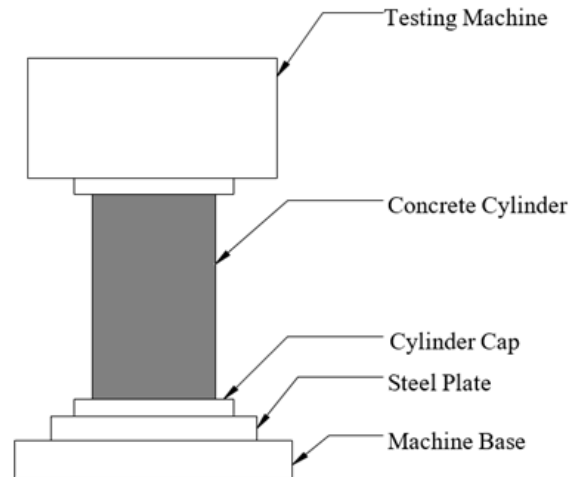


Figure 23. Compressive test setup

3.4.2.2. Flexural Strength Test

The flexural strength test has been undertaken in accordance with ASTM (C1609). Three prisms from each mix with a square cross section of 100×100 mm and a span of 500 mm were molded for 24 hours, then they were removed and moist-cured for 28 days, then they were tested. The concrete prisms were turned on their side and centered on a four-point loading apparatus and load was applied until rupture. The average value of the three tested cylinders was taken as the representative value for the corresponding mix. The test setup can be shown in Figure 25.



Figure 24. Flexural test setup.

3.4.2.3. The Direct Tensile Test

Due to lack of a standard test that can be used to determine the direct tensile strength for concrete, a uniaxial tensile test was carried based on some available methods founded in the literature [84]. Specimens with the dimensions shown in Figure 26 were used in the test. Before casting, the upper and lower squares of the specimen were both reinforced with $\phi 8$ steel bar as shown in Figure 26. This was done to prevent the failure at these two zones and to ensure a failure in the middle region between the two necks. After 28 days of curing, the specimens were ready for testing. The samples then were fixed to the universal testing machine by inserting two steel bars inside the upper and lower tubes then they were connected to the grips that hold the specimen as shown in Figure 27. To obtain the strain readings, strain gauge of type (PL-60-11-3L) was installed between the two necks. In addition, an LVDT was fixed as can be depicted in Figure 27 to track the behavior after

cracking as any crack might damage the strain gauge. For safety purpose, all the tested samples were covered with a several layers of cellophane.

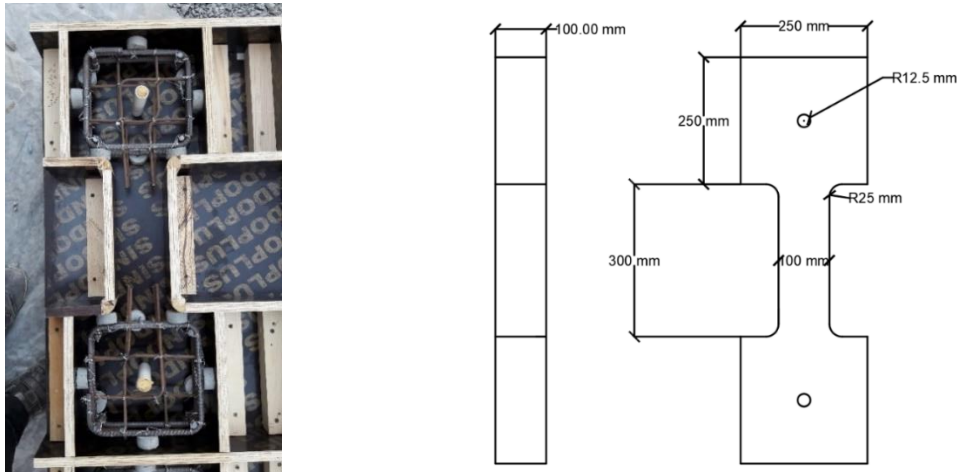


Figure 25. Formwork and dimensions for direct tensile test specimen

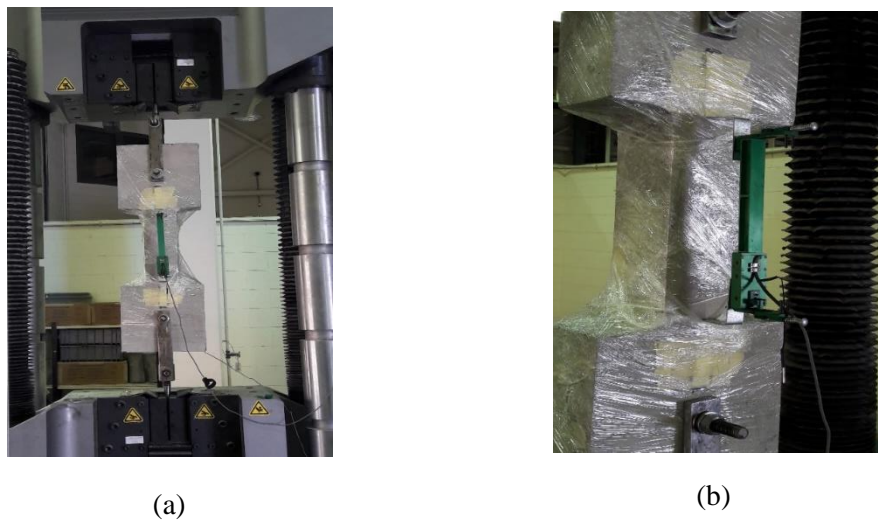


Figure 26. a) Direct tensile test setup; b) 200 mm LVDT

3.5. Beam Tests

This part of the testing program is investigating the shear performance of BFRC beams reinforced with BFRP bars and transverse glass FRP stirrups. A total of 14 beams loaded at four-points with a loading span of 1,600 mm were tested. The beams are designed to have the flexural capacity higher than the shear capacity. All beams dimensions were selected to have a cross section of 165 mm in width \times 260 mm in height, and a length of 2000 mm.




3.5.1. Test Setup and Instrumentation

The test specimens were constructed as shown in Table 4 where the formwork manufacturing, reinforcement cages assembling, concrete mix preparation, casting and curing were done at (AKC Contracting Company). All specimens have been loaded until failure using an existing universal testing machine (UTM) in the Structures lab, at Qatar University. The actuator has a maximum load capacity of 1500 KN and a maximum stroke of 150 mm. The loading was displacement control. The deflections at the mid-span of the RC beams were recorded using LVDT, and the strain for both the reinforcement and the concrete were recorded using the strain gauges made by the Japanese company (Tokyo Sokki Kenkyujo Co. Ltd. (TML)). BFLA-5-8-5L (for composite reinforcement) strain gauges of 5-mm were placed at the bottom BFRP bars at mid-span and at the mid height of the GFRP stirrups, FLA-5-11-5L strain gauges were used for steel stirrups, and concrete strains were measured using 60-mm length specialized strain gages (PL-60-11-3L) at mid-span of the top surface of the beam. The three strain gauges types are shown in Figure 28. Two crack transducers made by the latter company were placed diagonally at the mid

height of each beam's shear span between the point load and the support. The electrical LVDT, strain, and transducers were connected through a master panel to a data acquisition system (TML Data Logger Multi-Channel Digital Strain meter DRA-30A), as seen in Figure 29. The analog electrical signals of deflections, strains, and crack widths were converted through the data acquisition system to digital signals and then were displayed and recorded for each load increment.

Table 4

Steps of beam specimen's preparation

		
Longitudinal reinforcement placement	Placement of stirrups	Cage assembly
		
Beams formwork	Beams ready to be casted	Concrete casting
		
Concrete after casting	Concrete curing	Beam testing

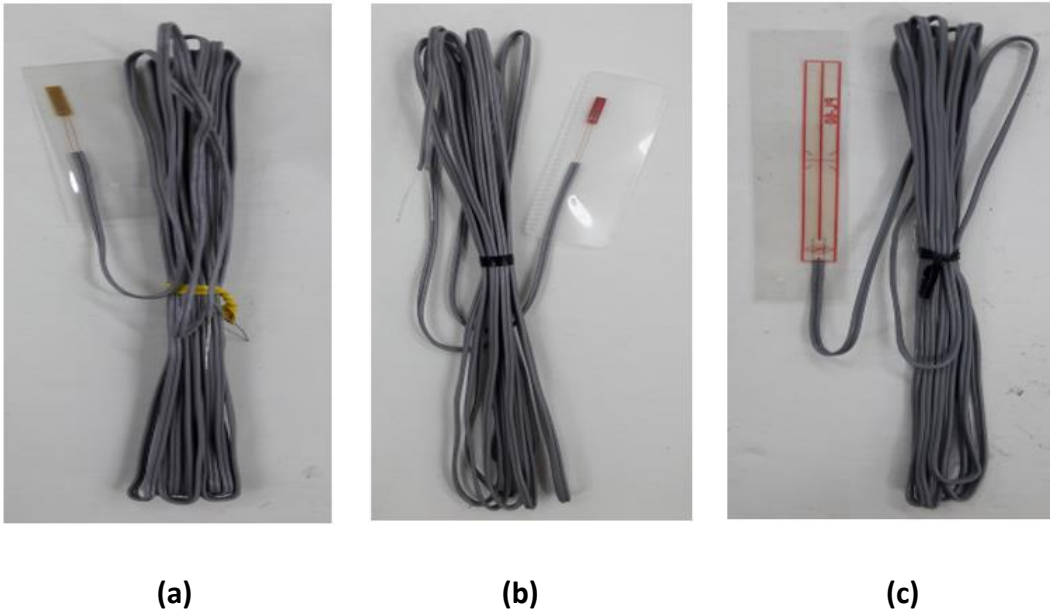


Figure 27. Strain gauges used: (a) FRP- strain gauge, (b) Steel- strain gauge, (c) Concrete- strain gauge

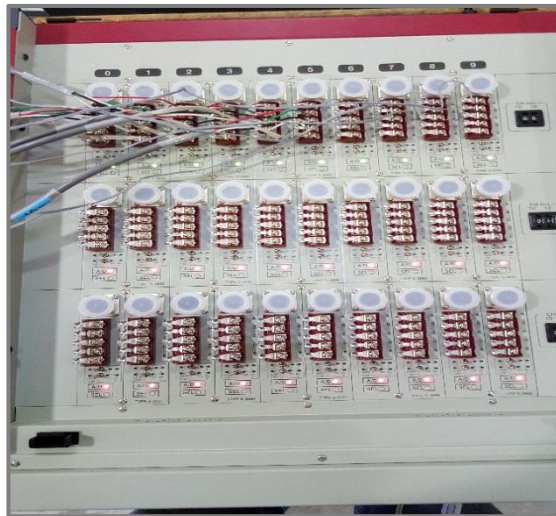


Figure 28. The data acquisition system

3.5.2. *The Test Variables*

It is intended here to reach for experimentally-driven conclusive remarks the effect of following parameters, as shown in Table 1: i.) Beam main reinforcement ratio: beam specimens will be reinforced with BFRP bars at three different ratios (i. e. $\rho_1 = 2.054 \rho_b$, $\rho_2 = 3.11 \rho_b$, $\rho_3 = 4.53 \rho_b$). As noted, for beams reinforced with BFRP bars, over-reinforced specimens were investigated to ensure failure by concrete crushing at the compression zone rather than fracture in the flexural bars at ultimate.; ii.) Span-to-depth ratio of the beams (a/d): two different values were investigated in this study (i. e. $a/d = 2.5$, $a/d = 3.3$); iii.) Volume fraction of the basalt macro fibers: three different volume fractions of basalt fibers were used in this study (i. e. 0%, 0.75%, and 1.5 %). The basalt macro fibers were placed in the concrete mix during casting at the assigned volume fractions.; iii.) Stirrups spacing: stirrups were placed at two different spacings (spacing 1 = 250 mm, Spacing 2 = 170 mm) as indicated in Figure 30. The testing specimens comprised 14 beams. Two beams reinforced with transverse steel stirrups and one beam having no basalt fibers will serve as control specimens. The main variables of the tested specimens are summarized in Table 5.

Table 5

Testing parameters

Parameters	Span to Depth ratio (a/d)	Volume Fraction of Chopped Basalt Fiber, V_f	Spacings of stirrups, mm	Reinforcement Ratio
14 specimens	a/d = 2.5	0.75%, and 1.5%	170 mm, and 250 mm	$\rho_s = 2.054 \rho_b$, $\rho_s = 3.11 \rho_b$, and $\rho_s = 4.53 \rho_b$
	a/d = 3.3	0%, 0.75%, and 1.5 %	170 mm, and 250 mm	$\rho_s = 2.054 \rho_b$, $\rho_s = 3.11 \rho_b$, and $\rho_s = 4.53 \rho_b$



(a)



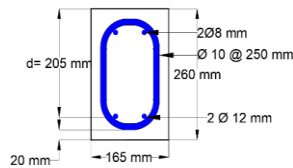
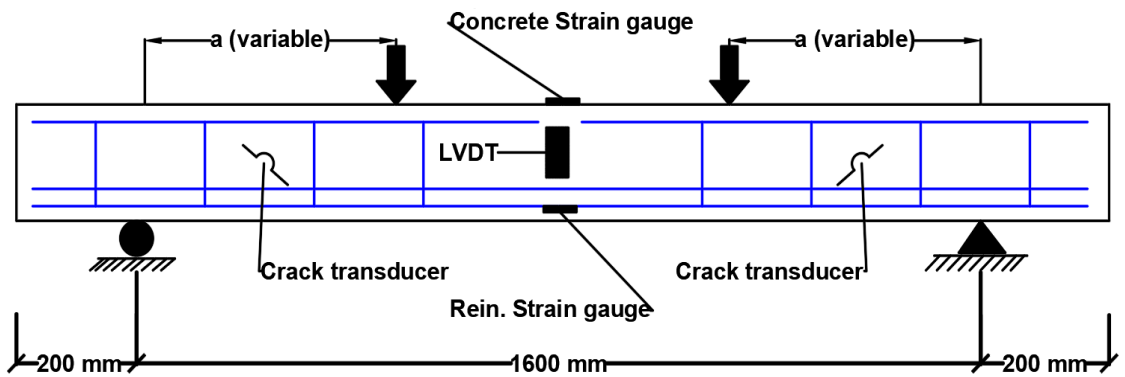
(b)

Figure 29. Stirrups spacings: 170 mm; and 250 mm

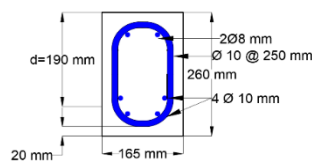
3.5.3. *Beams Designations*

The designation of beams specimens consists of four parts, the numbers 2.5 and 3.3 indicates the span to depth ratio, the following lower case **pf** denotes the reinforcement ratio, where **pf1**, **pf2**, and **pf3** correspond to $2\phi 12$, $4\phi 10$, and $4\phi 12$, respectively. The

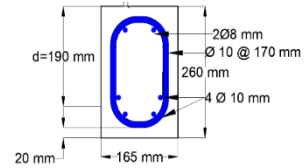
following numbers indicates the percentage of the fibers used in the mix and the spacings between stirrups with the stirrups type where the letter G corresponds to glass and the letter S corresponds to steel. For instance the beam 2.5-pf1-0.75%-G250 refers to the beam with span to depth ratio of 2.5, with reinforcement ratio of $2 \phi 12$, with 0.75% volume fractions of BMF, and 250 mm spacing of glass stirrups. The detailed sketch and the testing matrix of the tested beams are shown in Figure 31 and Table 6, respectively.



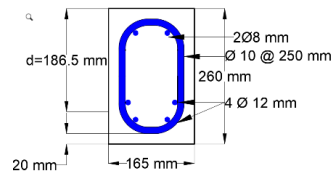
(a)



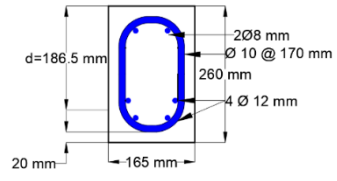
(b)



(c)



(d)



(e)

Figure 30. Beams and their sections details

Table 6

Tentative testing matrix of tested beams

Sample #	Description	Target Strength MPa	$\rho\%$ Long. Reinforcement	BFRP Bars Long. Reinfor.	Basalt Fiber Dosage % by Volume	Type of Stirrups	Stirrups Spacing
A1	2.5-pf1-0.75%-G250	35	$\rho_{f1} \%$	2 ϕ 12 BFRP Bars	0.75	GFRP	S1=250
A2	2.5-pf1-1.5%-G250	35	$\rho_{f1} \%$	2 ϕ 12 BFRP Bars	1.5	GFRP	S1=250
A3	2.5-pf2-0.75%-G250	35	$\rho_{f2} \%$	4 ϕ 10 BFRP Bars	0.75	GFRP	S1=250
A4	2.5-pf2-0.75%-G170	35	$\rho_{f2} \%$	4 ϕ 10 BFRP Bars	0.75	GFRP	S2=170
A5	3.3-pf2-1.5%-G250	35	$\rho_{f2} \%$	4 ϕ 10 BFRP Bars	1.5	GFRP	S1=250
A6	3.3-pf2-0%-G170	35	$\rho_{f2} \%$	4 ϕ 10 BFRP Bars	0	GFRP	S2=170
A7	3.3-pf2-0.75% - G170	35	$\rho_{f2} \%$	4 ϕ 10 BFRP Bars	0.75	GFRP	S2=170
A8	3.3-p2-1.5% -G170	35	$\rho_{f2} \%$	4 ϕ 10 BFRP Bars	1.5	GFRP	S2=170
A9	3.3-p3-0.75%-G170	35	$\rho_{f3} \%$	4 ϕ 12 BFRP Bars	0.75	GFRP	S2= 170
A10	2.5-p3-1.5% -G170	35	$\rho_{f3} \%$	4 ϕ 12 BFRP Bars	1.5	GFRP	S2= 170
A11	2.5-p3-0.75%-G250	35	Pf3 %	4 ϕ 12 BFRP Bars	0.75	GFRP	S1= 250
A12	2.5-p3-0.75%-G170	35	Pf3%	4 ϕ 12 BFRP Bars	0.75	GFRP	S2= 170
A13	2.5-p3-0.75%-S170	35	Pf3 %	4 ϕ 12 BFRP Bars	0.75	Steel	S2= 170
A14	2.5-p3-1.5%-S170	35	Pf3 %	4 ϕ 12 BFRP Bars	1.5	Steel	S2= 170

CHAPTER 4: RESULTS AND DISCUSSION

Throughout this chapter, the mechanical properties of hardened concrete will be investigated through the application of material characterization tests on small cylinders and prisms mentioned in the previous chapter. Then, the tested large scale BFRP beams will be analyzed and the effect of four main variables will be discussed: 1) Percentage of fibers; 2) Main reinforcement ratio; 3) span to depth ratio; 4) stirrups spacing. The discussion on counterpart beams is done in terms of maximum load, maximum deflection, the concrete and FRP bar strains at midspan, cracks width and distribution, and the mode of failure.

4.1. The Mechanical Properties of Fresh Concrete

4.1.1. Slump Test Results

It has been noticed during the casting time that both mixes (with and without fibers) were easy in handling and placing in their formwork. Interestingly, the addition of 1.5% volume fraction of fibers (which is equivalent to 28.5 Kg/m^3) noticed not to impede the concrete's workability. This can be referred to the uniform distribution of fibers among the concrete mix that is clearly shown in Figure 32, which resulted in well-spaced fibers that eliminated the probability for the balling phenomenon (fibers localized at one location in the mix causing a concrete ball) to exist. This fact has been proved by running the slump test which resulted in a 180 mm slump for the plain concrete mix, and a 150 mm slump for the mix with 1.5% volume fractions of fibers. The slump for mixes without fibers and with fibers can be shown in Figure 33.



Figure 31. Fibers distribution.



(a)



(b)

Figure 32. a) Slump for plain concrete; b) Slump for concrete with 1.5% basalt volume fraction.

4.2. The Mechanical Properties of Hardened Concrete

4.2.1. Compressive Test Results

The measured average compressive strength of the three concrete mixes are listed in Table 7. The test results revealed that the addition of fibers did not show a clear enhancement on the compressive strength in comparison to the plain concrete specimens. However, the fibers addition has significantly altered the mode of failure from an explosive, and brittle type of failure into a ductile failure. The BFRC specimens keep sustaining load even after the occurrence of significant cracking and remain coherent and intact after failure. Typical failure of normal concrete cylinders without fibers and with fibers can be depicted from Figures (34a, and 34b), respectively. This behavior can indicate the advantages of fibers in inhibiting the brittle nature of concrete and maintaining the integrity of a structural element even after failure.



(a)



(b)

Figure 33. Failure modes of a) Plain concrete; b) 0.75% and 1.5% concrete cylinders under compressive test.

Table 7

Compressive test results

Fibers % by volume	Actual Compressive Strength (MPa)	Average Compressive Strength (MPa)
0	40.44	
0	37.36	37.89
0	35.89	
0.75	35.91	
0.75	34.36	35.15
0.75	35.19	
1.5	34.84	
1.5	35.58	35.07
1.5	34.8	

4.2.2. Flexural Test Results

The measured average flexural strength of the three concrete mixes are listed in Table 8. An obvious better performance was noticed for the BFRC specimens over the control specimen. In comparison to compression test results, the effect of fibers was more noticeable in the flexural test results. It can be clearly seen from the test results that the flexural strength was increased by 6% and 25% when volume fractions of 0.75% and 1.5% of the basalt chopped fibers were added, respectively. It is known that when the plain concrete cracks, the tensile capacity of concrete falls to zero, therefore, this increase in the flexural strength can be attributed to the post cracking behavior of fibers that are bridging the cracks and keep carrying the load beyond the fracture point as can be shown in figure

(35b). Specimens without fibers were observed to fail suddenly into two pieces as in figure (35a), whereas although specimens with fibers were failed, they remained as one piece due to the presence of fibers that are shown in figure (35c, and 35d).



(a)



(b)



(c)



(d)

Figure 34. Failure types of prisms under flexural strength test

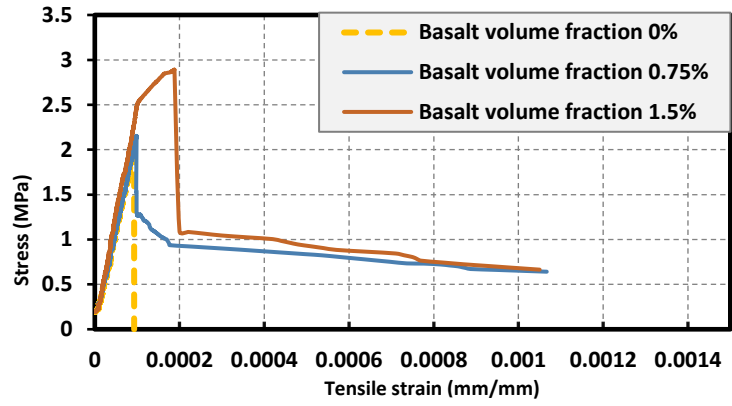
Table 8

Flexural test results

Fibers % by volume	Actual Flexural strength(MPa)	Avg Flexural strength (MPa)
0	5.84	
0	5.99	5.9
0	5.86	
0.75	6.02	
0.75	6.36	6.14
0.75	6.03	
1.5	7.95	
1.5	7.25	7.42
1.5	7.06	

4.2.3. Direct Tensile Test Results

The measured average direct tensile strength of the three concrete mixes are listed in Table 9. This test showed a more pronounced effect of fibers on the tensile strength. The test results for 0.75% and 1.5% specimens highlighted an increase of 14%, and 35%, respectively compared to its counterpart specimens made with plain concrete. Referring to Figure 36, the specimens with 0% of fibers have encountered steep drop in the loading until reaching zero, while the FRC specimens noticed to provide some residual tensile stresses after failure until fibers ruptured or pulled out, and hence, this indicates that higher tensile strain of FRC at failure can be achieved than the normal concrete specimens. This finding can clearly validate the usefulness of the basalt fibers as a reinforcing component for concrete that significantly increases its tensile strength and enhances its ductility.



(a)



(b)



(c)

Figure 35. (a) Stress strain diagram; (b) Failure occurs at the mid height; (c) Failure occurs near the upper neck

Table 9

Direct tensile test results

Fibers % by volume	Actual Tensile strength (MPa)	Average Tensile strength (MPa)
0	1.99	
0	1.79	1.89
0.75	2.15	
0.75	2.15	2.15
1.5	2.7	
1.5	2.4	2.55

4.3. *Large – Scale BFRP-RC Beams*

In this section the behavior of each beam loaded under two symmetrical concentrated loads that are displacement controlled will be described until failure. The description will comprise four different stages:

- 1- The behavior before cracking
- 2- The behavior after first flexural crack
- 3- The behavior after first diagonal crack
- 4- The failure mode

4.3.1. *Beam A1(2.5- ρ_f 1-0.75%-G250)*

Stage 1: Beam A1 has been made with 2 \emptyset 12 BFRP bars as main reinforcement, and \emptyset 10 GFRP stirrups spaced at 250 mm with 0.75% of fibers, and $a/d=2.5$. Initially, no flexural cracks were observed at this stage when the applied load was in the range below (28 kN). Within this range, the load vs midspan deflection graph demonstrated a linear relationship. This behavior remains the same until the load reaches (29 kN).

Stage 2: Once the applied load exceeds (28 kN) to (29 kN), the first flexural crack appeared at the extreme concrete fiber within the constant moment zone. As the load was increasing more adjacent cracks were existed. The cracks then started to get wider and propagate toward the neutral axis of the beam. The beam at this stage begins to experience a midspan deflection that is increasing in a faster rate than the previous stage due to the reduction in the moment of inertia after cracking.

Stage 3: At a load of (34 kN), the cracks were shifted into the shear span, and a flexural crack started to develop at the extreme bottom fibers of the beam extending upward, then an inclined cracks started to develop on top of at (59 kN). When more load was applied the crack was diagonally extending up toward the point load, and more adjacent flexure shear cracks started to appear at a distance equal to the beam depth from the support approximately.

Stage 4: When the load was further increased to (99 kN) the diagonal crack widened more and the lower portion of the crack extended diagonally beyond the main reinforcement level, at which the diagonal section completely cracked and a diagonal tension failure occurred with a (45°) as shown in Figure 37. At failure no concrete spallation was noticed. The maximum compressive and tensile strains in concrete, and BFRP bars were recorded as (0.002), and (0.011), respectively. The beam's maximum midspan deflection was 17 mm.



Figure 36. Beam A1 (Diagonal tension failure).

4.3.2. Beam A2 (2.5- ρ_f -1.5%-G250)

Stage 1: Beam A2 has been made with 2 \emptyset 12 BFRP bars as main reinforcement, and \emptyset 10 GFRP stirrups spaced at 250 mm with 1.5% of fibers, and $a/d=2.5$. Initially, no flexural cracks were observed at this stage when the applied load was in the range below (32 kN). Within this range, the load vs midspan deflection graph demonstrated a linear relationship. This behavior remains the same until the load reaches (33 kN).

Stage 2: Once the applied load exceeds (32 kN) to (33 kN), the first flexural crack appeared at the extreme concrete fiber within the constant moment zone. As the load was increasing more adjacent cracks were existed. The cracks then started to get wider and propagate toward the neutral axis of the beam. The beam at this stage begins to experience a midspan deflection that is increasing in a faster rate than the previous stage due to the reduction in the moment of inertia after cracking.

Stage 3: At a load of (40 kN), the cracks were shifted into the shear span, and a flexural crack started to develop at the extreme bottom fibers and acquire more inclination as they extending upward, then an inclined cracks started to develop at (64 kN). When more load was applied, more adjacent shear cracks starts to exist, and were diagonally extending up toward the point load and down close to the reinforcement level at the range between [64-125 kN].

Stage 4: When the load was further increased to (128 kN) one of the diagonal cracks widened more and the lower portion of the crack extended diagonally beyond the main reinforcement level, at which the diagonal section completely cracked and a diagonal tension failure occurred with a (33°) as shown in Figure 38. At failure no concrete spallation

was noticed. The maximum compressive and tensile strains in concrete, and BFRP bars were recorded as (0.00326), and (0.012), respectively. The beam's maximum midspan deflection was 31 mm.



Figure 37. Beam A2 (Diagonal tension failure).

4.3.3. Beam A3 (2.5-pf2-0.75%-G250)

Stage 1: Beam A3 has been made with 4 \emptyset 10 BFRP bars as main reinforcement, and \emptyset 10 GFRP stirrups spaced at 250 mm with 0.75% of fibers, and $a/d = 2.5$. Initially, no flexural cracks were observed at this stage when the applied load was in the range below (30 kN). Within this range, the load vs midspan deflection graph demonstrated a linear relationship. This behavior remains the same until the load reaches (31 kN).

Stage 2: Once the applied load exceeds (30 kN) to (31 kN), the first flexural crack appeared at the extreme concrete tension fiber within the constant moment zone. As the

load was increasing more adjacent cracks were existed. The cracks then started to get wider and propagate toward the neutral axis of the beam. The beam at this stage begins to experience a midspan deflection that is increasing in a faster rate than the previous stage due to the reduction in the moment of inertia after cracking.

Stage 3: At a load of (34 kN), the cracks were shifted into the shear span, and a flexural crack started to develop at the extreme bottom fibers of the beam extending upward, then an inclined cracks started to develop on top of them at (60 kN). When more load was applied several adjacent flexure shear crack were diagonally extending up toward the point load, accompanied by some shear cracks started to develop at the mid height of the beam then these cracks were extended down toward the reinforcement level at a distance equivalent to the beam depth from support and up toward the loading point in the loading range of (85 – 110 kN).

Stage 4: When the load was further increased to (115 kN), one shear crack started to widen more than the other cracks. The load keeps increasing until (122 kN), after it starts to progressively decrease to (69 kN). The beam keeps deflecting until rupture in the main reinforcement and diagonal tension failure was observed at an angle of (40) as shown in Figure 39. The maximum compressive and tensile strains in concrete, and BFRP bars were recorded as (0.0019), and (0.011), respectively. The beam's maximum midspan deflection was 22 mm.

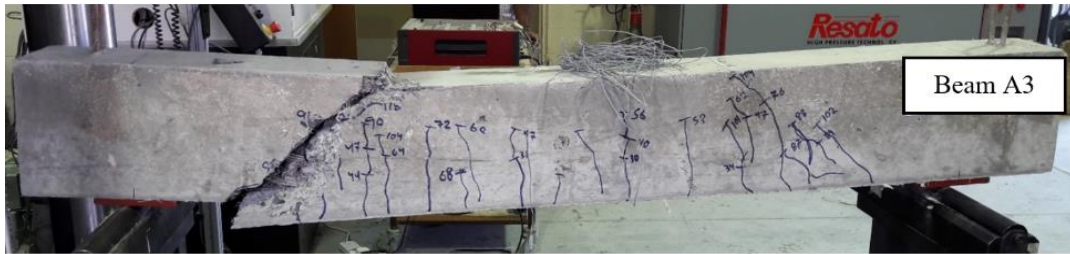


Figure 38. Beam A3 (Diagonal tension failure)

4.3.4. Beam A4 (2.5- ρ_f -0.75%-G170)

Stage 1: Beam A4 has been made with 4 ϕ 10 BFRP bars as main reinforcement, and ϕ 10 GFRP stirrups spaced at 170 mm with 0.75% of fibers. Initially, no flexural cracks were observed at this stage when the applied load was in the range below (32 kN). Within this range, the load vs midspan deflection graph demonstrated a linear relationship. This behavior remains the same until the load reaches (33 kN).

Stage 2: Once the applied load exceeds (32 kN) to (33 kN), the first flexural crack appeared at the extreme concrete tension fiber within the constant moment zone. As the load was increasing more adjacent cracks were existed. The cracks then started to get wider and propagate toward the neutral axis of the beam. The beam at this stage begins to experience a midspan deflection that is increasing in a faster rate than the previous stage due to the reduction in the moment of inertia after cracking.

Stage 3: At a load of (42 kN), the cracks were shifted into the shear span, and a flexural crack started to develop at the extreme bottom fibers of the beam extending

upward. When more load was applied the crack was diagonally extending up toward the point load, and more adjacent shear cracks started to develop at the mid height of the beam then these cracks were extended down toward the support location and up toward the loading point in the loading range of (110 – 125 kN).

Stage 4: When the load was further increased to (147 kN) the beam continues to displace downward, and the load started to progressively decreases. Then, the compression zone at the midspan started to crush as shown in Figure 41, however no concrete spallation was noticed at this stage. The beam keeps deflecting until clear and wide flexural cracks were observed. The maximum compressive and tensile strains in concrete, and BFRP bars were recorded as (0.0035), and (0.02), respectively. The beam's maximum midspan deflection was 86 mm.

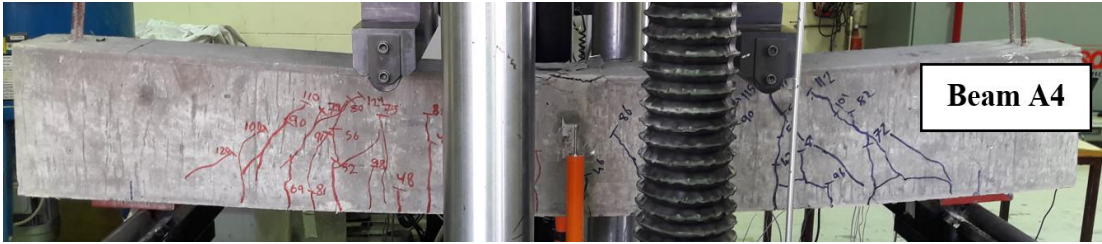


Figure 39. Beam A4 (Compression flexural failure)

4.3.5. Beam A5 (3.3- ρ_f 2-1.5%-G250)

Stage 1: Beam A7 has been made with 4 ϕ 10 BFRP bars as main reinforcement, and ϕ 10 GFRP stirrups spaced at 250 mm with 1.5% of fibers, and $a/d=3.3$. Initially, no flexural cracks were observed at this stage when the applied load was in the range below (30kN). Within this range, the load vs midspan deflection graph demonstrated a linear relationship.

This behavior remains the same until the load reaches (31 kN), at which an equal tensile stress to the modulus of rupture of concrete has been created by the applied load.

Stage 2: Once the applied load exceeds (30 kN) to (31 kN), the developed tensile stresses exceeds the flexural tensile strength for the concrete and as a result the first flexural crack appeared at the extreme concrete fiber within the constant moment zone. As the load was increasing more adjacent cracks were existed. The cracks then started to get wider and propagate toward the neutral axis of the beam. The beam at this stage begins to experience a midspan deflection that is increasing in a faster rate than the previous stage due to the reduction in the moment of inertia after cracking.

Stage 3: At a load of (46 kN), the cracks were shifted into the shear span, and a flexural crack started to develop at the extreme bottom fibers of the beam extending upward and acquire more inclination as they extend upward. Clear inclination of cracks was noticed at (58 kN) on top of the flexural crack. When more load was applied more shear cracks were developed at the mid height of beam and the cracks were diagonally extending up toward the point load, and down close to the reinforcement level at the range between [58-106 kN].

Stage 4: When the load was further increased to (124 kN) the shear cracks stops increasing and the compression zone at the midspan starts crushing with an excessive flexural crack at the beam's midspan as can be depicted from Figure 42. At failure no concrete spallation was noticed. The maximum compressive and tensile strains in concrete, and BFRP bars were recorded as (0.003), and (0.025), respectively. The beam's maximum midspan deflection was 80 mm.

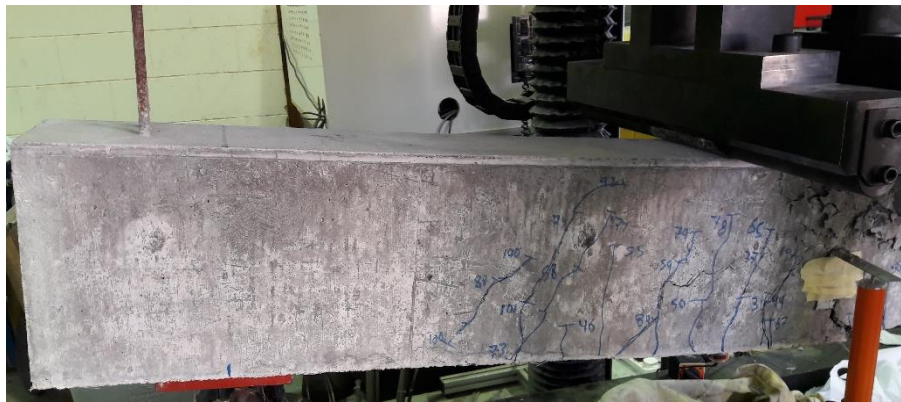
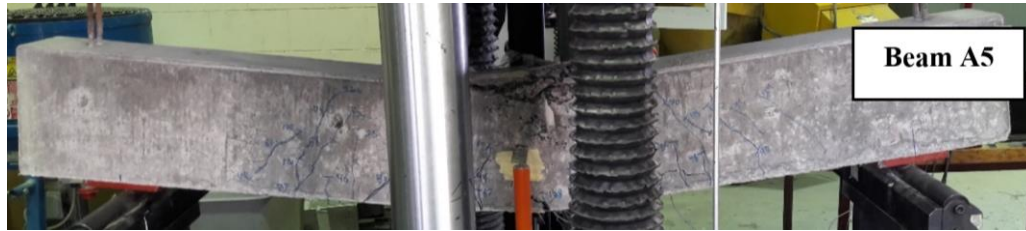


Figure 40. Beam A5 (Compression flexural failure)

4.3.6. Beam A6 (3.3-pf2-0%-G170)

Stage 1: Beam A6 has been made with 4 \emptyset 10 BFRP bars as main reinforcement, and \emptyset 10 GFRP stirrups spaced at 170 mm with 0% of fibers, and $a/d=3.3$. Initially, no flexural cracks were observed at this stage when the applied load was in the range below (22 kN). Within this range, the load vs midspan deflection graph demonstrated a linear relationship. This behavior remains the same until the load reaches (23 kN).

Stage 2: Once the applied load exceeds (22 kN) to (23 kN), the first flexural crack appeared at the extreme concrete tension fiber within the constant moment zone. As the load was increasing more adjacent cracks were existed. The cracks then started to get wider and propagate toward the neutral axis of the beam. The beam at this stage begins to experience a midspan deflection that is increasing in a faster rate than the previous stage due to the reduction in the moment of inertia after cracking.

Stage 3: At a load of (41 kN), the cracks were shifted into the shear span, and a flexural crack started to develop at the extreme bottom fibers of the beam extending upward, then an inclined cracks started to develop on top of them at (47 kN). When more load was applied the crack was diagonally extending up toward the point load, and more adjacent shear cracks started to develop at the mid height of the beam then these cracks were extended up toward the loading point and downward to below the flexural reinforcement in the loading range of (70 – 100 kN). Some of the cracks were extended toward the support.

Stage 4: When the load was further increased to (99 kN) the beam continues to displace downward, and the load started to progressively decreases to (88 KN). Then, the compression zone at the loading point started to crush and a diagonal crack extending from below the crushed zone to the support with an angle of (43) keeps widening until failure occurs as shown in Figure 43. The maximum compressive and tensile strains in concrete, and BFRP bars were recorded as (0.0027), and (0.015), respectively. The beam's maximum midspan deflection was 47 mm.



Figure 41. Beam A6 (Compression shear failure)

4.3.7. Beam A7 (3.3- ρ_f 2-0.75% -G170)

Stage 1: Beam A7 has been made with 4 \emptyset 10 BFRP bars as main reinforcement, and \emptyset 10 GFRP stirrups spaced at 170 mm with 0.75% of fibers. Initially, no flexural cracks were observed at this stage when the applied load was in the range below (30 kN). Within this range, the load vs midspan deflection graph demonstrated a linear relationship. This behavior remains the same until the load reaches (31 kN).

Stage 2: Once the applied load exceeds (30 kN) to (31 kN), the first flexural crack appeared at the extreme concrete tension fiber within the constant moment zone. As the load was increasing the crack started to get wider and propagate toward the neutral axis of the beam. The beam at this stage begins to experience a midspan deflection that is increasing in a faster rate than the previous stage due to the reduction in the moment of inertia after cracking.

Stage 3: At a load of (37 kN), the cracks were shifted into the shear span, and a flexural crack started to develop at the extreme bottom fibers of the beam extending upward, then an inclined cracks started to develop on top of them at (52 kN). When more load was applied the crack was diagonally extending up toward the point load, and more adjacent flexure shear were observed. Then a diagonal shear cracks begins to formulate at the mid height of the beam and propagate toward the loading point and to below the flexural reinforcement in the loading range of (70 – 100 kN).

Stage 4: When the load was increased to (101 KN) the beam continues to displace downward, and the load started to progressively decreases. Then, the compression zone at the midspan started to crush as shown in Figure 44, however no concrete spallation was noticed at this stage. The beam keeps deflecting until clear and wide flexural cracks were observed then the test was stopped. The maximum tensile strain in BFRP bars was recorded as (0.022). The beam's maximum midspan deflection was 68 mm.



Figure 42. Beam A7 (Compression flexural failure).

4.3.8. Beam A8 (3.3- ρ 2-1.5% -G170)

Stage 1: Beam A8 has been made with 4 \emptyset 10 BFRP bars as main reinforcement, and \emptyset 10 GFRP stirrups spaced at 170 mm with 1.5% of fibers, and $a/d = 3.3$. Initially, no flexural cracks were observed at this stage when the applied load was in the range below (31 kN). Within this range, the load vs midspan deflection graph demonstrated a linear relationship. This behavior remains the same until the load reaches (32 kN).

Stage 2: Once the applied load exceeds (31 kN) to (32 kN), the first flexural crack appeared at the extreme concrete tension fiber within the constant moment zone. As the load was increasing more adjacent cracks were existed. The cracks then started to get wider and propagate toward the neutral axis of the beam. The beam at this stage begins to experience a midspan deflection that is increasing in a faster rate than the previous stage due to the reduction in the moment of inertia after cracking.

Stage 3: At a load of (37 kN), the cracks were shifted into the shear span, and a flexural crack started to develop at the extreme bottom fibers of the beam extending upward and acquire more inclination as they extend upward. Clear inclination of cracks was noticed at (70 kN) on top of the flexural crack. Shear cracks starts developing at (62 kN). When more load was applied more shear cracks were developed at the mid height of beam and the cracks were diagonally extending up toward the point load, and down close to the reinforcement level at the range between [62-114 kN].

Stage 4: When the load was further increased to (118 kN) the load is then experience a progressive decreasing at this stage and the diagonal cracks stops propagating, however, the concrete at the compression zone of the midspan begins to crush as shown in

Figure 45 with a clear and wide flexural cracks at later stages. Then the load starts decreasing gradually until it reaches (35 kN) at which an excessive flexural crack was noticed. The test is then being stopped. The maximum compressive and tensile strains in concrete, and BFRP bars were recorded as (0.0029), and (0.02) , respectively. The beam's maximum midspan deflection was 87 mm.

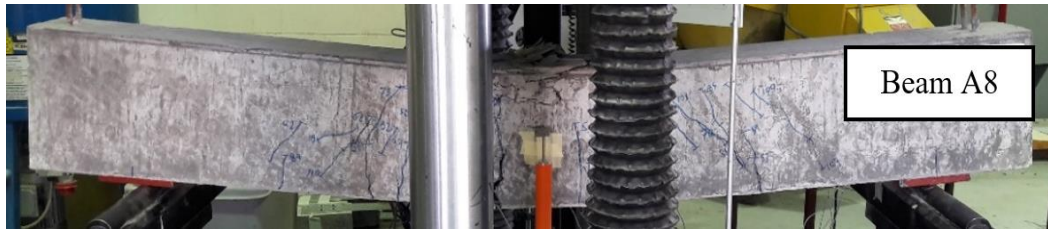


Figure 43. Beam A8 (Compression flexural failure)

4.3.9. *Beam A9 (3.3- ρ 3-0.75%-G170)*

Stage 1: Beam A9 has been made with 4 \emptyset 12 BFRP bars as main reinforcement, and \emptyset 10 GFRP stirrups spaced at 170 mm with 0.75% of fibers, and $a/d= 3.3$. Initially, no flexural cracks were observed at this stage when the applied load was in the range below (24 kN). Within this range, the load vs midspan deflection graph demonstrated a linear relationship. This behavior remains the same until the load reaches (25 kN).

Stage 2: Once the applied load exceeds (24 kN) to (25 kN), the first flexural crack appeared at the extreme concrete tension fiber within the constant moment zone. As the load was increasing the crack started to get wider and propagate toward the neutral axis of the beam. The beam at this stage begins to experience a midspan deflection that is increasing in a faster rate than the previous stage due to the reduction in the moment of inertia after cracking.

Stage 3: At a load of (33 kN), the cracks were shifted into the shear span, and a flexural crack started to develop at the extreme bottom fibers of the beam extending upward, then an inclined cracks started to develop on top of them at (61 kN). When more load was applied the crack was diagonally extending up toward the point load, and more adjacent flexure shear were observed. Then a diagonal shear cracks begins to formulate at the mid height of the beam and propagate toward the loading point and to below the flexural reinforcement in the loading range of (61 – 124 kN). After this stage no increase in the number of cracks was noticed.

Stage 4: When the load was further increased to (125 kN) the beam continues to displace downward, then, the compression zone at the midspan started to crush as in Figure

46, however no concrete spallation was noticed at this stage and the load started to progressively decreases and wide flexural cracks were figured out at the midspan of the beam. The maximum compressive and tensile strains in concrete, and BFRP bars were recorded as (0.0027), and (0.024), respectively. The beam's maximum midspan deflection was 89 mm.

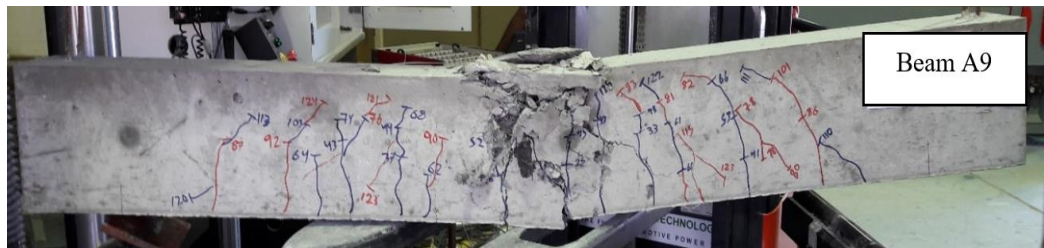


Figure 44. Beam A9 (Compression flexural failure).

4.3.10. Beam A10 (2.5- ρ_3 -1.5% -G170)

Stage 1: Beam A10 has been made with 4 ϕ 12 BFRP bars as main reinforcement, and ϕ 10 GFRP stirrups spaced at 170 mm with 0.75% of fibers, and $a/d = 2.5$. Initially, no flexural cracks were observed at this stage when the applied load was in the range below (36 kN). Within this range, the load Vs midspan deflection graph demonstrated a linear relationship. This behavior remains the same until the load reaches (37 kN).

Stage 2: Once the applied load exceeds (36 kN) to (37 kN), the first flexural crack appeared at the extreme concrete tension fiber within the constant moment zone. As the load was increasing more adjacent cracks were existed. The cracks then started to get wider and propagate toward the neutral axis of the beam. The beam at this stage begins to experience a midspan deflection that is increasing in a faster rate than the previous stage due to the reduction in the moment of inertia after cracking.

Stage 3: At a load of (45 kN), the cracks were shifted into the shear span, and a flexural crack started to develop at the extreme bottom fibers of the beam extending upward, then an inclined crack started to develop on top of them at (72 kN). When more load was applied several adjacent flexure shear cracks were diagonally extending up toward the point load, accompanied by some shear cracks started to develop at the mid height of the beam then these cracks were extended down toward the reinforcement level at a distance equivalent to the beam depth from support or toward the support and up toward the loading point in the loading range of (72 – 135 kN). After this stage no increase in the number of cracks was noticed.

Stage 4: When the load was further increased to (153 kN) the load remains constant at this stage and the diagonal cracks stops widening, however, the concrete at the compression zone of the midspan begins to crush as shown in Figure 47 with a clear and wide flexural cracks at the midspan. Then the load starts decreasing gradually. The maximum compressive and tensile strains in concrete, and BFRP bars were recorded as (0.0033), and (0.02), respectively. The beam's maximum midspan deflection was 80 mm.

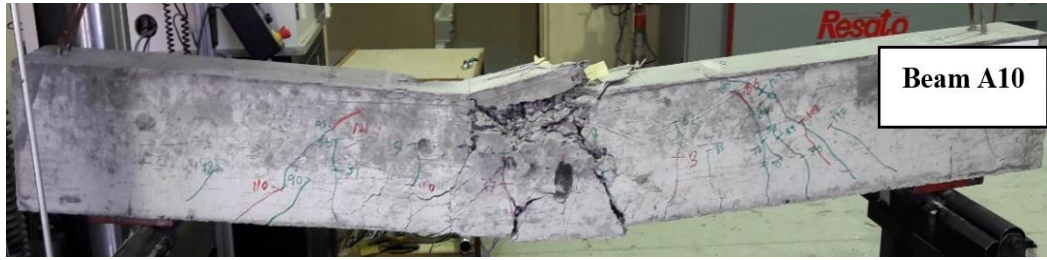


Figure 45. Beam A10 (Compression flexural failure)

4.3.11. Beam A11 (2.5- ρ_3 -0.75%-G250)

Stage 1: Beam A11 has been made with 4 \emptyset 12 BFRP bars as main reinforcement, and \emptyset 10 GFRP stirrups spaced at 250 mm with 0.75% of fibers, and $a/d = 2.5$. Initially, no flexural cracks were observed at this stage when the applied load was in the range below (33 kN). Within this range, the load vs midspan deflection graph demonstrated a linear relationship. This behavior remains the same until the load reaches (34 kN).

Stage 2: Once the applied load exceeds (33 kN) to (34 kN), the first flexural crack appeared at the extreme concrete tension fiber within the constant moment zone. As the load was increasing more adjacent cracks were existed. The cracks then started to get wider and propagate toward the neutral axis of the beam. The beam at this stage begins to experience a midspan deflection that is increasing in a faster rate than the previous stage due to the reduction in the moment of inertia after cracking.

Stage 3: At a load of (41 kN), the cracks were shifted into the shear span, and a flexural crack started to develop at the extreme bottom fibers of the beam extending upward, then an inclined crack started to develop on top of them at (66 kN). When more load was applied several adjacent flexure shear cracks were diagonally extending up toward the point load, accompanied by some shear cracks started to develop at the mid height of the beam then these cracks were extended down toward the reinforcement level at a distance equivalent to the beam depth from support and up toward the loading point in the loading range of (88 – 125 kN).

Stage 4: When the load was further increased to (125 kN), one shear crack started to widen more than the other cracks. The load keeps increasing until (133.7 kN). Then it starts to progressively decrease to (69 kN). The beam keeps deflecting until diagonal tension failure was observed at an angle of (45) as shown in Figure 48. The maximum compressive and tensile strains in concrete, and BFRP bars were recorded as (0.00217), and (0.0081), respectively. The beam's maximum midspan deflection was 17.6 mm.



Figure 46. Beam A11 (Diagonal tension failure).

4.3.12. *Beam A12 (2.5- ρ 3-0.75%-G170)*

Stage 1: Beam A12 has been made with 4 \emptyset 12 BFRP bars as main reinforcement, and \emptyset 10 GFRP stirrups spaced at 170 mm with 0.75% of fibers, and $a/d = 2.5$. Initially, no flexural cracks were observed at this stage when the applied load was in the range below (32 kN). Within this range, the load Vs midspan deflection graph demonstrated a linear relationship. This behavior remains the same until the load reaches (33 kN).

Stage 2: Once the applied load exceeds (32 kN) to (33 kN), the first flexural crack appeared at the extreme concrete tension fiber within the constant moment zone. As the load was increasing more adjacent cracks were existed. The cracks then started to get wider and propagate toward the neutral axis of the beam. The beam at this stage begins to experience a midspan deflection that is increasing in a faster rate than the previous stage due to the reduction in the moment of inertia after cracking.

Stage 3: At a load of (51 kN), the cracks were shifted into the shear span, and a flexural crack started to develop at the extreme bottom fibers of the beam extending upward, then an inclined crack started to develop on top of them at (71 kN). When more load was applied several adjacent flexure shear cracks were diagonally extending up toward the point load, accompanied by some shear cracks started to develop at the mid height of the beam then these cracks were extended down toward the reinforcement level at a distance equivalent to the beam depth from support or toward the support and up toward the loading point in the loading range of (70 – 124 kN). After this stage no increase in the number of cracks was noticed.

Stage 4: When the load was further increased to (130 kN), one shear crack started to widen more than the other cracks. The load keeps increasing until (144 kN), after that the load was steeply decreases to (81 kN) because the concrete at the diagonally cracked section has splitted and diagonal tension failure was observed at an angle of (33) as shown in Figure 49. The maximum compressive and tensile strains in concrete, and BFRP bars were recorded as (0.003), and (0.01), respectively. The beam's maximum midspan deflection was 24 mm.

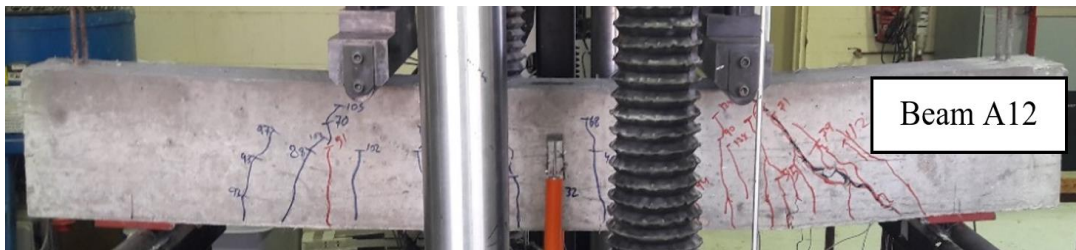


Figure 47. Beam A12 (Diagonal tension failure).

4.3.13. Beam A13 (2.5- ρ 3-0.75%-S170)

Stage 1: Beam A13 has been made with 4 \emptyset 12 BFRP bars as main reinforcement, and \emptyset 10 steel stirrups spaced at 170 mm with 0.75% of fibers, and $a/d = 2.5$. Initially, no flexural cracks were observed at this stage when the applied load was in the range below

(42 kN). Within this range, the load vs midspan deflection graph demonstrated a linear relationship. This behavior remains the same until the load reaches (43 kN).

Stage 2: Once the applied load exceeds (42 kN) to (43 kN), the first flexural crack appeared at the extreme concrete tension fiber within the constant moment zone. As the load was increasing more adjacent cracks were existed. The cracks then started to get wider and propagate toward the neutral axis of the beam. The beam at this stage begins to experience a midspan deflection that is increasing in a faster rate than the previous stage due to the reduction in the moment of inertia after cracking.

Stage 3: At a load of (52 kN), the cracks were shifted into the shear span, and a flexural crack started to develop at the extreme bottom fibers of the beam extending upward, then an inclined cracks started to develop on top of them at (77 kN). When more load was applied several adjacent flexure shear crack were diagonally extending up toward the point load, accompanied by some shear cracks started to develop at the mid height of the beam then these cracks were extended down toward the reinforcement level at a distance equivalent to the beam depth from support and up toward the loading point in the loading range of (75 – 135 kN).

Stage 4: When the load was further increased to (175 kN), the number of cracks remains the same, however, one shear crack started to widen more than the other cracks. The load keeps increasing until (187 Kn) because the concrete at the diagonally cracked section has splitted and diagonal tension failure was observed at an angle of (37) as can be seen in Figure 50. The maximum compressive and tensile strains in concrete, and BFRP

bars were recorded as (0.0032), and (0.0125), respectively. The beam's maximum midspan deflection was 25 mm.

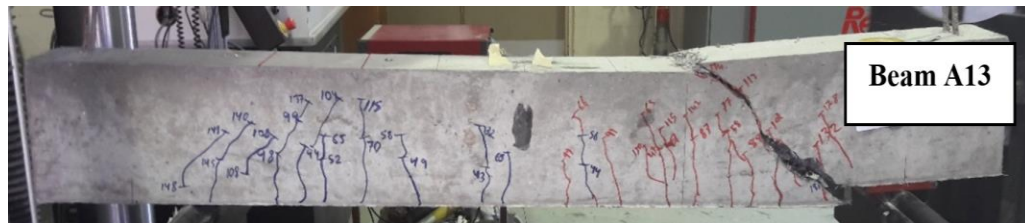


Figure 48. Beam A13 (Diagonal tension failure).

4.3.14. Beam A14 (2.5- ρ_3 -1.5%-S170)

Stage 1: Beam A14 has been made with 4 \emptyset 12 BFRP bars as main reinforcement, and \emptyset 10 GFRP stirrups spaced at 170 mm with 1.5% of fibers, and $a/d = 2.5$. Initially, no flexural cracks were observed at this stage when the applied load was in the range below (42 kN). Within this range, the load Vs midspan deflection graph demonstrated a linear relationship. This behavior remains the same until the load reaches (43 kN).

Stage 2: Once the applied load exceeds (42 kN) to (43 kN), the first flexural crack appeared at the extreme concrete tension fiber within the constant moment zone. As the load was increasing more adjacent cracks were existed. The cracks then started to get wider and propagate toward the neutral axis of the beam. The beam at this stage begins to

experience a midspan deflection that is increasing in a faster rate than the previous stage due to the reduction in the moment of inertia after cracking.

Stage 3: At a load of (63 kN), the cracks were shifted into the shear span, and a flexural crack started to develop at the extreme bottom fibers of the beam extending upward and acquiring more inclination as they extend upward. Shear cracks starts developing at (78 kN). When more load was applied more shear cracks were developed at the mid height of beam and the cracks were diagonally extending up toward the point load, and down close to the reinforcement level at the range between [78-140 kN].

Stage 4: When the load was further increased above (140 kN) up to (186 kN) no new cracks were observed and the diagonal cracks stopped propagating. The load is then experience a progressive decreasing at this stage and the diagonal cracks stops propagating, however, the concrete at the compression zone of the midspan begins to crush as in Figure 51. Then the load starts decreasing gradually until it reaches (70 kN). Wide flexural cracks at the midspan were observed at this stage. The maximum compressive and tensile strains in concrete, and BFRP bars were recorded as (0.0033), and (0.025), respectively. The beam's maximum midspan deflection was 85 mm.



Figure 49. Beam A14 (Compression flexural failure)

4.4. Discussion of Test Results

Starting from left to right, Table (10) summarizes the detailed results of the tested beams in terms of beam number and designation, maximum load, maximum deflection at failure, maximum strain values for both the longitudinal BFRP reinforcement and the concrete at the midspan, the cracking moment, the failure type, and the angle of failure.

Table 10

Summary of test results

Beam No.	Beam designation	Max load P/2 (KN)	Δ_{Max} (mm)	Max ϵ FRP	Max ϵ concrete	Mcr (KN.m)	Failure type	Angle of failure
A1	2.5-pf1-0.75%-G250	49.5	17	0.011	0.002	7.4	Diag tension	45
A2	2.5-pf1-1.5%-G250	64.35	31	0.012	0.00326	8.4	Diag tension	33
A3	2.5-pf2-0.75%-G250	61	22	0.011	0.0019	7.4	Diag tension	40
A4	2.5-pf2-0.75%-G170	73.5	86	0.02	0.0035	7.8	Flex comp	-
A5	3.3-pf2-1.5%-G250	62.25	80	0.025	0.003	9.7	Flex comp	-
A6	3.3-pf2-0%-G170	49.5	46	0.015	0.0027	7.2	Shear comp	43
A7	3.3-pf2-0.75%-G170	50.5	68	0.022	0.0012	9.7	Flex comp	-
A8	3.3-p2-1.5% -G170	59	87	0.02	0.0029	10	Flex comp	-
A9	3.3-p3-0.75%-G170	62.5	89	0.024	0.0027	7.7	Flex comp	-
A10	2.5-p3-1.5% -G170	76.5	80	0.02	0.0033	8.6	Flex comp	-
A11	2.5-p3-0.75%-G250	66.85	17.6	0.0081	0.00217	7.9	Diag tension	45
A12	2.5-p3-0.75%-G170	72	24	0.01	0.003	5.8	Diag tension	33
A13	2.5-p3-0.75%-S170	93.5	25	0.0125	0.0032	10	Diag tension	37
A14	2.5-p3-1.5%-S170	98	85	0.025	0.0033	10	Flex comp	-

4.4.1. The Effect of Fiber Percentage

It was observed that the fibers addition has enhanced the behavior of the tested beams from three main aspects; 1) the ultimate load carrying capacity; 2) the stiffness; 3) the mode of failure.

By referring to Figure 54, beam A1 and beam A2 were fabricated with 0.75% and 1.5% volume fraction of fibers, respectively. The ultimate load capacity in beam A2 has experienced an increase of 30% in comparison to beam A1, and they have both failed by diagonal tension failure. Similarly, beam A8 (with 1.5%) have also shown an increase in the ultimate load over beam A7 (with 0.75%) by 20% when both beams have failed by compression flexural failure. However, this increase becomes marginal in beams A10 and A14 (both made with 1.5%) which failed by compression flexural failure, compared respectively to their counterpart beams A12 and A13 (both made with 0.75%), that have failed by diagonal tension failure, where the results showed an increase of 6-7% only. This minor effect might have occurred because increasing the fiber percentages have increased the shear capacity beyond the flexural capacity, and hence the flexural capacity of beams A10, and A14 was reached earlier than their shear capacity.

Compared to the control beam A6 that was made with 0% volume fraction of fibers, the carried tests highlighted a clear enhancement of stiffness when fibers were presented in both percentages (0.75% and 1.5%). At maximum load of beam A6 (0%), beam A7(0.75%) and beam A8(1.5%) have shown lesser deflection by 75% as can be depicted from Figure 54. This enhancement can be attributed to the effect of fibers in controlling the flexural cracks and delaying their propagation and widening by means of crack

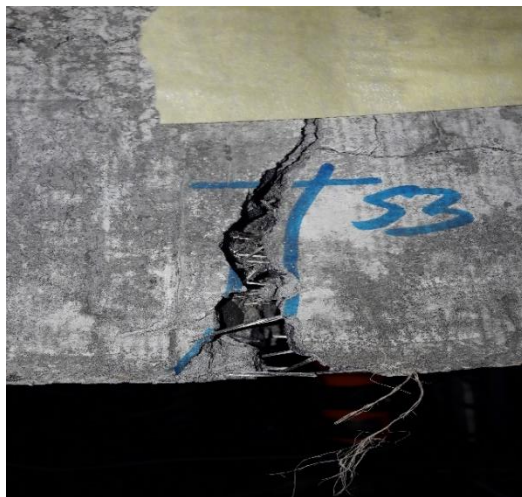
arresting mechanism that bridges the cracked zone as in Figure 52a. However, beams made with 0.75% of fibers behaved almost similar to beams made with 1.5% of fibers in terms of beams stiffness, whereas the main difference among them was in the loading capacity. Prior to the first flexural crack all beams were behaving similarly in terms of stiffness, but their effect was very apparent in preserving the beams stiffness from high reduction when the extreme tension fibers of the beams started to crack. As a result, Figure 56 shows that after the existence of first flexural crack, beams with higher percentages of fibers revealed a considerable reduction in the longitudinal BFRP strain values at all loading stages that was ranging from (20-45%) between 1.5% and 0.75% FRC beams, and from (85-95%) between 1.5% FRC beam and the control beam (0%). This can attract our attention toward an important outcome which is the ability of the fibers to reduce the axial stresses created on the flexural reinforcement by reducing the deflection, thus increasing the beam's loading capacity. Additionally, the appearance of inclined cracks was retarded or slowed down by the addition of fibers as shown in Figure 55a and therefore, the stirrups are expected to be stressed in a later stage.

Interestingly, the presence of fibers has altered the mode of failure in several beams from brittle shear failure into ductile flexural failure, allowing them to have a higher load bearing capacity. Although beam A6 (with 0% of fibers) was failed by compression shear failure, beam A7 (with 0.75% of fibers) and beam A8 (with 1.5% of fibers) have failed under compression flexural failure. In some cases, high percentage of fibers (such as: 1.5%) was needed to change the failure type in the tested beams. This can be noticed by referring to beams (A12 and A13) that were made with 0.75% of fibers compared to their counterpart beams made with 1.5% (A10 and A14), respectively, where the mode of failure was altered

from diagonal tension failure into compression flexural failure. Hence, this can clearly indicate the efficiency of fibers in increasing the shear capacity of RC beams and providing a noticeable ductile behavior throughout the test, which is represented in Figure 54 by the progressive declining in the applied load. This enhancement in the shear capacity can be referred to several reasons: 1) the presented fibers have significantly reduced the width of the diagonal crack and slows down their widening according to Figure 55, where it is clear that beams A8 and A7 (with 1.5%, and 0.75% of fibers, respectively) observed to have a much lesser crack width than the reference beam A6 (with 0% of fibers) in all loading stages after the existence of the crack. At the ultimate load of beam A6 the crack width reached 6 mm, whereas at the same loading stage, beams A8 and A7 have got a crack width of 0.82 mm. Similar observation is illustrated in Figure 55d, and hence the concrete contribution to shear resistance resulted from the interlocking of coarse aggregate will be preserved for a longer time, and this provides a more durable structure that allows additional transfer of shear through the interfacial surface; 2) the transfer of tensile stresses through diagonal cracks; 3) the resisted principal tensile stresses until fibers ruptured or pulled out. This can be depicted in Figure 52b.

It was interesting to observe beam A5 which was made with stirrups spacing of 250 mm and a fiber % of 1.5 to present a 25% increase in the ultimate load over beam A6 which was made with lesser stirrups spacing of 170 mm and 0% of fibers. Even though beam A6 was provided with a more number of stirrups along the shear span, the shear failure was not prevented, while the 1.5% of fibers in beam A5 were able to alter the failure mode into a flexural failure. Hence, this can demonstrate clearly the ability of fibers in partially substituting the FRP stirrups and enhancing the beam's ductility as can be depicted in

Figure 53b. The inclusion of fibers provides an excellent adhesion among the entire concrete and as a result prevented the spalling of concrete during all loading stages, including the failure load. By contrast, beams without fibers have experienced a failure that was accompanied by concrete spallation as shown in Figure 53. This can lead as to the conclusion that when fibers are introduced, catastrophic failure can be avoided.



(a)

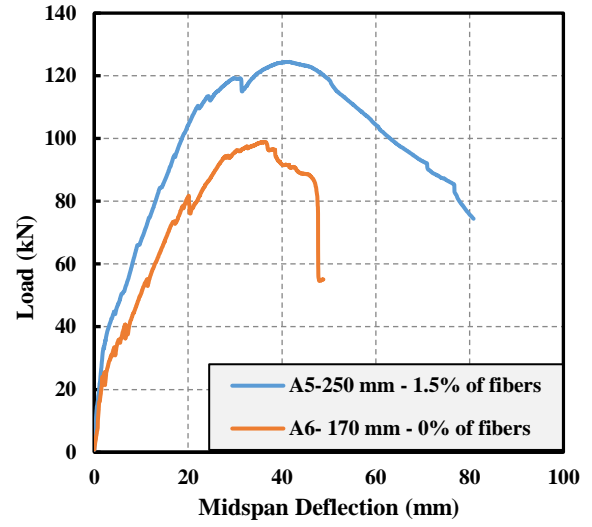


(b)

Figure 50. a) fibers bridging the flexural crack; b) fibers across inclined crack.

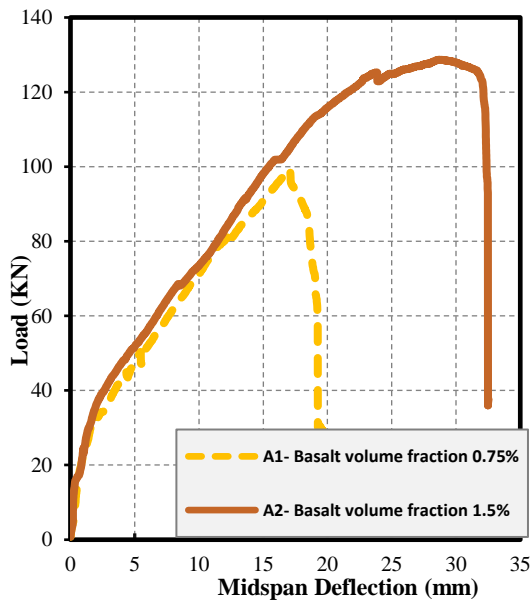


(a)

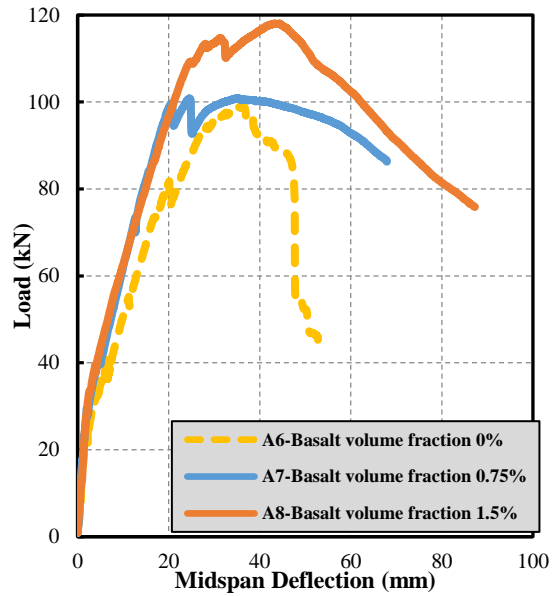


(b)

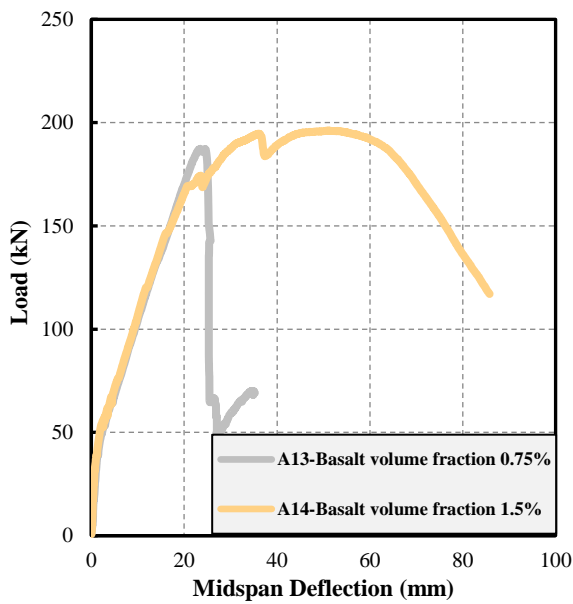
Figure 51. a) Concrete spallation in beam A6 (without fibers); b) The effect of fibers in partially substituting the glass stirrups.



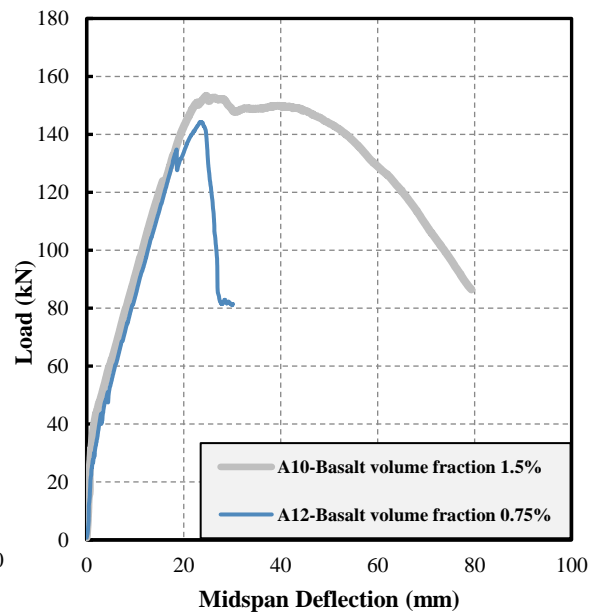
(a) A1 vs A2



(b) A6 vs A7 vs A8

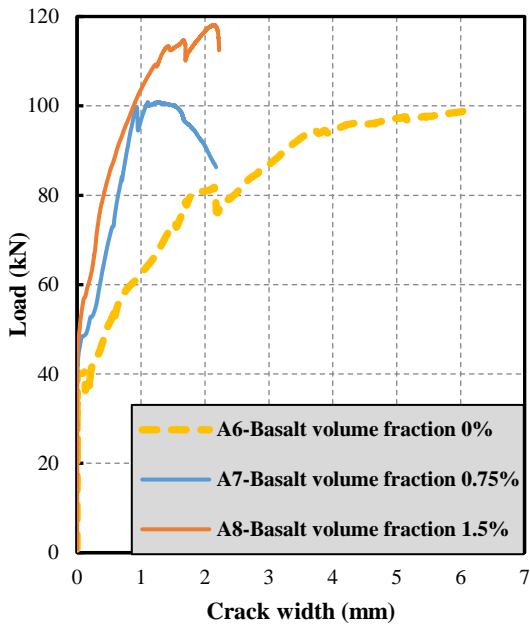


(c) A13 vs A14

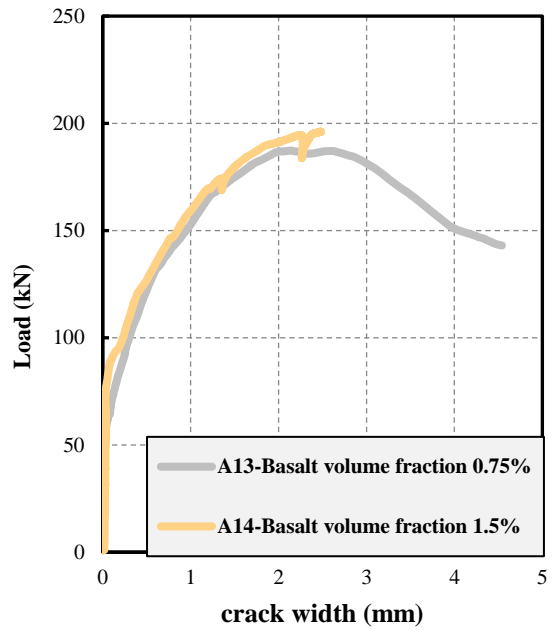


(d) A10 vs A12

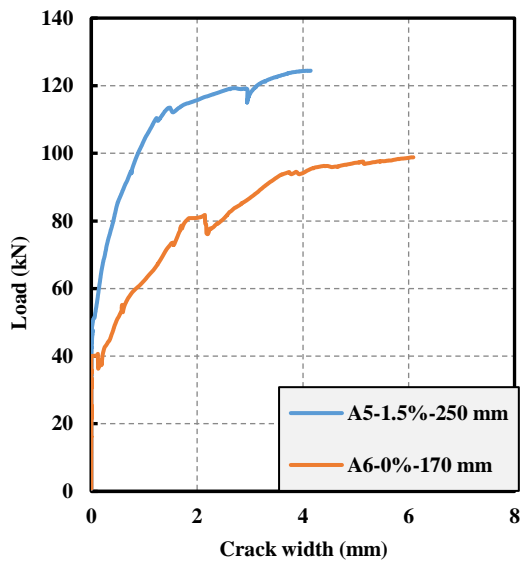
Figure 52. Load displacement diagrams for identical beams with different fiber percentages



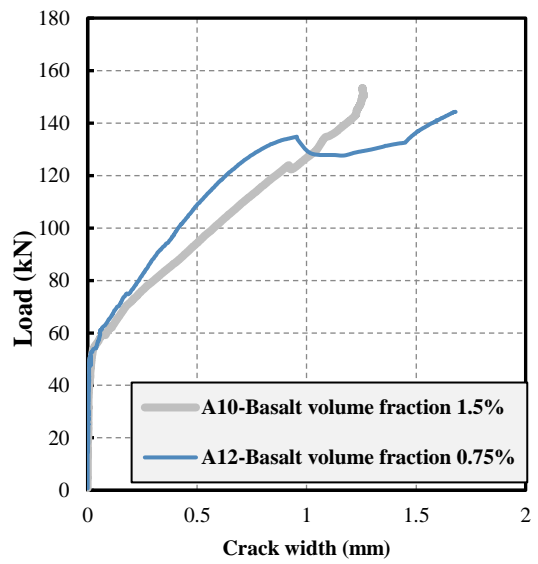
(a) A6 vs A7 vs A8



(b) A13 vs A14

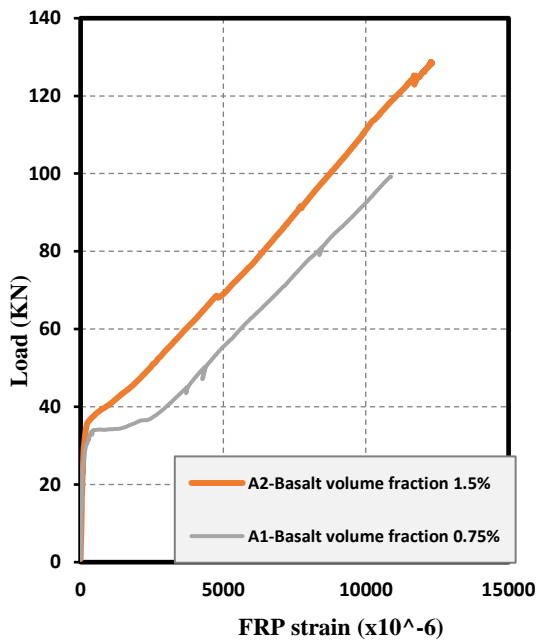


(c) A5 vs A6

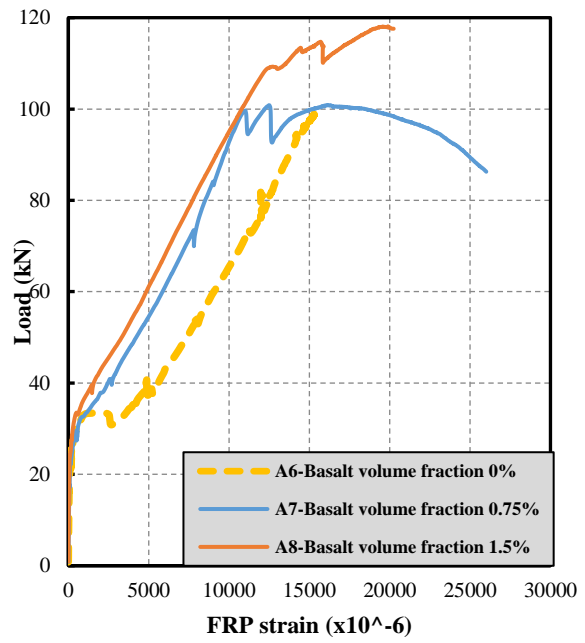


(d) A10 vs A12

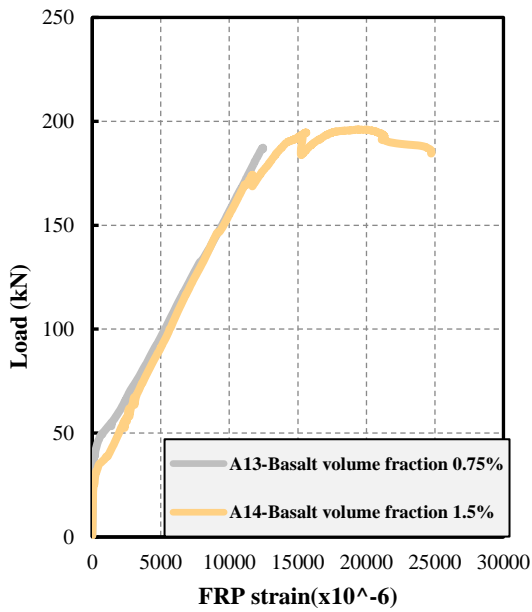
Figure 53. Load vs Crack width diagrams for identical beams with different fiber percentages



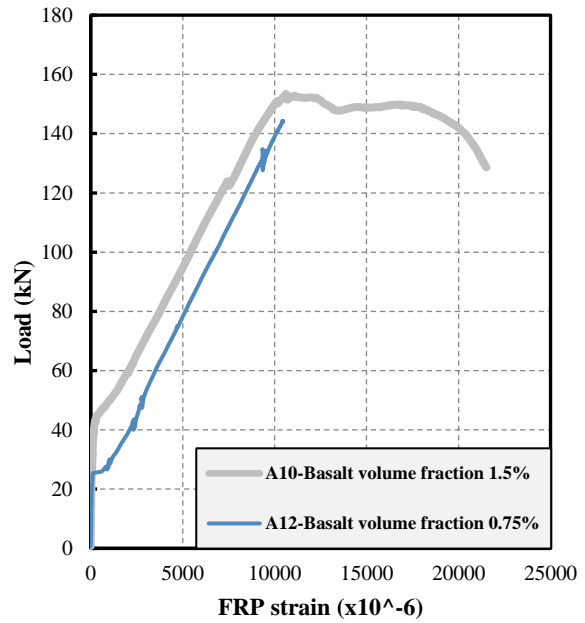
(a) A1 vs A2



(b) A6 vs A7 vs A8

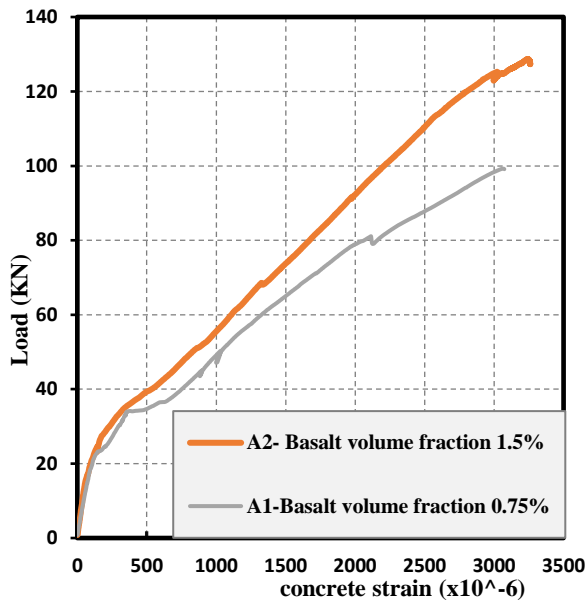


(c) A13 vs A14

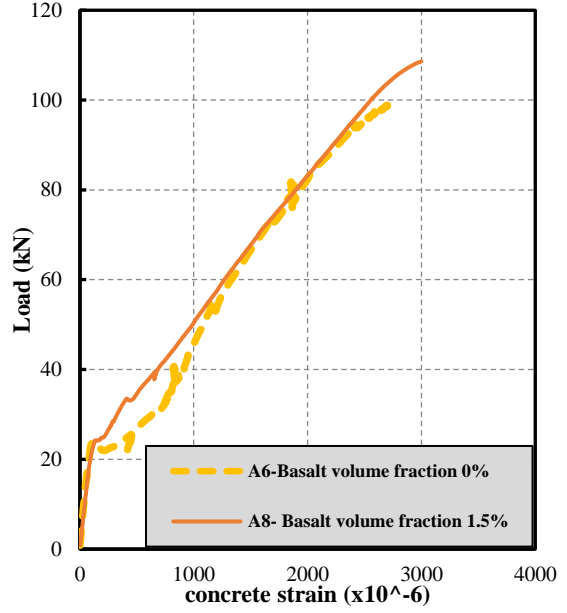


(d) A10 vs A12

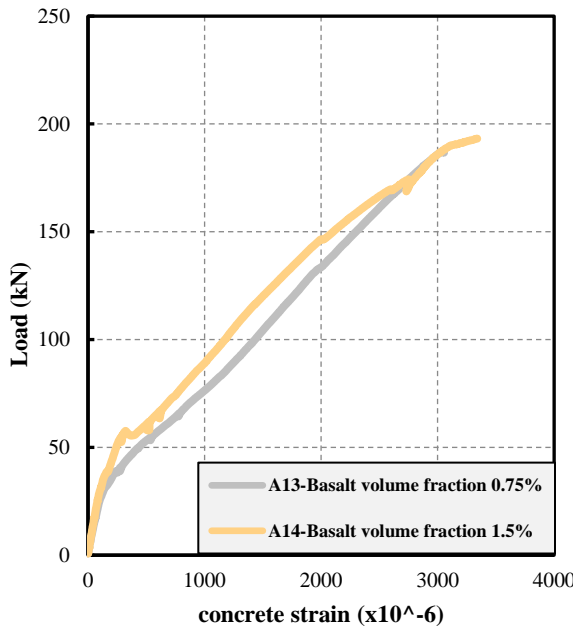
Figure 54. Load vs longitudinal FRP strain diagrams for identical beams with different fiber percentages



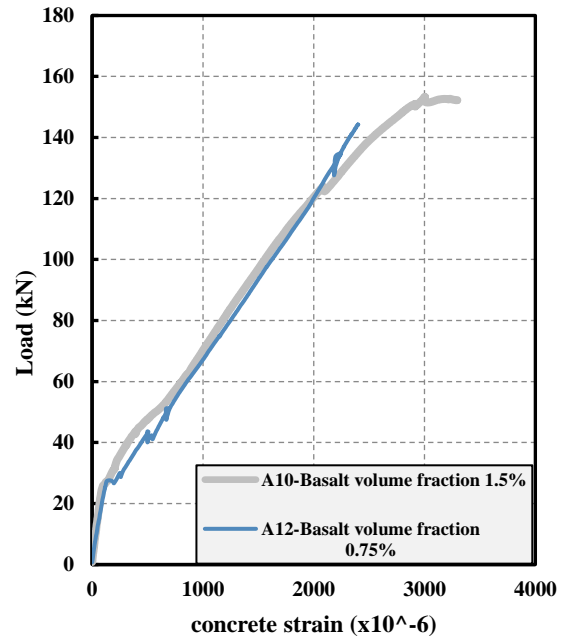
(a) A1 vs A2



(b) A6 vs A8



(c) A13 vs A14



(d) A10 vs A12

Figure 55. Load vs concrete strain diagrams for identical beams with different fiber percentages.

4.4.2. *The Effect of Reinforcement Ratio*

The analysis revealed an increase in the ultimate load capacity by 24% when the reinforcement ratio was increased from 0.0067 in beam A1 to 0.01 in beam A3. Additionally, beam A11 has revealed 48% enhancement in the shear strength over beam A1 when the reinforcement ratio was further increased to 0.0147. This enhancement in the shear strength of beams with high reinforcement ratio can be referred to the increased compression zone required to balance the high amount of reinforcement, the reduced crack width shown in Figure 59 that will maintain the effectiveness of the aggregate interlocking mechanism, and the boosted dowel capacity.

All beams have experienced a linear behavior in the load-deflection diagrams prior to the initiation of the first flexural crack. Subsequently, deflection was observed to increase linearly but with higher increments due to the reduction in the moment of inertia which reduces the BFRP beams stiffness. However, this reduction in stiffness was clearly influenced by the reinforcement ratio. Using higher reinforcement ratio has improved the beam stiffness after the initiation of the first flexural crack up to the failure point as shown in Figure 58.

The strain values for both the longitudinal bars and the concrete was mainly influenced by the amount of reinforcement ratio. Results obtained in Figure 60 and Figure 61 have shown that at the same loading level, less strain values were obtained when higher reinforcement ratio was used. Also, it can be noticed that the strain values for the longitudinal reinforcement have experienced a sudden jump after the first flexural crack formation, which is expected due to the transmission of most of the tensile stresses to the

longitudinal BFRP bars which is recognized to have a low elastic modulus. However, by looking at Figure 56, it can be observed that this jump in the strain values can be significantly controlled by using higher percentage of fibers. Also using higher reinforcement ratio as in Figure 60 showed a moderate control over this jump.

Although beam A12 was made with higher reinforcement ratio (0.0147) than beam A4 (0.01), the ultimate load capacity was same for both. This could be referred to some variations in the concrete properties resulted from different vibration or compaction of concrete.

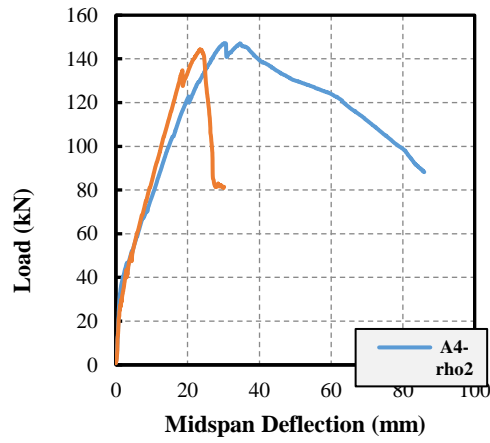
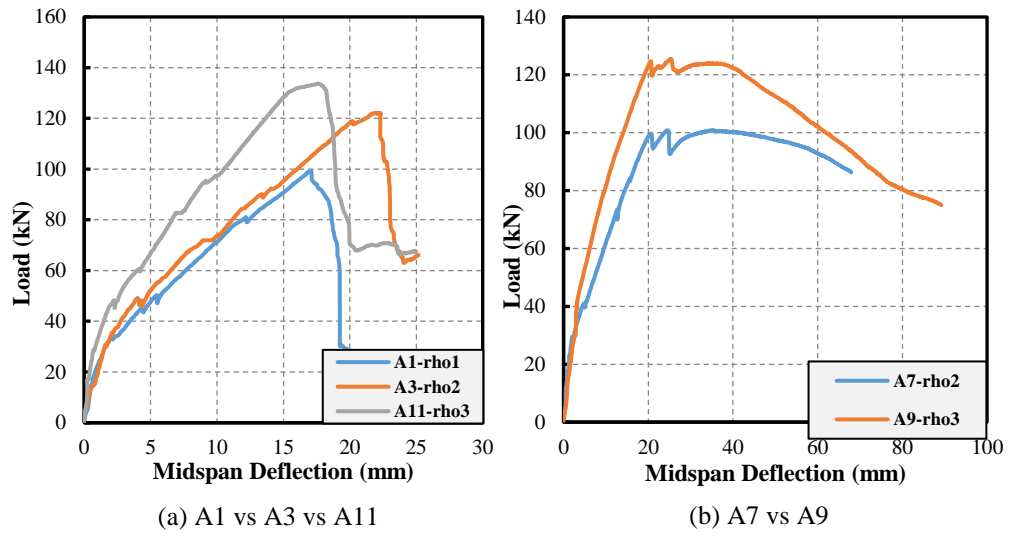
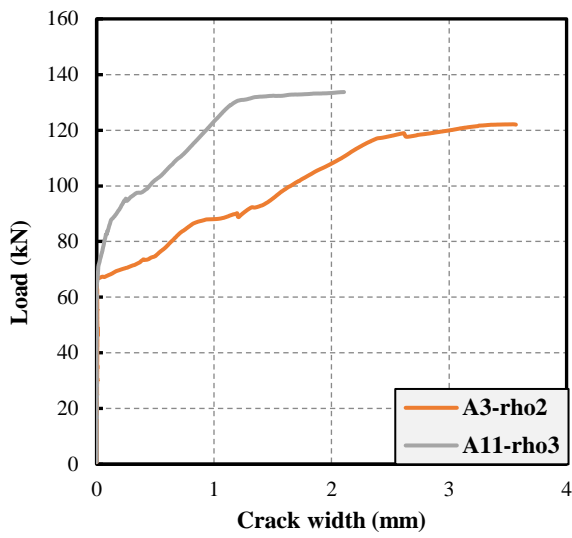
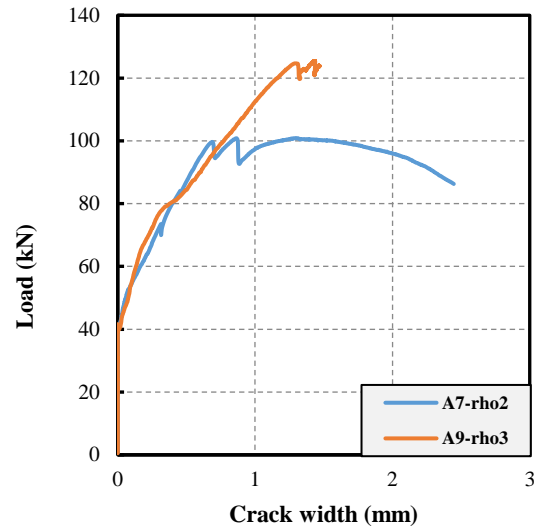


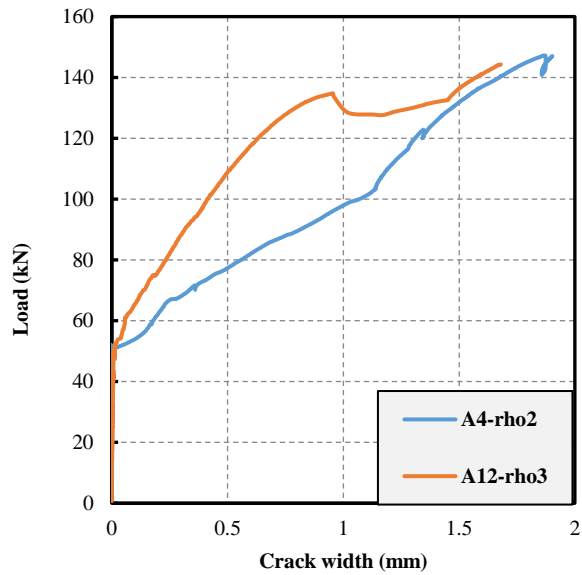
Figure 56. Load displacement diagrams for identical beams with different reinforcement ratios



(a) A3 vs A11

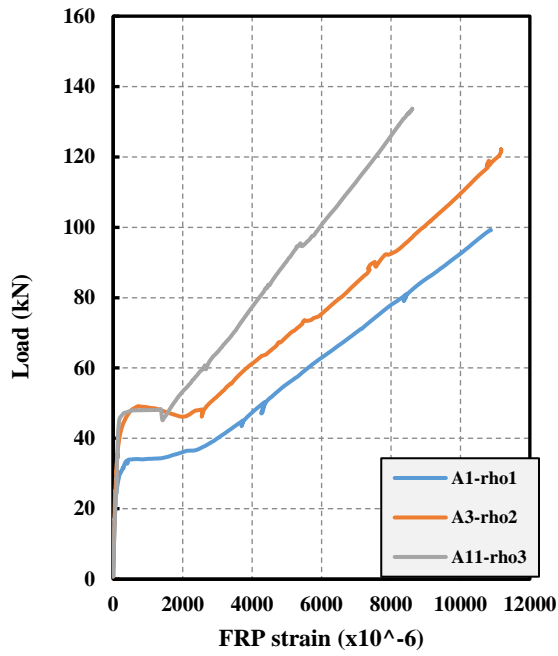


(b) A7 vs A9

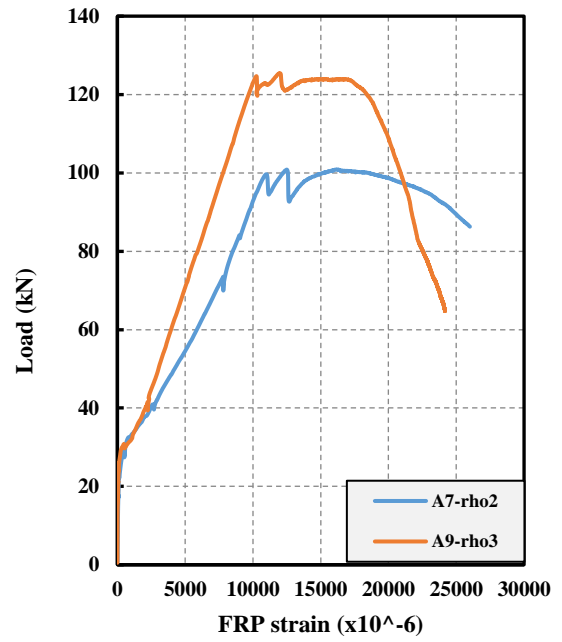


(c) A4 vs A12

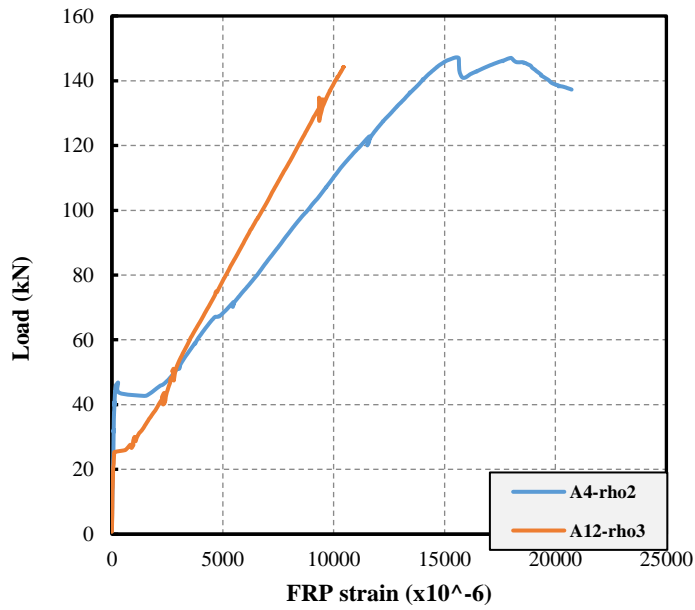
Figure 57. Load vs crack width diagrams for identical beams with different reinforcement ratios



(a) A1 vs A3 vs A11

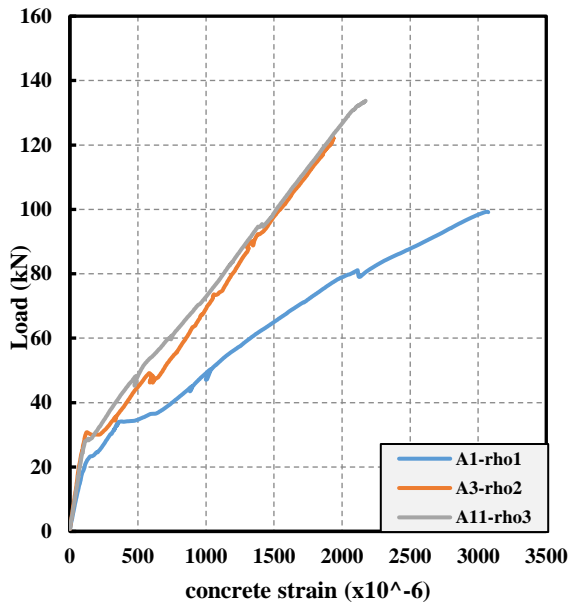


(b) A7 vs A9

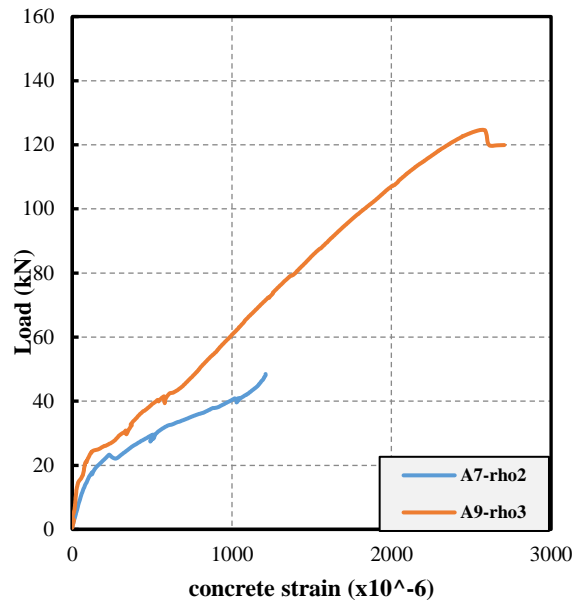


(c) A4 vs A12

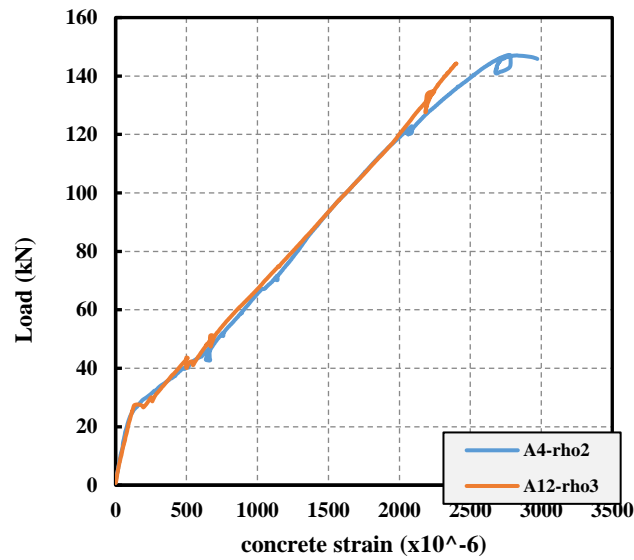
Figure 58. Load vs Longitudinal FRP strain diagrams for identical beams with different reinforcement ratios



(a) A1 vs A3 vs A11



(b) A7 vs A9



(c) A4 vs A12

Figure 59. Load vs concrete strain diagrams for identical beams with different reinforcement ratios

4.4.3. The Effect of Span to Depth Ratio

The observation to emerge from the data comparison of counterpart beams with different span to depth ratio (a/d) was an increase in the ultimate load capacity as smaller (a/d) ratio is used. Beams A4 and A12 which had a (a/d) ratio of (2.5) resulted in an increase in the loading capacity of 46% and 18%, respectively over beams A7 and A9 which had a (a/d) of (3.3).

The (a/d) ratio has also affected the stiffness of BFRP beams as can be depicted from Figure 62, where beams with lower (a/d) ratios (2.5) highlighted an increased stiffness compared to those beams with higher (a/d) ratio (3.3). This is because having a higher (a/d) ratio will increase the moment arm (longer shear span), which in turn will produce a higher moment value that is responsible to initiate the flexural cracking in earlier stage than beams with lower (a/d) ratio due to higher tensile stresses, and with a more number of cracks, reducing by that the beam stiffness. Consequently, at the same loading level, beams with higher (a/d) ratio founded to experience a higher strain values for the main reinforcement and the concrete at the midspan. This is clearly shown in Figure 64 and Figure 65.

The failure in BFRP-RC beams witnessed a change in mode with varying (a/d) ratios. Beams with lower (a/d) ratio (2.5) such as: beam A12 have failed by diagonal tension failure, while its counterpart beam with higher (a/d) ratio (3.3) such as: beam A9 have failed by compression flexural failure. Despite the formation of a critical shear crack in the latter beams, it was inhibited by the stirrup and therefore a change in the failure mode was observed. Also, it can be due to the increased number of flexural cracks at the constant moment zone that were propagating closer to the extreme compression fiber of the concrete

beam, causing by that a higher reduction in the beam stiffness and a higher deflection, as a result the flexural capacity of the beam was reached at earlier loading stage before the shear capacity is reached.

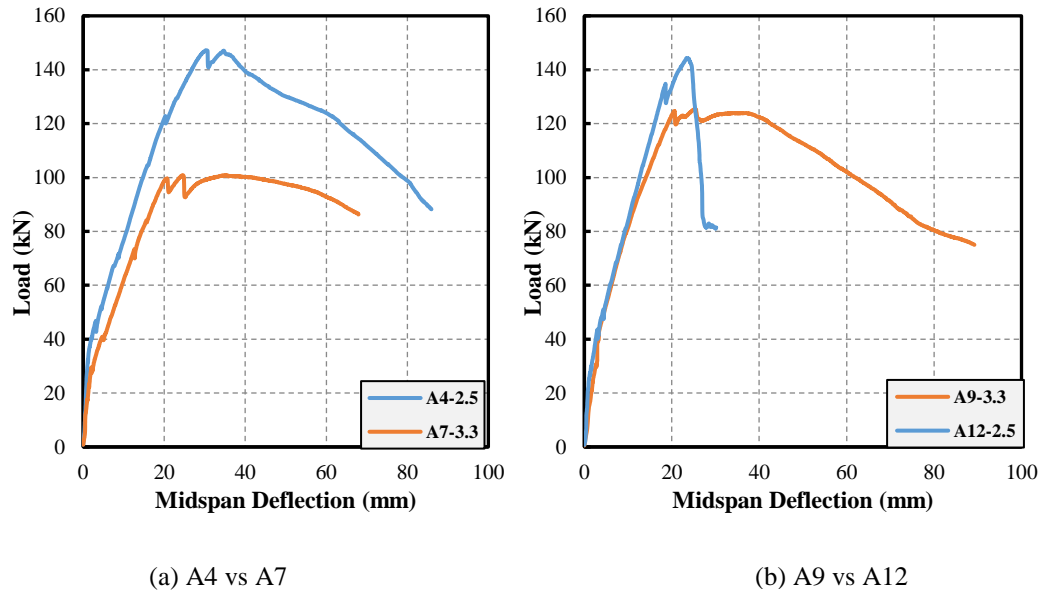


Figure 60. Load displacement diagrams for identical beams with different span to depth (a/d) ratios

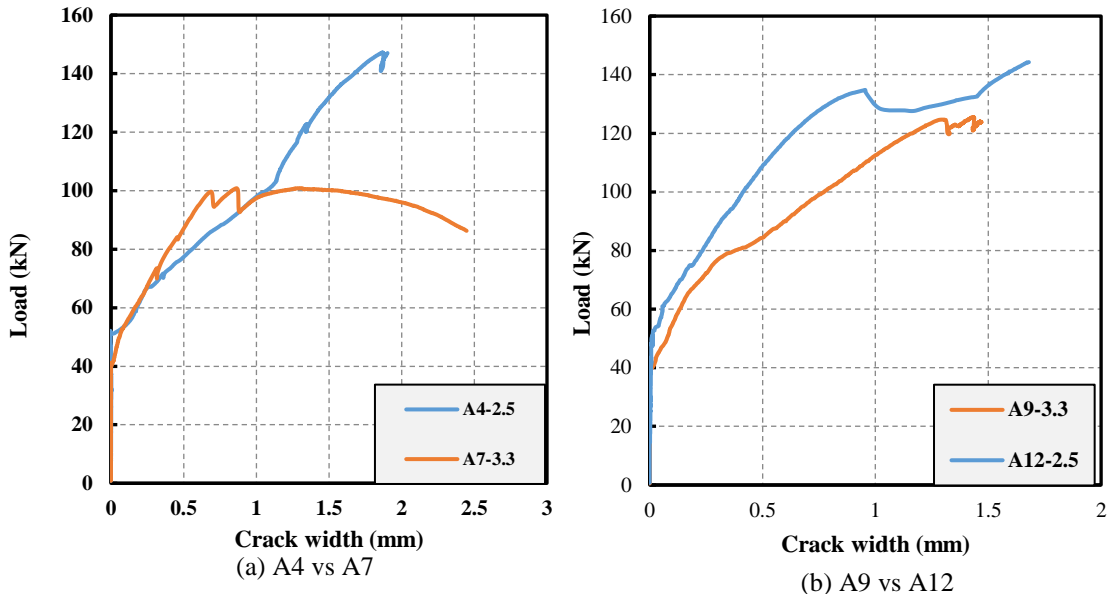


Figure 61. Load vs crack width diagrams for identical beams with different span to depth (a/d) ratios

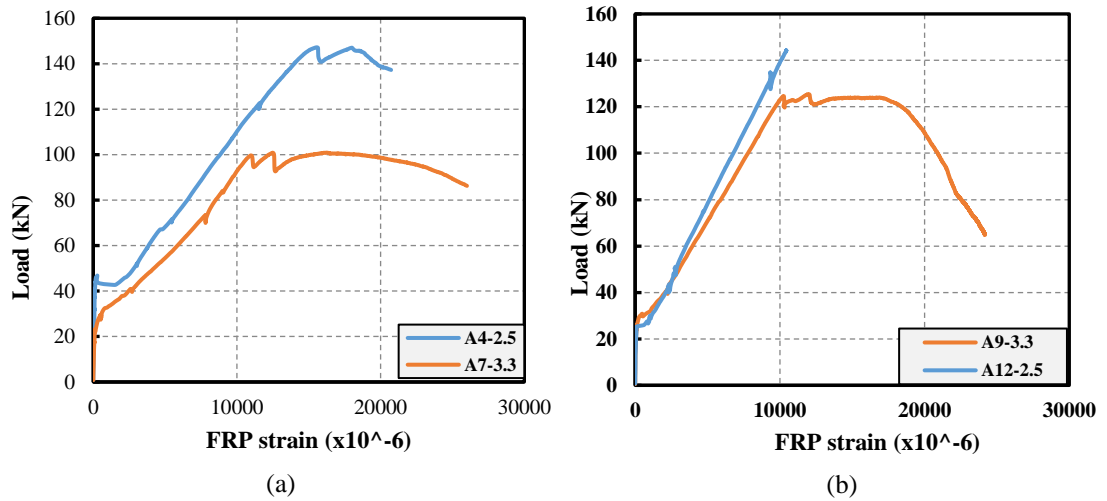


Figure 62. Load vs longitudinal FRP strain diagrams for identical beams with different span to depth (a/d) ratios

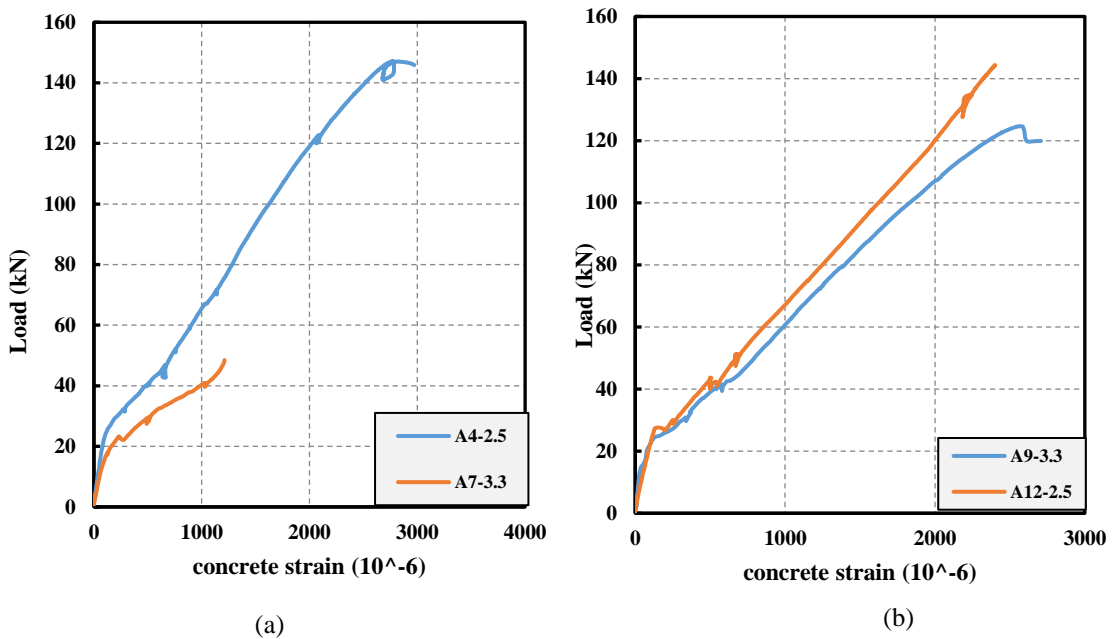
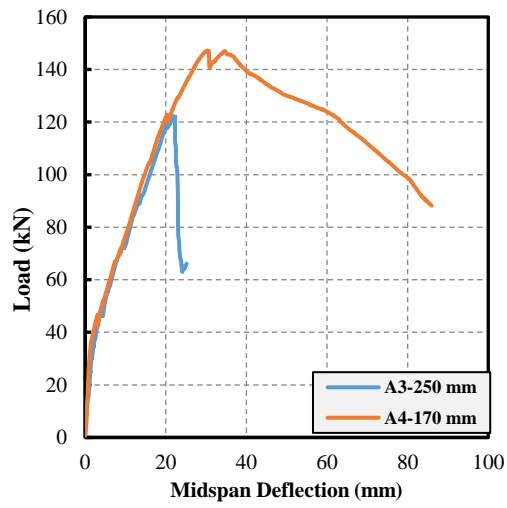


Figure 63. Load vs concrete strain diagrams for identical beams with different span to depth (a/d) ratios

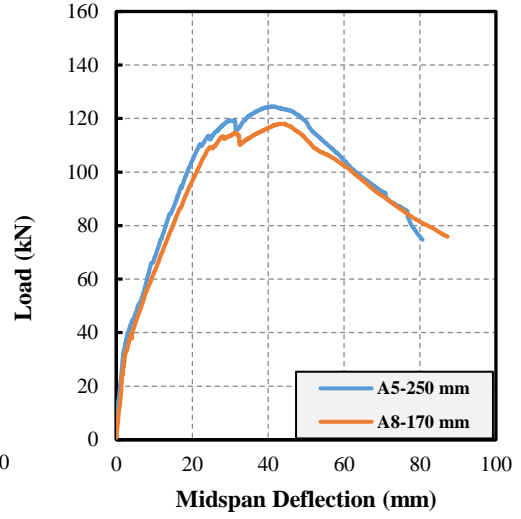
4.4.4. The Effect of Stirrups Spacing

Results indicated a quite good improvement in the ultimate loading capacity when lesser spacing for stirrups was used. Beam A4 and A12 with (170 mm) spacing of stirrups have demonstrated an increase in the ultimate load capacity by 20% and 8% over beam A3 and beam A11, respectively which have a higher spacing of (250 mm). The increase in the shear capacity for beams with lesser spacing of stirrups is expected as the shear force is distributed among more number of stirrups and the diagonal cracks are counteracted by more stirrups that act as dowels, which slows down their widening as shown in Figure 67 and this as a result can lead to a better contribution of the aggregate interlock along the entire

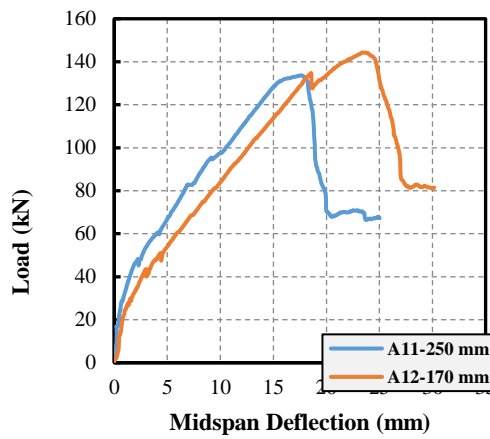
inclined plane. Furthermore, beam A3 failed by a diagonal tension failure whereas the failure type was converted into compression flexural failure with lesser spacing in beam A4. Beam A5 and beam A8 have shown almost a similar behavior throughout the test because they have both experienced a flexural compression failure. Even though shear cracks were developed along the shear span of those beams, the presence of stirrups has prevented their widening and propagation and altered their failure mode into a compression flexural failure as can be depicted from the load displacement diagrams in Figure 66a and 66b.



(a) A3 vs A4

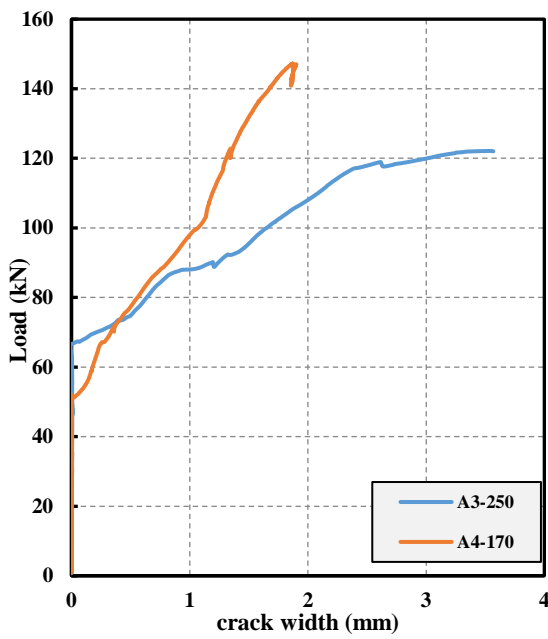


(b) A5 vs A8

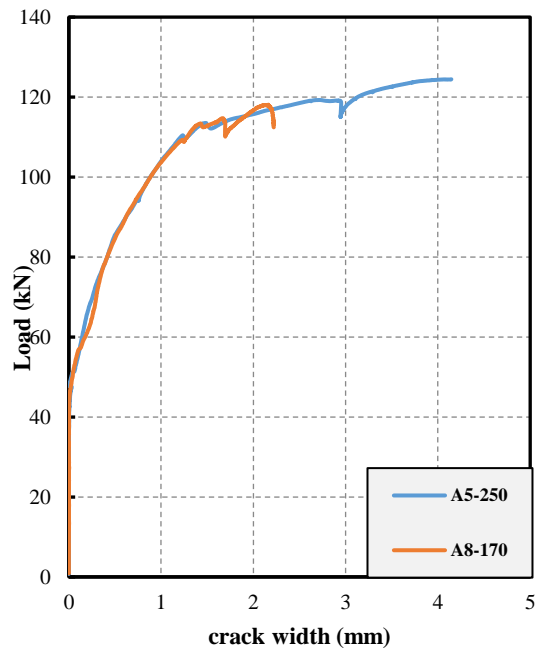


(c) A11 vs A12

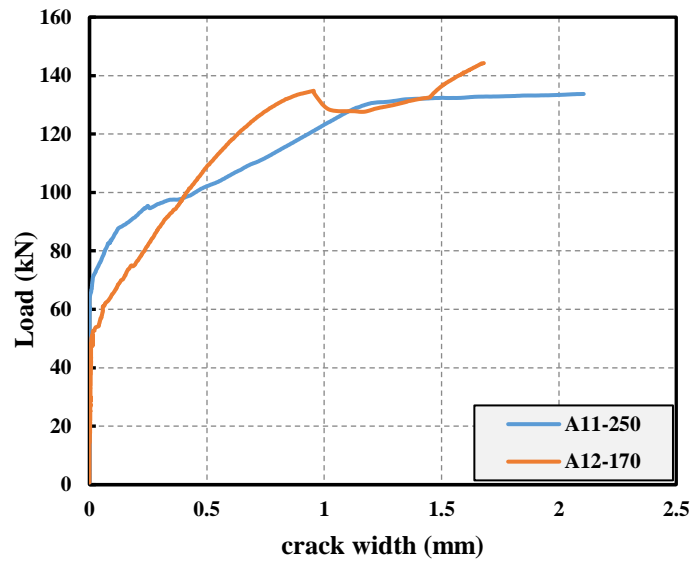
Figure 64. Load displacement diagrams for identical beams with different spacings of stirrups



(a) A3 vs A4



(b) A5 vs A8



(c) A11 vs A12

Figure 65. Load vs crack width diagrams for identical beams with different spacings of stirrups

4.4.5. The GFRP Stirrups Vs Steel Stirrups

The use of GFRP stirrups as a shear reinforcement have shown a significant reduction in the beams ultimate load carrying capacity. Compared to the control beams A13 and A14 which made with steel stirrups, the ultimate loads in beams A12 and A10 have decreased by 30% and 28%, respectively. Also, the control beams demonstrated a clear improvement in the beams stiffness, and this can be attributed to the lower axial stiffness (EA) of the GFRP stirrups in comparison to steel stirrups, therefore by looking at Figure 68, higher strain values of the GFRP stirrups were obtained at similar loading which leads to a higher deformation (Figure 69), a wider cracks (Figure 70), and greater strain values at the midspan for both the longitudinal rebars (Figure 71), and the concrete (Figure 72) . However, no change in the failure mode was noticed.

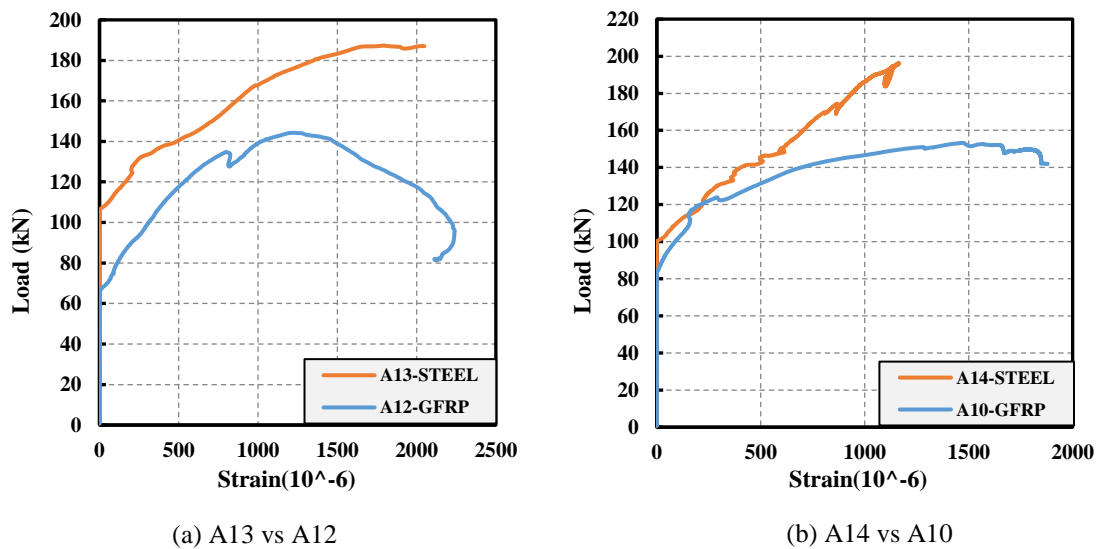
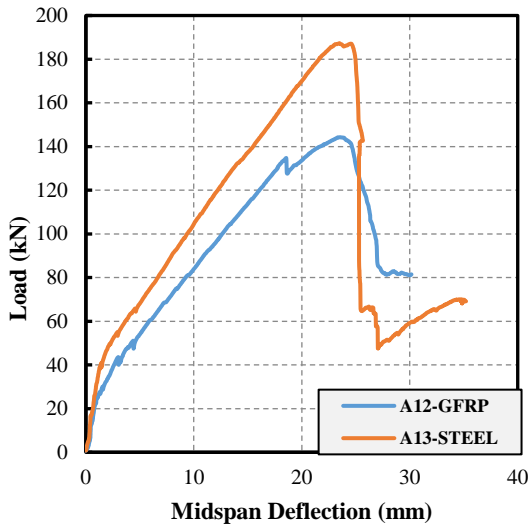
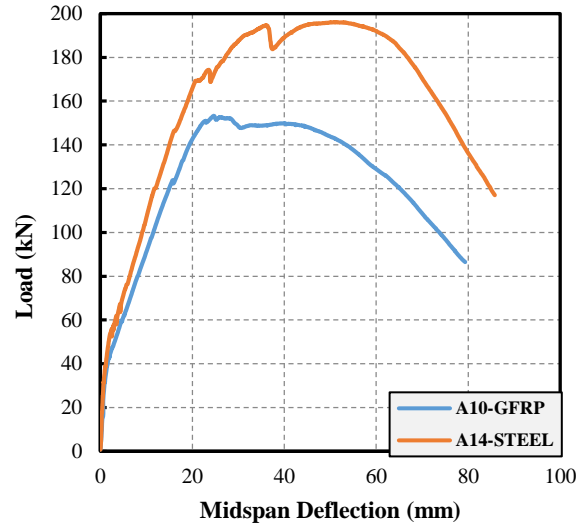


Figure 66. Load vs stirrups strain diagrams for identical beams with different type of stirrups (GFRP vs Steel)

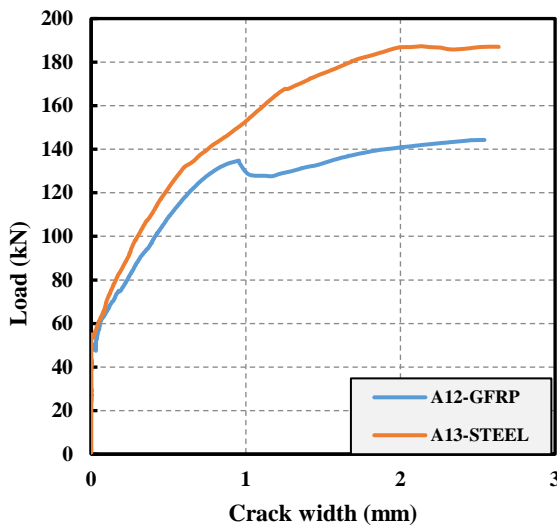


(a) A12 vs A13

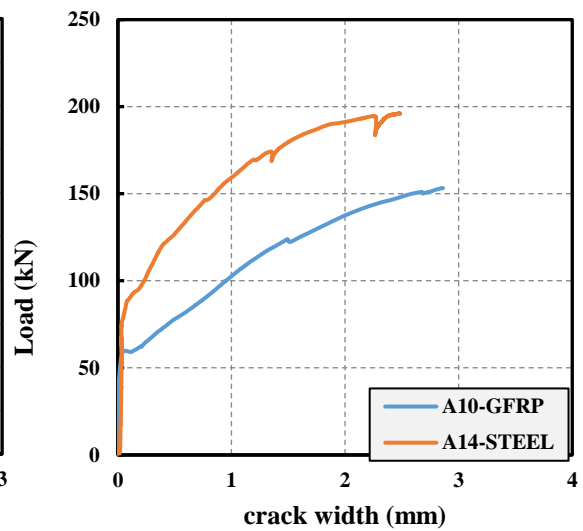


(b) A10 vs A14

Figure 67. Load displacement diagrams for identical beams with different type of stirrups (GFRP vs Steel)

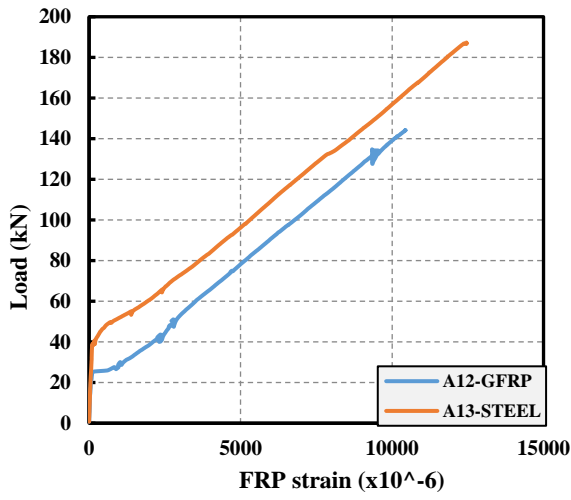


(a) A12 vs A13

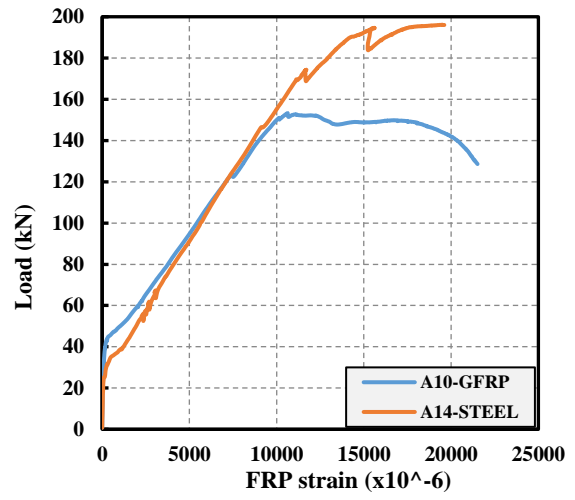


(b) A10 vs A14

Figure 68. Load vs crack width diagrams for identical beams with different type of stirrups (GFRP vs Steel).

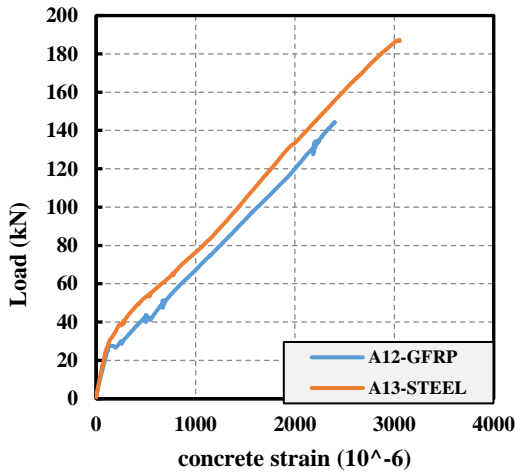


(a) A12 vs A13

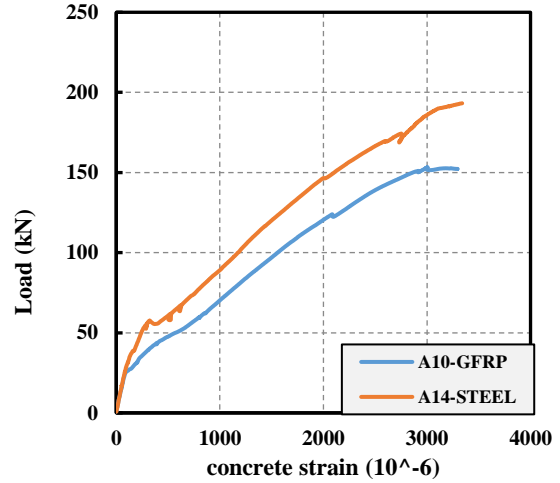


(b) A10 vs A14

Figure 69. Load vs longitudinal FRP strain diagrams for identical beams with different type of stirrups (GFRP vs Steel).



(a) A12 vs A13



(b) A10 vs A14

Figure 70. Load vs concrete strain diagrams for identical beams with different type of stirrups (GFRP vs Steel)

CHAPTER 5: ANALYTICAL PROGRAM

The analytical program aims at investigating the shear capacity of FRC beams reinforced with BFRP bars and GFRP stirrups by validating the findings with the available code-based equations that are evaluating the concrete, stirrups, and the fibers contribution to the shear strength of FRC beams reinforced with BFRP reinforcing bars. A number of design guidelines that addresses the design and construction of concrete structures reinforced with glass, aramid and carbon FRP bars are available in USA, Canada, and Japan [9,10,30,31]. These documents, however, do not provide specific provisions for RC structures reinforced with basalt FRP bars. As a common basis, all these guidelines assumed that shear contributions of the internal stirrups, and shear capacity of concrete are independently contribute to the ultimate shear resistance of the RC beam reinforced with FRP bars as follow: $V_n = V_{frp} + V_c$, where V_{frp} , and V_c are the contributions of the internal FRP stirrups, and shear capacity of concrete, respectively. To calculate the fibers effect, various models available in the literature that have been proposed for shear strength prediction of FRC beams were investigated as well and compared to our test results.

5.1. Design Equations for Shear Strength

ACI 440.1R-15 [9].

$$V_c = \frac{2}{5} \sqrt{f'_c} b_w k d \quad (3)$$

Where, $V_c =$ *Shear resistance provided by concrete*

$b_w =$ *width of web, mm*

$f'_c =$ *concrete compressive strength, MPa*

$d =$ effective depth, mm

$c = kd$, cracked transformed section neutral axis depth, mm.

$$k = \sqrt{2\rho n + (\rho n)^2} - \rho n$$

$$\rho = \frac{A}{b_w d}$$

$A =$ Area of tensile reinforcement, mm²

$$V_f = \frac{A_{fv} f_{fv} d}{s} \quad (4)$$

Where, $V_f =$ Shear resistance provided by FRP stirrups.

$A_{fv} =$ Area of shear reinforcement within stirrups spacing s , mm²

$f_{fv} =$ tensile strength of FRP taken as the smallest of design tensile strength f_{fu} , strength of bent portion of FRP stirrups f_{fb} , or stress corresponding to $0.004E_f$, (MPa).

$s =$ Spacings of FRP stirrups.

CSA-S806-12 [31].

$$V_c = 0.05\lambda k_m k_r (f'c)^{\frac{1}{3}} b_w d_v, \text{ for } d \leq 300 \text{ mm} \quad (5)$$

provided that $0.11\sqrt{f'c} b_w d_v \leq V_c \leq 0.22\sqrt{f'c} b_w d_v$

$$k_m = \sqrt{\frac{V_f d}{M_f}} \leq 1.0, \quad \text{where } \left(\frac{V_f d}{M_f}\right) \text{ is equivalent to } \left(\frac{d}{a}\right)$$

$$k_r = 1 + (E_f \rho)^{\frac{1}{3}}$$

$E_f =$ elastic modulus of the longitudinal FRP reinforcement

d_v is taken as the greater of $0.9 d$ or $0.72 h$, where h is the overall thickness of a member

$V_f =$ ultimate shear, $M_f =$ ultimate moment

$$V_f = \frac{0.4\Phi_f A_{fv} f_{fu} d_v}{s} \cot\theta \quad (6)$$

$$f_{fu} \leq 0.005E_f$$

$$\theta = 30^\circ + 7000\varepsilon_l$$

provided that $30^\circ \leq \theta \leq 60^\circ$

$$\varepsilon_l = \frac{\frac{M_f}{d_v} + V_f + 0.5N_f}{E_f A_{fv}}, \quad N_f = \text{axial load normal to the member cross section. In our case} = 0$$

JSCE-97 [10].

$$V_c = \beta_d \beta_p \beta_n f_{vcd} b_w d / \gamma_b \quad (7)$$

$$\beta_d = \left(\frac{1000}{d}\right)^{\frac{1}{4}} \leq 1.5$$

$$\beta_p = \left(\frac{1000\rho E}{E_s}\right)^{\frac{1}{4}} \leq 1.5$$

$$E_s = \text{elastic modulus for steel } \left(\frac{200\text{KN}}{\text{mm}^2}\right)$$

$\beta_n = 1$ if no axial force applied

$$f_{vcd} = 0.2\sqrt[3]{f'c} \quad \text{provided that } f_{vcd} \leq 0.72 \frac{N}{\text{mm}^2}$$

$$\gamma_b = 1.3$$

$$V_f = [A_{fv} E_{fv} \varepsilon_{fwd} (\cos\alpha_s + \sin\alpha_s) / s] z / \gamma_{bs} \quad (8)$$

E_{fv} = elastic modulus of the FRP shear reinforcement

α_s = angle formed by shear reinforcement and member axis

$$z = \frac{d}{1.15}$$

$$\gamma_{bs} = 1.15$$

$$\varepsilon_{fwd} = 0.0001 \left(f'_{mcd} \left(\frac{\rho E_f}{\rho_w E_{fv}} \right) \right)^{\frac{1}{2}} \left[1 + 2 \left(\frac{\sigma_n}{f'_{mcd}} \right) \right] \quad (9)$$

$$\rho_w = A_{fv} / b_w s$$

$$f'_{mcd} = \left(\frac{h}{0.3} \right)^{-\frac{1}{10}} f'c$$

ISIS 2007 [30].

$$V_c = 0.2 \lambda \sqrt{f'c} b_w d \sqrt{\frac{E_f}{E_s}} \quad (10)$$

$$V_f = \frac{A_{fv} f_{fv} d_v \cot \theta}{s} \quad (11)$$

$$d_v = 0.9d$$

$$f_{fv} = \frac{(0.05 \left(\frac{rb}{db} \right) + 0.3) f_{fu}}{1.5}, \quad \text{or } f_{fv} = E_{fv} \varepsilon_{fwd1} \quad (12)$$

5.1.1. Design Equations for Concrete Beams Reinforced with Longitudinal FRP Bars.

The available codes have used the same concept for concrete members reinforced with steel in developing the design equations for FRP reinforced concrete members. However, due to the difference in characteristics among the FRP and steel, some modifications were done to account for the effects of the FRP material on the shear behavior. In general, the modifications in designing codes are mainly considering the effect of the axial stiffness ($E_f \rho_f$) for FRP bars on the concrete shear resistance which is known to be much lower than that for steel, and therefore can result in an increase in the crack widths and a reduction in depth of the uncracked compression region which are both considerably contributing to the shear strength of concrete.

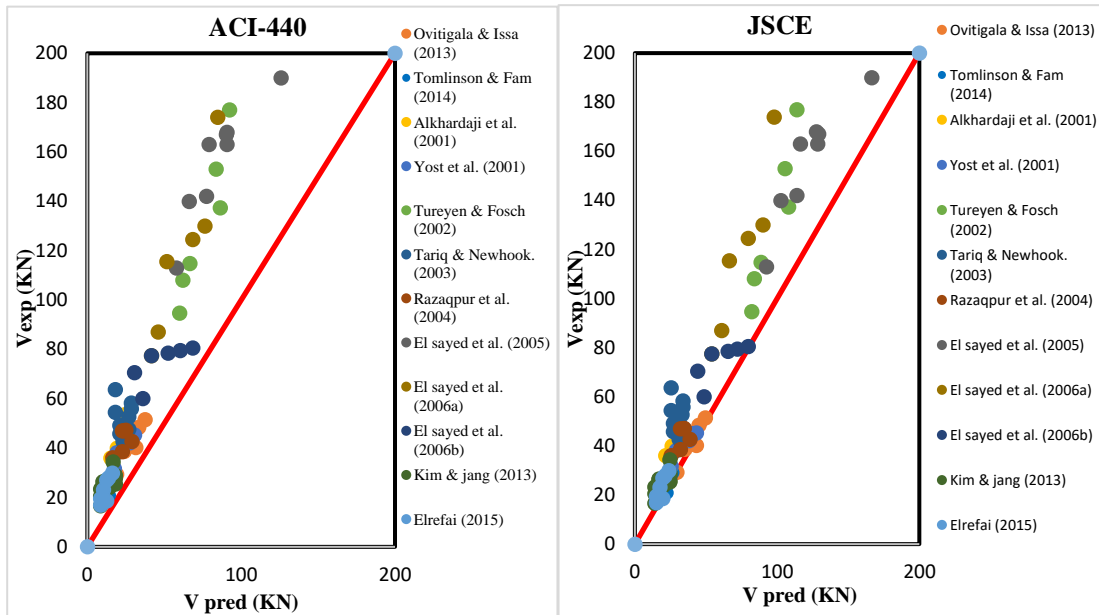
The accuracy of the design codes equations on predicting the concrete shear capacity was investigated on a large number of specimens that includes 86 concrete beams reinforced with different FRP bars and a comparison of the experimental values to the predicted values was then carried. 7 beams [25], 6 beams [40], 2 beams [50] reinforced with BFRP bars as a longitudinal reinforcement were combined to this large database to evaluate their behavior in comparison to the rest of FRP bars. All safety and reduction factors of the design equations were set to 1 in this study. Figure (73) is showing the predicted shear values relative to the experimental ones. The y-axis representing the experimental shear values, while the x-axis representing the predicted shear values. The 45° line represents a measure of how scattered the experimental values from the exact prediction of the design equations are. Figure 73 indicated a good agreement of the BFRP beams (The beams that referred to Ovitigala and Issa (2013), Tomlinson and Fam (2014), and Elrefai et al. (2015)) with the other types of FRP beams because they were following the same trend, especially with the GFRP and AFRP beams due to almost similar elastic modulus. Consequently, it can be concluded that the BFRP beams have a similar shear behavior as those with other FRP bars. By referring to Table 11 and Figure 73, it can be depicted that the ACI-440 code has shown a very conservative prediction with mean values for the ratio $V_{exp.}/V_{pre.}$ of 1.89. The ISIS, and JSCE equations were capable to predict more reasonable values for the shear strength with a mean value $V_{exp.}/V_{pre.}$ of 1.26 and 1.35, respectively but the ISIS have overestimated some predictions. Whereas, although some predictions were overestimated by CSA-S806-12, it has been observed to predict the experimental results more accurately than the other design codes with a mean value of the ratio $V_{exp.}/V_{pre.} = 1.12$, and a coefficient of variation of 18.9%, which indicates the lesser

scatter among the design codes. This is because the CSA-S806-12 equation is including all the parameters that are affecting the shear strength such as: the span to depth ratio (a/d), the reinforcement ratio, and the concrete compressive strength. On the other hand the rest of codes have a drawback of not including any effect for the (a/d) ratio, and it was shown in the previous sections that the (a/d) ratio has a considerable effect on the shear strength, which establishes the importance of including its effect on the design codes equations. Moreover, the ISIS equation does not consider the reinforcement ratio effect on the shear strength of concrete, and therefore, it was founded to have larger scattering in the predicted values than other design equations with a coefficient of variation of 29.6%.

Table 11

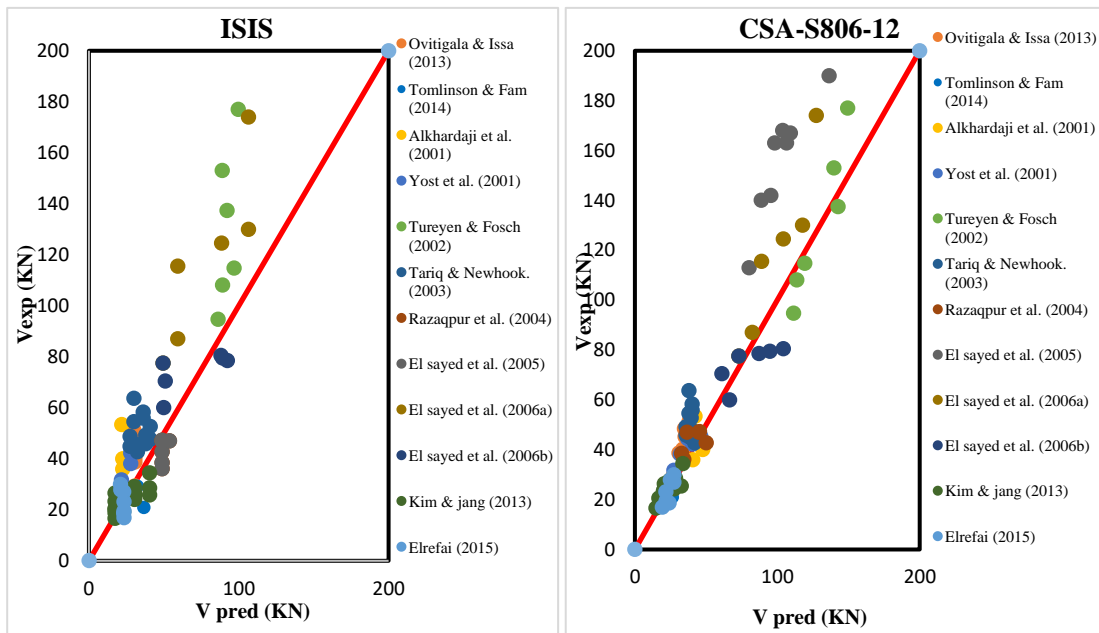
Statistics summary for the experimental concrete shear capacity compared to the predicted ones

	V_{exp}/V_{pre}			
	ACI 440-15	CSA-S806-12	JSCE	ISIS
Mean	1.89	1.12	1.35	1.26
St. Dev.	0.37	0.21	0.26	0.37
Coeff. Of. Var. (%)	20	18.9	19.7	29.6



a) ACI-440

b) JSCE



c) ISIS

d) CSA-S806-12

Figure 71. Comparison of experimental and predicted shear strength for beams reinforced with longitudinal FRP bars only.

5.1.2.Design Equations for Beams with FRP Stirrups

To evaluate the accuracy of the design equations, a large database that includes 92 beams reinforced with longitudinal FRP bars and vertical FRP stirrups was obtained from [37],[40], and [50], the predicted results were then compared to the experimental results, noting that all safety and reduction factors were taken equal to 1.

Due to the low elastic modulus of FRP, the design codes have specified an upper limit for the stress and strain levels to be developed on the FRP stirrups to ensure the integrity of the member through controlling the crack width, furthermore, to avoid failure at the bent region which will experience a considerable reduction in strength after bending as mentioned earlier. Although FRP shear reinforcement can attain larger strain at failure, the permissible strain in FRP stirrups ranges from 0.0025 to 0.004 in different design standards (i.e. ACI, ISIS, and JSCE), which is very close to the yielding strain in steel. According to ACI-440 code, the upper limit of 0.004 was specified to prevent the aggregate that interlocked with the surrounded concrete from being degraded. Even though, shear failure in steel was usually observed to take place at 3 or 4 times the yielding strain [37]. Therefore, standards are predicting more conservative values of shear strength for beams reinforced with FRP stirrups as can be depicted from Figure 74, where JSCE and ISIS guidelines observed to show an excessive conservative prediction of the shear strength with $V_{exp.}/V_{pred.}$ of 2.6 and 2.84, respectively. Whereas ACI-440 and CSA-S806-12 guidelines resulted in much more accurate predictions with $V_{exp.}/V_{pred.}$ of 1.47 and 1.38 respectively. Despite being accurate and conservative for most of the predictions, some predictions in ACI and CSA-S806-12 were overestimated.

In shear reinforcement, the stress level f_{fv} is limited according to ACI-440 and CSA-S806-12 guidelines to $0.004E_f$ and $0.005E_f \leq f_{fb}$, respectively. In JSCE and ISIS the stress can be obtained from $f_{fv} = E_{fv}\varepsilon_{fwd} \leq f_{fb}$, where the strain formula expression (ε_{fwd1}) is obtained from equation (9). However, the design standards are generally specifying a very conservative strain limits for the FRP shear reinforcement as stated earlier, therefore, for better prediction of the shear reinforcement contribution to the shear strength, a research work is required to re-evaluate the strain formula (equation 9) based on the strains values obtained from previous experimental tests. The approach to this issue has been proposed by Shanour et al [39], where a regression analysis was applied on the experimentally obtained strain values so that a modification to the strain equation (9) yields equation (13):

$$\varepsilon_{fwd1} = 0.0001 \left(f'_c \left(\frac{\rho E_f}{\rho_w E_{fv}} \right) \right)^{\frac{1}{2}} \rightarrow \varepsilon_{fwd2} = 0.000396 \left(f'_c \left(\frac{\rho E_f}{\rho_w E_{fv}} \right) \right)^{\frac{1}{2}} \quad (13)$$

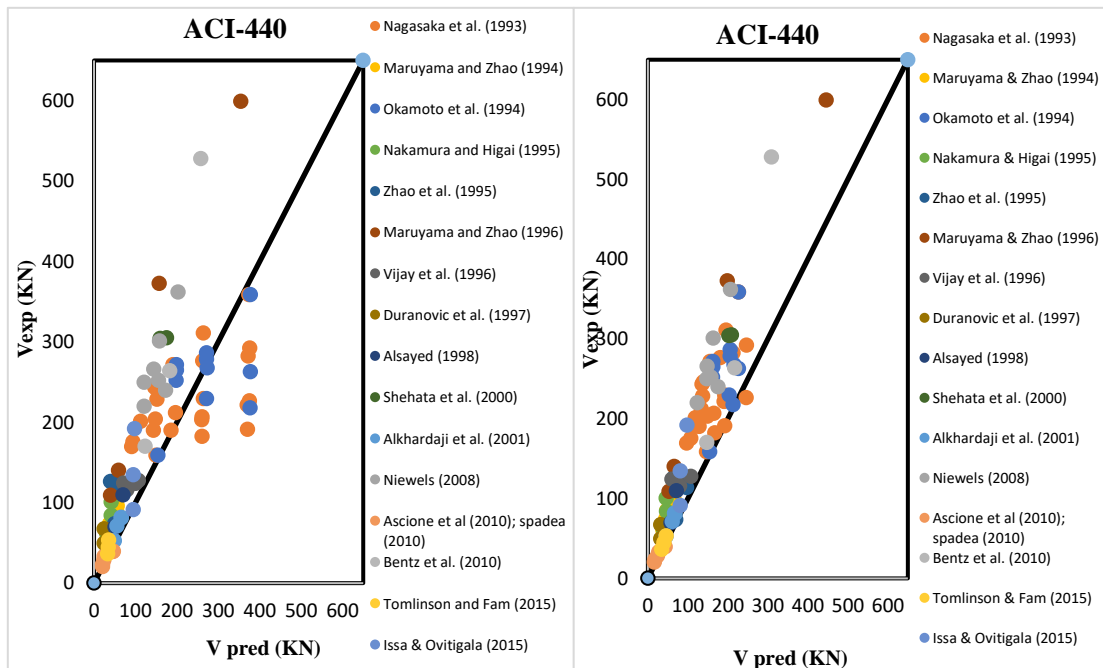
∴ Hence, the maximum stress value to be developed on FRP stirrups can be calculated based on equation (14):

$$f_{fv} = 0.000396 \left(f'_c \left(\frac{\rho E_f}{\rho_w E_{fv}} \right) \right)^{\frac{1}{2}} * E_{fv} \leq f_{fb} \quad (14)$$

Where $f_{fb} = \left(0.05 \left(\frac{rb}{db} \right) + 0.3 \right) f_{fuv} \leq f_{fuv}$

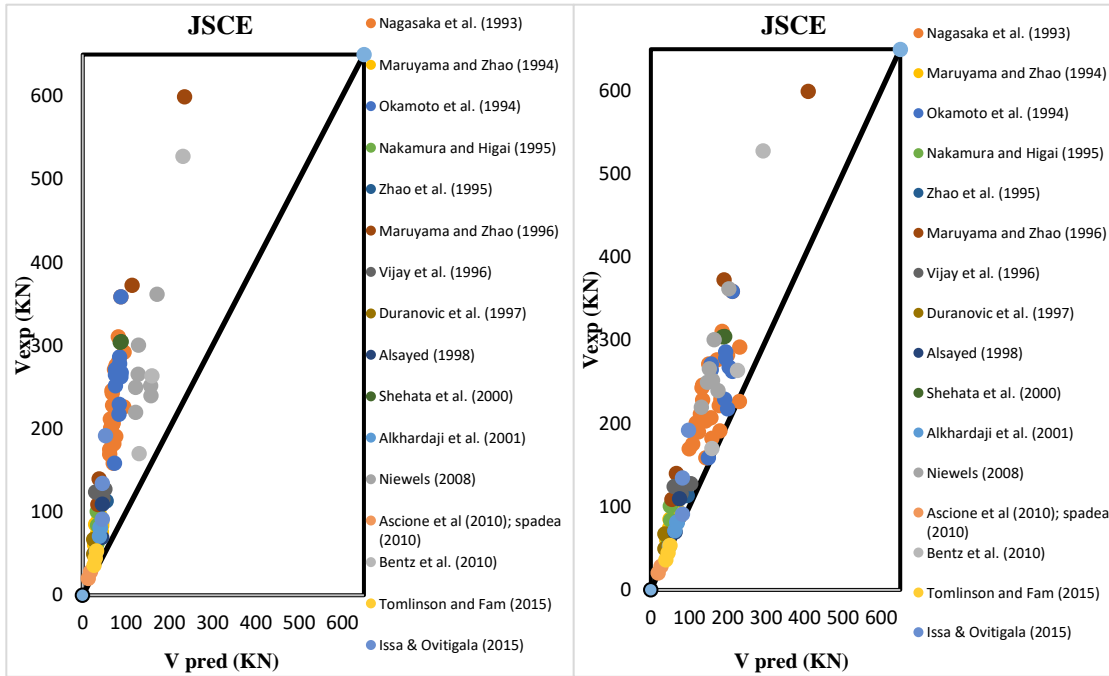
Figure 61 is showing the comparison between the experimental and predicted shear strength for equations before strain formula's modification (to the left) and after strain formula's modification (to the right). Noticeable improvement in the predicted values were

observed when the proposed equation from [39] was incorporated in the V_f equation and combined with the V_c design equations. Results have shown more accurate, consistent and conservative results with less coefficient of variation when we refer to Table 12, where the coefficient of variation in ACI, JSCE, CSA-S806-12, and ISIS was reduced from 36.5, 28.1, 25.2, and 27.6 to 20.7, 20.5, 20.7, and 22.8, respectively, which indicates a clear improvement in consistency between the different results. Also, some predicted values were over estimated by ACI equation, but they were conservatively predicted after the strain modification. Both equations have resulted in conservative predictions for most of the beams, however by employing the strain modification, more accurate predictions were achieved as the predictions are generally shown to be closer to the 45 degree line with a V_{exp}/V_{pred} being reduced from 1.47, 1.38, 2.6, 2.84 to 1.47, 1.21, 1.46, 1.47 in ACI, CSA-S806-12, JSCE, and ISIS, respectively.



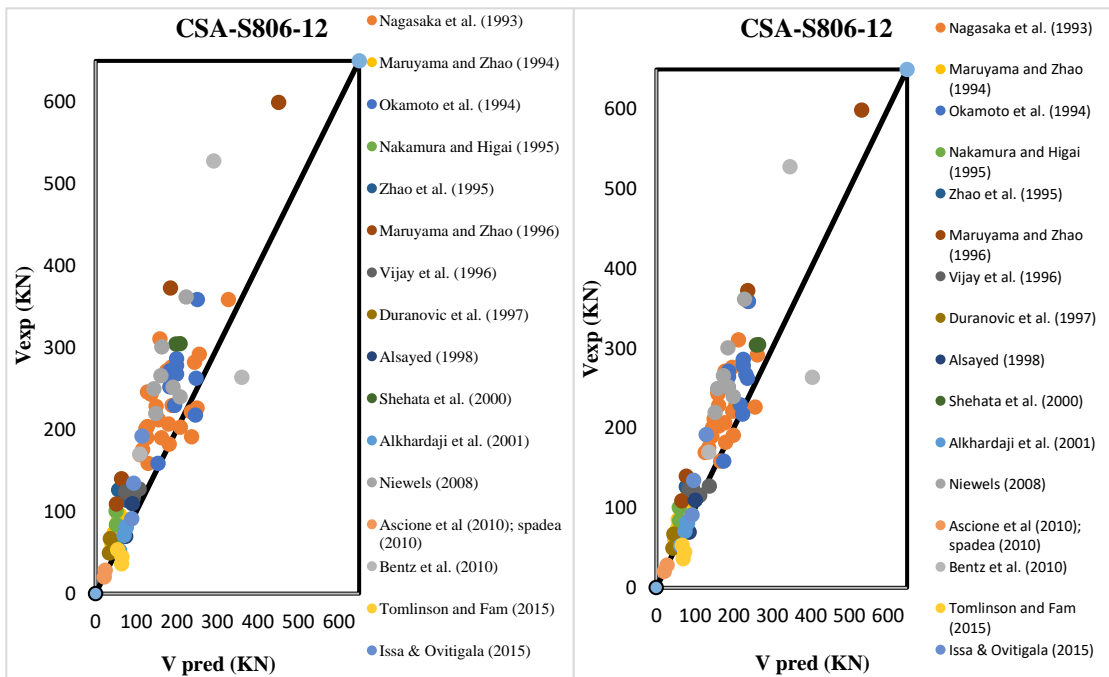
a) ACI-440 before strain modification

b) ACI-440 after strain modification



c) JSCE before strain modification

d) JSCE after strain modification



e) CSA-S806-12 before strain modification

f) CSA-S806-12 after strain modification

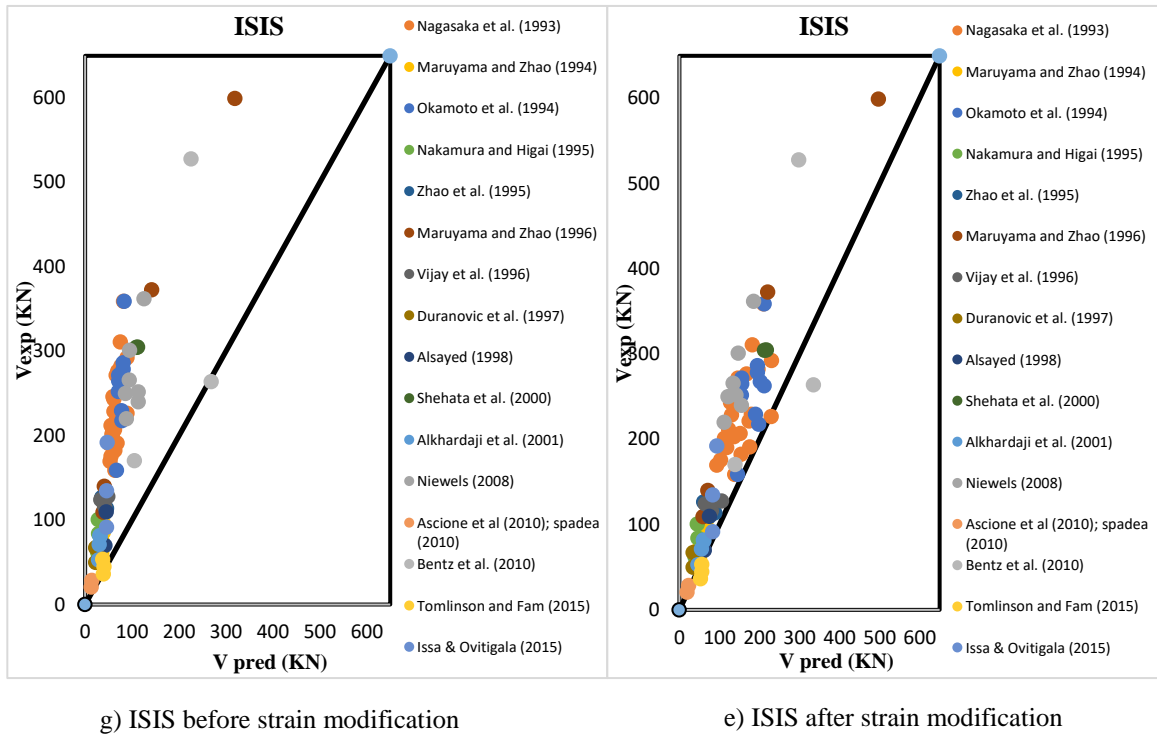


Figure 72. Comparison of experimental and predicted shear strength for beams reinforced with longitudinal FRP bars and stirrups

Table 12

Statistics summary for the experimental shear capacity of beams reinforced FRP bars and stirrups compared to the predicted ones

	V_{exp}/V_{pre}							
	ACI 440-15		CSA-S806-12		JSCE		ISIS	
	Before strain modific	After strain modific.	Before strain modific.	After strain modific	Before strain modific.	After strain modific.	Before strain modific.	After strain modific.
Mean	1.47	1.47	1.38	1.21	2.6	1.46	2.84	1.48
St. Dev.	0.54	0.31	0.35	0.26	0.73	0.3	0.78	0.34
Coeff. Of. Var. (%)	36.5	20.7	25.2	20.7	28.1	20.5	27.6	22.8

5.1.3. Design Equations for FRC Beams Reinforced with Basalt Chopped Fibers

In the literature, many researchers have conducted experimental tests to study the shear behavior of FRC beams, then they were able to propose many analytical approaches that can predict the shear strength values for FRC beams. However, the main focus of these researches was on the steel chopped fibers, while there is no research founded in the literature to provide an analytical approach for beams reinforced with basalt chopped fibers. Some analytical equations that are used to predict the shear strength contribution of steel fibers are listed below:

Narayanan and Darwish [85].

$$v_b = 0.41\tau F \text{ (pull out resistance of fiber), where } \tau = 4.15 \text{ MPa} \quad (15)$$

$$F = (l_f/d_f)V_f k_f$$

$$(l_f/d_f) = \text{fiber aspect ratio (fiber length/ fiber diameter)}$$

$$V_f = \text{Volume fraction of fibers}$$

k_f = bond factor. It was assigned as 0.5 for round fibers, 0.75 for crimped fibers, and 1.0 for indented fibers.

Ta'an and Feel [86].

$$v_b = \frac{8.5}{9} k_f V_f (l_f/d_f) \quad (16)$$

Swamy et al [87].

$$v_b = 0.37 \tau k_f V_f (l_f/d_f) \quad (17)$$

Khuntia [88].

$$v_b = 0.25V_f(l_f/d_f)\sqrt{f'_c} \quad (18)$$

In general, the main difference between FRC and RC beams stems from the post cracking tensile strength behavior that the fiber presence provide, which presents an additional effect on the shear strength over the conventional RC beams. Khuntia et al [88] stated that the residual tensile stress is affected by several factors such as: the fiber aspect ratio, shape, volume fraction and the properties of concrete matrix, therefore many analytical studied [87, 89-94] have suggested the post cracking tensile stress to be expressed in terms of $V_f(l_f/d_f)$. According to Naaman et al [95], better bonding characteristics can be achieved with higher strength concrete, and this in turn can enhance the interfacial bond stress of the fiber with the surrounding matrix. Therefore, the same factors of Khuntia's equation will be considered in this study as it includes the compressive strength effect in addition to the effect of fiber geometry. The stiffness effect will be taken into consideration by including the term $\sqrt{E_f/E_s}$. Also, it was observed that the contribution of fibers was relatively better when higher reinforcement ratio was used as shown in Figure 75. This might be rational if we attributed it to the enhanced dowel action that would slow down the process of bond slip between the reinforcement and the concrete which will reduce the crack widening process and hence the fibers effect will be more prominent in combination with the reinforcement.

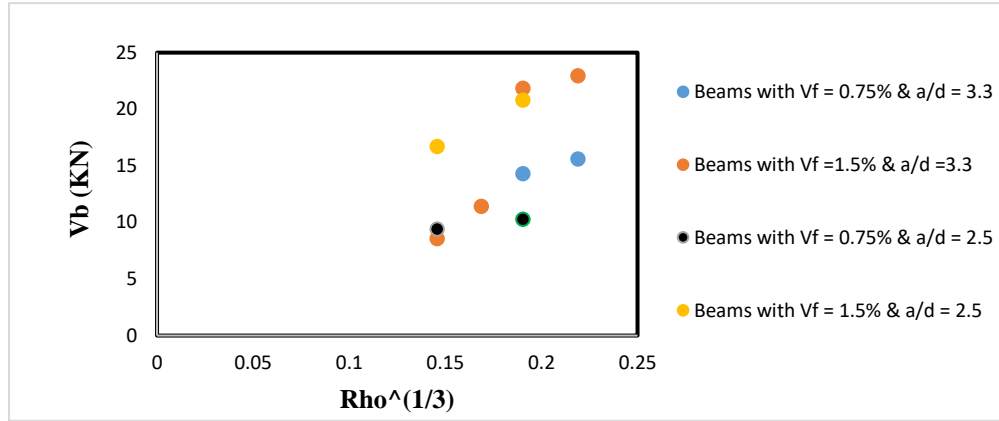


Figure 73. The effect of $\rho^{1/3}$ on the shear contribution of chopped fibers

To evaluate the contribution of the basalt fibers to the shear strength, a similar study to that in [25] but with the addition of basalt minibars was carried (note that this is a different study not mentioned in the experimental program, where FRP stirrups were not used). The increased capacity was calculated then a regression analysis was conducted on the test results and an equation for the fibers contribution was proposed as shown below in equation (19). Next the accuracy of equation (19) was investigated by comparing its predictions to the experimental contribution of basalt fibers to the shearing strength.

$$v_b = 2.84 V_f (l_f/d_f) k_f^3 \sqrt{\rho f'c} \sqrt{E_f/E_s} \quad \text{where } k_f = 0.5 \quad (19)$$

Looking at table (13) from an accuracy perspective it can be concluded that the predictions are showing good accuracy with V_{exp}/V_{pred} of 1.05 and relatively small scattering of 17%

Table 13

Results for evaluating the shear behavior of beams reinforced with longitudinal basalt bars and basalt chopped fibers.

Sample # for [25]	Sample # of current study	f _c (MPa)	a/d ratio	rho	Basalt fiber Volume fraction %	Ultimate shear V _u (KN) by [25]	Ultimate shear V _u (KN) by current study	V _b (KN) Experimental	V _b (KN) Theoretical	V _{exp} /V _{pred}
B-3.3-R3	B1	49	3.3	0.0069	0.75	18.6	32.9	14.3	10.8	1.33
	B2	49	3.3	0.0069	1.5	18.6	40.45	21.85	21.5	1.02
B-3.3-R4	B3	49	3.3	0.0105	0.75	27.85	43.45	15.6	11.3	1.38
	B4	49	3.3	0.0105	1.5	27.85	50.8	22.95	22.6	1.02
B-3.3-R5	B5	49	3.3	0.0152	0.75	29.9	41.5	11.6	12.6	0.92
	B6	49	3.3	0.0152	1.5	29.9	50.4	20.5	25.3	0.81
B-2.5-R1	B7	49	2.5	0.0031	0.75	19.5	28.9	9.4	8.3	1.13
	B8	49	2.5	0.0031	1.5	19.5	36.2	16.7	16.6	1.00
B-2.5-R3	B9	49	2.5	0.0069	0.75	27	37.25	10.25	9.5	0.96
	B10	49	2.5	0.0069	1.5	27	47.8	20.8	19.1	0.97
Average =										1.05
Stand. Dev. =										0.18
Coeff. Of Var. =										17%

After evaluating the shear contribution of the BMF and the proposed equation showed a good match with experimental values, the beams reinforced with longitudinal BFRP bars, GFRP stirrups, and BMF were then evaluated through equation (20), which combines equation (5) for concrete contribution, the stirrups contribution by taking into consideration the modification done in section 5.1.2. to the strain limit in stirrups, and the fibers contribution. This combination was made as these equations have shown the most accurate results among the rest of equations.

$$V_{BFRC} = 0.05\lambda k_m k_r (f'c)^{\frac{1}{3}} b_w d_v + \frac{A_{fv} E_{fv} \varepsilon_{fv} w_d z d_v}{s} + (2.84 V_f (l_f / d_f) k_f \sqrt{\rho f'c} \sqrt{\frac{E_f}{E_s}}) b_w d \quad (20)$$

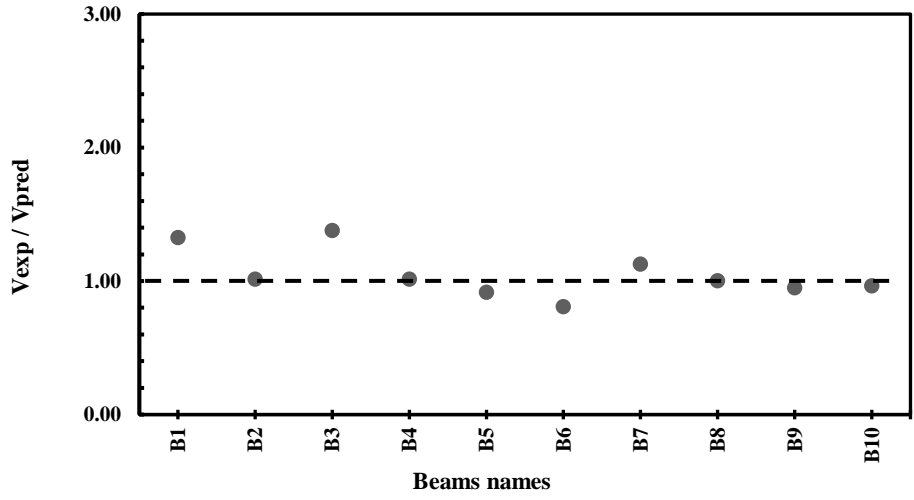
By referring to table (14), the proposed equation pointed out very good predictions with V_{exp}/V_{pred} of 1.00 and with small scattering of 9.8.

Table 14

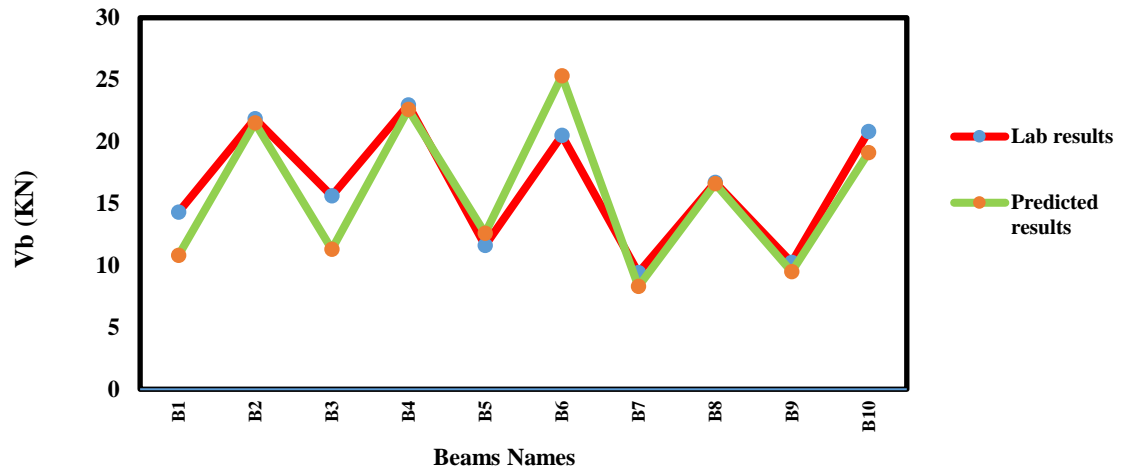
Results for evaluating the shear behavior of beams reinforced with longitudinal basalt bars, GFRP stirrups, and basalt chopped fibers.

Sample #	f_c (MPa)	ρ	ρ_w	Basalt fiber Volume fraction %	Experimental shear V_u (KN)	$V_{predicted}$ (KN)	V_{exp}/V_{pred}
A1	33.7	0.0067	0.0034	0.75	49.5	51.12	0.97
A2	35	0.0067	0.0034	1.5	64.35	61.58	1.04
A3	33.7	0.0100	0.0034	0.75	61	54.98	1.11
A4	33.7	0.0100	0.0051	0.75	73.5	59.03	1.25
A5	35	0.0100	0.0034	1.5	62.25	62.75	0.99
A6	38	0.0100	0.0051	0	49.5	47.91	1.03
A7	33.7	0.0100	0.0051	0.75	50.5	55.73	0.91
A8	35	0.0100	0.0051	1.5	59	66.87	0.88
A9	33.7	0.0147	0.0051	0.75	62.5	63.49	0.98
A10	35	0.0147	0.0051	1.5	76.5	79.70	0.96
A11	33.7	0.0147	0.0034	0.75	66.85	62.38	1.07
A12	33.7	0.0147	0.0051	0.75	72	67.19	1.07
A13	33.7	0.0147	0.0051	0.75	93.5	98.62	0.95
A14	35	0.0147	0.0051	1.5	98	110.60	0.89
Average							1.00
Stand. Dev.							0.098
Coeff. Of var.							9.8

In general, equations (20) and (21) were observed to follow the same trend that the experimental results are following as shown in the figures below (76) and (77). This indicates the ability of the proposed equations to grasp the change in the behavior from beam to beam with an acceptable accuracy.

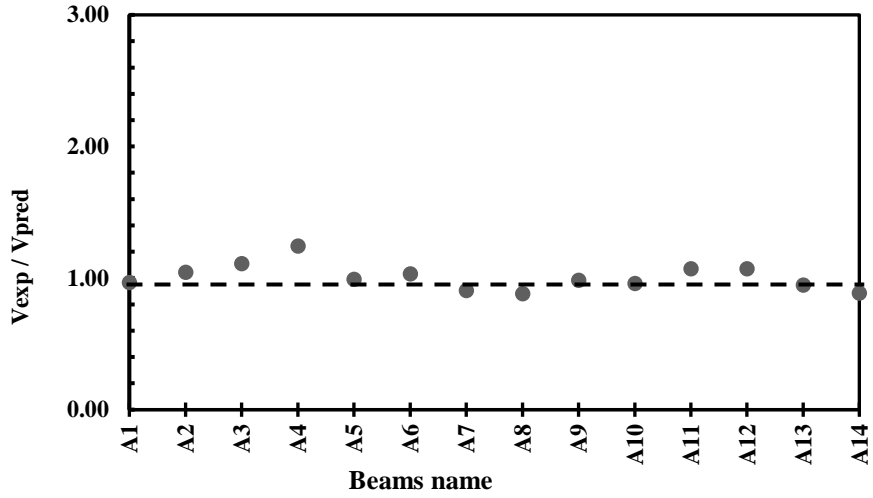


(a)

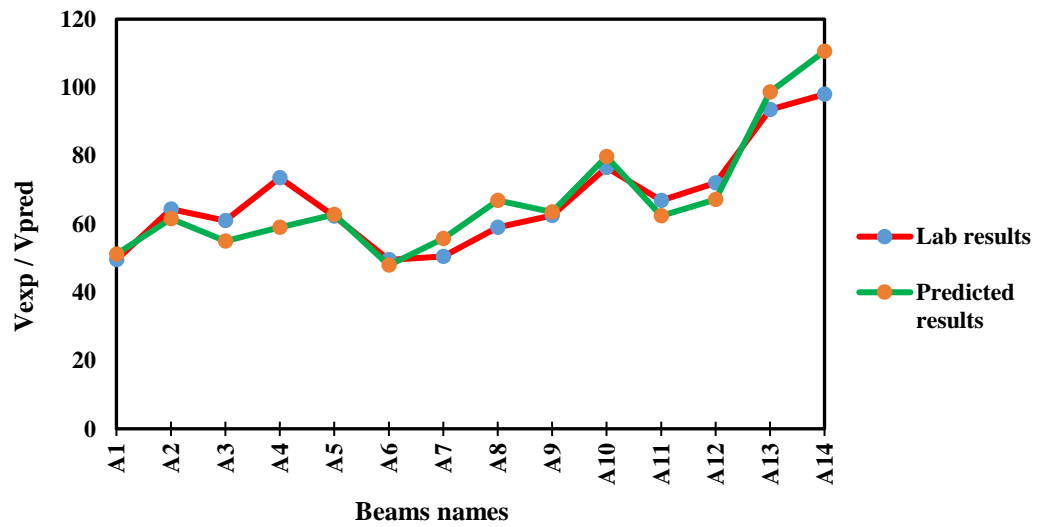


(b)

Figure 74. Comparison between the experimental and predicted values by equation (20)



(a)



(b)

Figure 75. Comparison between the experimental and predicted values by equation (21)

CHAPTER 6: SUMMARY, CONCLUSIONS AND RECOMMENDATIONS

Summary

This paper has investigated the shear behavior of reinforced concrete beams reinforced with BFRP bars and GFRP stirrups. The main variables considered in the study were: span to depth ratio, reinforcement ratio, stirrups spacings, and different volume fractions of basalt fibers. Test results were compared to several analytical models founded in the literature, then a new analytical approach was proposed.

Conclusions

At the end of this investigation the following conclusions can be drawn:

- 1- Adding 0.75% and 1.5% basalt fiber volume fraction to concrete mix observed not to disturb the mix workability.
- 2- The concrete compressive strength was not affected by fiber addition; however, the failure mode has been changed from an explosive type of failure into ductile one.
- 3- The effect of fibers on the flexural strength was more pronounced than the compressive strength, this is due to the post cracking behavior of fibers that are bridging the cracked zone and carrying load beyond the fracture point.
- 4- For the direct tensile test, the concrete in the FRC specimens does not fail once the crack appears as usual, but it keeps carrying the load until fiber rupture or pull out.
- 5- The ultimate load capacity of the large scale beams has experienced an increase of 30% due to the fibers addition.

- 6- In comparison to the reference beam (with 0% fibers), a clear enhancement in the stiffness for the FRC beams was recorded, this can be attributed to the ability of fibers to control cracks widening and propagation by means of crack arresting mechanism. As a result, less strain values in the longitudinal BFRP bars were shown, which indicates less stress values.
- 7- The presence of fibers has altered the mode of failure in several beams from brittle shear failure into ductile flexural failure, allowing them to have a higher load bearing capacity.
- 8- In all tests, the inclusion of fibers provides an excellent adhesion among the entire concrete, therefore catastrophic failure can be avoided.
- 9- Increasing the reinforcement ratio from 0.0067 to 0.01 revealed an increase in the ultimate load capacity of 24%. The loading capacity was further increased by 48% when increasing the reinforcement ratio from 0.0067 to 0.0147. This increase resulted from the increased depth of the uncracked zone, the reduced crack width, and the enhanced dowel capacity. Furthermore, a clear improvement in the beams stiffness were observed when higher reinforcement ratio was used.
- 10- Beams with lower a/d ratio have demonstrated higher loading capacity than their counterpart beams with higher a/d ratio, where this increase ranges from 18% to 46%.
- 11- Reducing the spacing of stirrups from 250 mm to 170 mm has shown a 20% increase in the loading capacity. Additionally, it prevents the diagonal crack widening and propagation thus, the failure mode was altered from shear failure into compression flexural failure.

- 12- Using GFRP stirrups instead of steel results in a 30% reduction in the ultimate load.
- 13- The accuracy of 4 design codes namely: ACI-440. 1R-15, CSA-S806-12, ISIS, and JSCE in predicting the shear strength of beams reinforced with FRP bars and stirrups were investigated. The ACI-440 equation was very conservative in predicting the shear contribution for concrete with V_{exp}/V_{pred} of 1.89, while the CSA-S806-12, ISIS, and JSCE provided reasonably accurate results with V_{exp}/V_{pred} of 1.12, 1.26, and 1.35, respectively.
- 14- In general, all design codes were more conservative for predicting the shear strength for beams reinforced with FRP stirrups, however, using the modification factor for the strain on fiber provided by Shanour et al [39] has significantly improved the predictions accuracy.
- 15- The effect of BMF on the shear strength was investigated, and an analytical approach was proposed to predict its contribution.
- 16- A new equation was proposed to predict the shear strength of beams reinforced with longitudinal FRP bars, FRP stirrups and BMF. The proposed equation's predictions showed very good matching with tested beams with V_{exp}/V_{pred} of 1.00 and a coefficient of variation of 9.8%.

Recommendations

Further work is required to study the performance of basalt stirrups as a shear reinforcement. For a more accurate prediction of the basalt fibers contribution to the shearing strength, more tests are required to investigate the effect of varying strengths of concrete in the bonding between the fiber with the surrounding concrete matrix, and the relation between the reinforcement ratio and the span to depth ratio on the fibers effect. Furthermore, it was observed in one of the observations that the fibers inclusion in a beam with bigger spacing between stirrups resulted in a much better behavior than a counterpart beam made without fibers and with smaller spacing between stirrups. Therefore, the ability of fibers in partially substituting the number of stirrups should be examined to find the optimum amount of fibers required to reduce the amount of shear reinforcement.

References

1. Bell, T. (n.d.). How and Why Do Metals Corrode? Retrieved May 31, 2018, from <https://www.thebalance.com/what-is-corrosion-2339700>.
2. ACI Committee 222, "Protection of Metals in Concrete Against Corrosion (ACI 222R-01)," ACI Manual of Concrete Practice, American Concrete Institute, Farmington Hills, MI.
3. The international Handbook of FRP COMPOSITES IN CIVIL ENGINEERING. Edited by Manoochehr Zoghi.
4. P. Balagury, A. Nanni, and J. Giancaspro, FRP Composites For Reinforced And Prestressed Concrete Structures, 1st ed. Taylor & Francis, 2009.
5. C. E. Bakis, A. Ganjehlou, D. I. Kachlakev, M. Schupack, P. N. Balaguru, D. J. Gee, V. M. Karbhari, D. W. Scott, C. A. Ballinger, T. R. Gentry, and others, "Guide for the Design and Construction of Externally Bonded FRP Systems for Strengthening Concrete Structures," 2002.
6. H. V. S. GangaRao, N. Taly, and P. V. Vijay, Reinforced Concrete Design with FRP Composite, 1st ed. Taylor & Francis, 2007.
7. ISIS-Canada (2003). An introduction to FRP composites for Construction, ISIS Canada, Toronto, Ontario, Canada, www.isiscanada.com.
8. Kiilunen, E (2016). Retrieved May 31, 2018, from http://ltap.unl.edu/Documents/ConferenceArchives/MINK16_Kiilunen.pdf.
9. ACI (American Concrete Institute). (2015). "Guide for the design and construction of structural concrete reinforced with FRP bars." ACI 440.1R-15, Farmington Hills, MI.

10. Japan Society of Civil Engineers (1997). Recommendation for design and construction of concrete structures using continuous fiber reinforcing materials. Concrete Engineering Series 23; Tokyo, Japan Society of Civil Engineers.
11. Al-Mahmoud, F., A. Castel, R. Francois, C. Tourneur, 2007, Effect of surface pre-conditioning on bond of carbon fibre reinforced polymer rods to concrete, *Cement and Concrete Composites*, 29, 677-689.
12. Minelli, F., and G. Plizzari. 2006. Steel fibers as shear reinforcement for beams. In *Proceedings of the second fib congress, Naples, Italy*.
13. Neville, A.M. & Brooks, J.J., 2001. *Concrete Technology*, revised edition. Essex U.K.; Pearson Education Limited.
14. Jóhann Helgi Óskarsson (2013) A master thesis on ‘The effect of steel fibres on the compressive ductility in lightweight aggregate concrete structures’, *Research and Applications in Structural Engineering, Mechanics and Computation*, (June), pp. 543–544. doi: doi:10.1201/b15963-273.
15. Sahoo, D.R., Maran, K. & Kumar, A., 2015. Effect of steel and synthetic fibers on shear strength of RC beams without shear stirrups. *Construction and Building Materials*, 83, pp.150–158. Available at:
<http://dx.doi.org/10.1016/j.conbuildmat.2015.03.010>.
16. Ellobody, E., 2013. Numerical modelling of fibre reinforced concrete-filled stainless steel tubular columns. *Thin-Walled Structures*, 63, 1-12.

17. Kanstad, T. et al., 2011. Forslag til retningslinjer for dimensjonering, utførelse og kontroll av fiberarmerte betongkonstruksjoner, COIN Project report 29 -2011. Trondheim; SINTEF Building and Infrastructure.
18. Abbas, U. (2013) 'Materials Development of Steel-and Basalt Fiber-Reinforced Concretes', (November).
19. Bentur A, Mindess S. Fibre reinforced cementitious composites. London: Taylor & Francis; 2007. XX, 601 s. : ill. p.
20. Hancock, Paul and Skinner, Brian J. "basalt." The Oxford Companion to the Earth. 2000. Encyclopedia.com.
21. Patnaik, A.K., Puli, R.K., and Mylavarapu, R., "Basalt FRP: A new FRP material for infrastructure market ?", 4th International Conference on Advanced Composite Materials in Bridges and Structures (ACMBS-IV) - Editors: M. El-Badry and L. Dunaszegi, Canadian Society of Civil Engineers, Montreal, Canada, July 2004, 8 pages.
22. Patnaik, A., "Applications of Basalt Fiber Reinforced Polymer (BFRP) Reinforcement for Transportation Infrastructure", Developing a Research Agenda for Transportation Infrastructure Preservation and Renewal, Transportation Research Board Conference (TRB-2009), Washington, D.C., Nov. 2009, 5 pages.
23. Patnaik, A., Adhikari, S., Bani-Bayat, P., and Robinson, P., "Flexural Performance of Concrete Beams Reinforced with Basalt FRP Bars", 3rd fib International Congress, Washington, D.C., May 2010, 12 pages.

24. Patnaik, A., “Basalt Fiber Reinforced Polymer (BFRP) Materials for Reinforced Concrete Applications“, 2011 DoD Corrosion Conference, NACE International, Palm Springs, CA July-Aug. 2011, 15 pages.
25. A. EI Refai, F. Abed. Concrete contribution to shear strength of beams reinforced with basalt fiber-reinforced bars. *J Compos Constr* 10.1061/(ASCE)CC.1943-5614.0000648, 04015082.
26. Sim, K., Park, C., and Moon, D. Y. (2005). “Characteristics of basalt fiber as a strengthening material for concrete structures.
27. J. Krassowska, A. Lapko, The influence of basalt fibers on the shear and flexural capacity of reinforced concrete continuous beams, in: First International Conference for Ph.D. Students in Civil Engineering, CE-PhD 2012, Cluj-Napoca, Romania, Nov. 4-7, 2012.
28. Thorhallsson, E., Erlendsson, J. & Erlendsson, Ö., 2013. Basalt fiber introduction. Ltu.Se, (November), pp.1–6. Available at: [http://www.ltu.se/cms_fs/1.111059!/file/BASALT_FIBER_INTRODUCTION .pdf](http://www.ltu.se/cms_fs/1.111059!/file/BASALT_FIBER_INTRODUCTION.pdf).
29. Rathod, N., Gonbare, M. & Pujari, M., 2013. Basalt Fiber Reinforced Concrete. *International Journal of Science and Research (IJSR) ISSN (Online Index Copernicus Value Impact Factor, 14(5), pp.2319–7064. Available at: www.ijsr.net.*
30. ISIS Canada, Reinforcing Concrete Structures with Fiber Reinforced Polymers. Design Manual N8 3 Version 2, Canada ISIS Canada Corporation, Manitoba, 2007.
31. CSA, S806-12: Design and Construction of Building Components with Fiber-Reinforced Polymers, Canadian Standards Association, Canada, 2012.

32. Sudeep Adhikari, 2013. MECHANICAL AND STRUCTURAL CHARACTERIZATION OF MINI-BAR REINFORCED CONCRETE BEAMS A Dissertation Presented to The Graduate Faculty of The University of Akron In Partial Fulfillment of the Requirements for the Degree Doctor of Philosophy.
33. Reinforced Concrete mechanics and design book By James K. Wight & James G. MacGregor.
34. Steel Fiber Reinforced Concrete Behavior, Modelling, and Design By Harvinder Singh.
35. Design of reinforced concrete (9th edition) By JACK C. McCROMAC & RUSSELL H. BROWN.
36. Lovísa, S., 2012. Experimental research on strengthening of concrete beams by the use of epoxy adhesive and cement-based bonding material. , (June).
37. Razaqpur, A. G., Isgor, B. O., Greenaway, S., and Selley, A. (2004). “Concrete contribution to the shear resistance of fiber reinforced polymer reinforced concrete members.” *J. Compos. Constr.*, Vol. 8:5, 452–460.
38. El-Sayed, A. K., El-Salakawy, E., and Benmokrane, B. (2006b). “Shear strength of FRP-reinforced concrete without transverse reinforcement.” *ACI Struct. J.*, 103(2), 235–243.
39. Shanour, A.S. et al., 2016. Experimental and analytical shear evaluation of concrete beams reinforced with glass fiber reinforced polymers bars reinforced with glass fiber reinforced polymers bars. *CONSTRUCTION & BUILDING MATERIALS*, 102(November 2015), pp.574–591. Available at: <http://dx.doi.org/10.1016/j.conbuildmat.2015.10.185>.

40. Issa, MA, Ovitigala, T & Ibrahim, M 2016, 'Shear Behavior of Basalt Fiber Reinforced Concrete Beams with and without Basalt FRP Stirrups' *Journal of Composites for Construction*, vol 20, no. 4, 4015083. DOI: 10.1061/(ASCE)CC.1943-5614.0000638
41. Yost, J. R, Gross, S. P, and Dinehart, D. W. (2001). "Shear strength of normal strength concrete beams reinforced with deformed GFRP bars." *J. Compos. Constr.*, 10.1061/(ASCE)1090-0268(2001)5:4(268), 268–275.
42. Kalpana, V.G. & Subramanian, K., 2011. Behavior of concrete beams reinforced with GFRP BARS.
43. Mahmoud, K. & El-salakawy, E., 2015. Shear strength of glass fiber reinforced polymer – reinforced concrete continuous beams without transverse reinforcement. , 1082(June 2014), pp.1073–1082.
44. Sergey, S. & Bogdanova, E., The Experimental Study of Concrete Beams Reinforced with Different Types of Bars Carrying Capacity. , 7, pp.1–4.
45. Bentz, E. C., Vecchio, F. J., and Collins, M. P. (2006). "Simplified modified compression field theory for calculating the shear strength of reinforced 15 concrete elements." *ACI Struct. J.*, 103(4), 614–624
46. Bentz, E. C., and Collins, M. P. (2006). "Development of the 2004 Canadian Standards Association (CSA) A23.3 shear provisions for reinforced concrete." *Can. J. Civ. Eng.*, 33(5), 521–534.
47. Morphy, R., Shehata, E., and Rizkalla, S. (1997). "Bent effect on strength of CFRP stirrups." *Proc. • 3rd Int. Symp. on Nonmetallic (FRP) Reinforcement for Concrete Struct.*, (2), 19 - 26.

48. Bentz, E.C. et al., 2010. Shear Strength of Large Concrete Members with FRP Reinforcement. , 14(December), pp.637–646.
49. Ehsani, M. R.; Saadatmanesh, H.; and Tao, S., 1995,“Bond of Hooked Glass Fiber Reinforced Plastic (GFRP) Reinforcing Bars to Concrete,” ACI Materials Journal, V. 92, No. 4, July-Aug., pp. 391-400.
50. Tomlinson, D., and Fam, A. (2014). “Performance of concrete beams reinforced with basalt FRP for flexure and shear.” J. Compos. Constr., 10.1061/(ASCE)CC.1943-5614.0000491, 04014036.
51. Ahmed, E. A., El-Sayed, A. K., El-Salakawy, E., and Benmokrane, B.(2014). “Bend strength of FRP stirrups: Comparison and evaluation of testing methods.” J. Compos. Constr., 10.1061/(ASCE)CC.1943-5614.0000050, 3–10.
52. Grace, N.F. et al., 1998. Behavior and Ductility of Simple and Continuous FRP Reinforced Beams. Journal of Composites for Construction, 2(November), pp.186–194.
53. Gross, S. P., Yost, J. R., Dinehart, D. W., Svensen, E., and Liu, N. (2003). “Shear strength of normal and high strength concrete beams reinforced with GFRP reinforcing bars.” Proc., Int. Conf. on High Performance Materials in Bridges, ASCE, Kona, Hawaii, 426–437.
54. Alam, M. S., and Hussein, A. (2013). “Size effect on shear strength of FRP reinforced concrete beams without stirrup.” J. Compos. Constr., 10.1061/(ASCE)CC.1943-5614.0000248, 119–126.
55. Laurent Massam, The Behaviour of GFRP Reinforced Concrete Beams in Shear,MSc, Department of Civil Engineering, University of Toronto, Canada,

2001.

56. Patnaik, A.K., Miller, L. & Standal, P.C., Fiber Reinforced Concrete Made From Basalt Frp Minibar.
57. High, C. et al., 2015. Use of basalt fibers for concrete structures. *Construction and Building Materials*, 96, pp.37–46. Available at:
<http://dx.doi.org/10.1016/j.conbuildmat.2015.07.138>.
58. Patnaik, A.K., MacDonald, C., MacDonald, M., and Ramakrishnan, V., “Review of ASTM C1399 Test for the Determination of Average Residual Strength of Fiber Reinforced Concrete“, the proceedings of the international conference on Recent Advances in Concrete Technology (RAC07), Baltimore, MD, Sep. 2007, 10 pages.
59. Juárez, C., P. Valdez, A. Durán, A., and K. Sobolev. 2007. The diagonal tension behavior of fiber reinforced concrete beams. *Cement and Concrete Composites* 29: 402–408. 3.14 Hollow Core Slabs (HCS) Made with FRC 45.
60. Conforti, A., F. Minelli, and G.A. Plizzari. 2013. Wide-shallow beams with and without steel fibers: A peculiar behaviour in shear and flexure. *Composites Part B: Engineering* 51:282–290.
61. Conforti, A. 2014. Shear behavior of deep and wide-shallow beams in fiber reinforced concrete. Ph.D. thesis, Department of civil, architectural, environmental, land planning engineering and of mathematics, University of Brescia, May 2014, Aracne Editrice, Roma, p. 232, ISBN 978-88-548-7009-3.

62. Minelli, F., G. Plizzari, and F. Vecchio. 2007. Influence of steel fibers on full-scale RC beams under shear loading. In Proceedings of the international conference framcos—high performance concrete, brick-masonry and environmental aspects, Catania, Italy.
63. Lim, D.H., and B.H. Oh. 1999. Experimental and theoretical investigation on the shear of steel fibre reinforced concrete beams. *Engineering Structures* 21: 937–944.
64. Minelli, F., A. Conforti, E. Cuenca, and G.A. Plizzari. 2014. Are steel fibres able to mitigate or eliminate size effect in shear? *Materials and Structures* 47(3): 459–473.
65. K. Holschemacher, T. Mueller, and Y. Ribakov (2010). “Effect of steel fibers on mechanical properties of high-strength concrete,” *Materials and Design*, 31(5), 2604-2615.
66. Y. Mohammadi, R. Carkon-Azad, S.P. Singh, and S. Kaushik (2009). “Impact resistance of steel fibrous concrete containing fibers of mixed aspect ratio,” *Construction and Building Materials*, 23(1), 183-189.
67. J. Katzer and J. Dowski (2012). “Quality and mechanical properties of engineered steel fibers used as reinforcement for concrete,” *Construction and Building Materials*, 34, 243-248.
68. Imam, Vandewalle, Mortelmans and V. Gemert. 1997. Shear domain of Fibre-Reinforced High-Strength Concrete Beams. *Engineering Structures* 19(9): 738–747.

69. Di-Prisco, Plizzari and Vandewalle. 2010. MC2010: Overview on the shear provisions for FRC. In *Shear and punching shear in RC and FRC elements*, vol. 57, ed. F. Minelli and G. Plizzari, 61–76. Italy: University of Brescia.
70. Kwak YK, Eberhard MO, Kim WS, Kim J. Shear strength of steel fiber-reinforced concrete beams without stirrups. *ACI Struct J* 2002;99(4):530–8.
71. Parra-Montesinos GJ. Shear strength of beams with deformed steel fibers. *Concr Int* 2006; 28(11):57–66.
72. Sahoo DR, Sharma A. Effect of steel fiber content on behavior of concrete beams with and without stirrups. *ACI Struct J* 2014;111(5):1157–66.
73. ACI 318-08. Building code requirements for structural concrete (ACI 318-08) and Commentary (ACI 318R-08). Farmington Hills, MI: American Concrete Institute; 2008. p.465.
74. El-dieb, A.S., El-maaddawy, T.A. & Al-rawashdah, O., 2014. Shear behavior of ultra - high - strength steel fiber - reinforced self - compacting concrete beams. , pp.972–979.
75. Ding, Y., You, Z. & Jalali, S., 2011. The composite effect of steel fibres and stirrups on the shear behaviour of beams using self-consolidating concrete. *Engineering Structures*, 33(1), pp.107–117. Available at: <http://dx.doi.org/10.1016/j.engstruct.2010.09.023>.
76. Amin, A. & Foster, S.J., 2016. Shear strength of steel fibre reinforced concrete beams with stirrups. *Engineering Structures*, 111, pp.323–332. Available at: <http://dx.doi.org/10.1016/j.engstruct.2015.12.026>.
77. Mansur, M. A.; Ong, K. C. G.; and Paramsivam, P., “Shear Strength of Fibrous

- Concrete Beams without Stirrups,” *Journal of Structural Engineering*, V. 112, No. 9, Sept. 1986, pp. 2066-2079.
78. V. Ramakrishnan, N. S. Tolmare, and V. Brik, *Performance Evaluation of 3-D Basalt Fiber Reinforced Concrete & Basalt Rod Reinforced Concrete*, 1998.
79. T. Ayub, N. Shafiq, M. F. Nuruddin, and S. U. Khan, “Mechanical properties of high-strength concrete reinforced with PVA and basalt fibres,” in *InCIEC 2013*, pp. 567–575, Springer, 2014.
80. L. J. Y. Y. Meng and Z. Yan, “Experimental research on the mechanical behavior of chopped basalt fiber reinforced concrete,” *Industrial Construction*, vol. 6, article 002, 2007.
81. Jianxun Ma, Xuemei Qiu, Litao Cheng, Yunlong Wang, *Experimental research on the fundamental mechanical properties of presoaked basalt fiber concrete*, in: Lieping Ye, Peng Feng, Qingrui Yue (Eds.), *Advances in FRP Composites in Civil Engineering*, Springer, Berlin, Heidelberg, 2011, pp. 85–88, <http://link.springer.com/chapter/10.1007/978-3-642-17487-2_16>.
82. S. Bajaj (2012). “Effect of corrosion on physical and mechanical properties of reinforced concrete,” M. Sc. Thesis, University of Akron, USA.
83. Li, V. C., Ward, R. and Hamza, A. M. (1992) ‘Steel and Synthetic Fibres As Shear Reinforcement’, *ACI Materials Journal*, 89(5), pp. 499–508.
84. Adhikari, S. and Patnaik, D. A. (2013) ‘Mechanical and Structural Characterization of Mini-Bar Reinforced Concrete Beams’, *The Graduate Faculty of The University of Akron*, p. 71.

85. Narayanan R, Darwish IYS. Use of steel fibres as shear reinforcement. *ACI Struct J* 1987;84(3):1125–32.
86. Ta'an A, Feel A. Evaluation of shear strength of fibre reinforced concrete beams. *Cement Concrete Compos* 1990;12(2):87–94.
87. Swamy RN, Jones R, Chiam ATP. Influence of steel fibres on the shear resistance of lightweight concrete T-beams. *ACI Struct J* 1993;90(1):103–14.
88. Khuntia, M., Stojadinovic, B., and Goel, S. C. (1999) 'Shear strength of normal and high-strength fiber reinforced concrete beams without stirrups', *ACI Structural Journal*, 99(96), pp. 530–538.
89. Lim, T. Y.; Paramasivam, P.; and Lee, S. L., "Shear and Moment Capacity of Reinforced Steel-Fiber-Concrete Beams," *Magazine of Concrete Research*, V. 39, No. 140, Sept. 1987, pp. 148-160.
90. Lim, T. Y.; Paramasivam, P.; and Lee, S. L., "Analytical Model for Tensile Behavior of Steel-Fiber Concrete," *ACI Materials Journal*, V. 84, No. 4, July-Aug. 1987, pp. 286-298.
91. Naaman, A. E., "High-Performance Fiber Reinforced Cement Composites," *Proceedings of the IABSE Symposium on Concrete Structures for the Future*, Paris, France, Sept. 1987, pp. 371-376.
92. Naaman, A. E.; Moavenzadeh, F.; and McGarry, F. J., "Probabilistic Analysis of Fiber-Reinforced Concrete," *Journal of Engineering Mechanics Division*, V. 100, No. EM2, Apr. 1974, pp. 397-413.
93. Nammur, G. G., and Naaman, A. E., "Strain Rate Effects on Tensile Properties of Fiber Reinforced Concrete," *Proceedings of MRS Symposium on "Cement Based*

Composites: Strain Rate Effects on Fracture,” V. 64, S. Mindess, ed., Materials Research Society, Pittsburg, Pa. 1986, pp. 97-118.

94. Swamy, R. N., and Mangat, P. S., “Interfacial Bond Stress in Steel Fiber Cement Composites,” Cement and Concrete Research, V. 6, 1976, pp. 641-650.

95. Naaman, A. E., and Najm, H., “Bond-Slip Mechanisms of Steel Fibers in Concrete,” ACI Materials Journal, V. 88, No. 2, Mar.-Apr. 1991, pp. 135-145.